MACHINE SCIENCE

1
2021

International scientific–technical journal

Contents

For the anniversary of prof., DSc (Technical) Rasim Alizade!

Rasim Ismayil Alizade - Chairman of the Azerbaijan Committee of the International Federation for the development of science "Theory of Mechanisms and Machines" (AzC IFToMM at the Azerbaijan Technical University was approved by the IFToMM Assembly in 1995).

Born on 28.11.1941 in Ganja, Azerbaijan. He graduated from the mechanical faculty of the Kharkov Institute of Transport Engineers (1965), post-graduate studies at the Moscow State Institute of Machine Science of the USSR Academy of Sciences in the specialty "Mechanisms, machines and theory of automatic lines" (1966-1968) and in 1968 in Moscow he defended his thesis for the degree of candidate of Technical Sciences. In 1973, he was confirmed as an associate Professor, and in 1991 he was awarded the academic title of Professor. In 1992, he defended his doctoral dissertation on the topic "Modular method of kinematic analysis and synthesis of spatial lever mechanisms". Since September 1968 he began to work at Azerbaijan Technical University: assistant, senior lecturer of the Department "Theory mechanisms and machines, machine parts" (1968-1969); head of the Department "Textile and food machines" (1970-1978); Dean of Mechanical (1979-1987), Robot-technical (1987-1990) faculties; Vice-rector of the Azerbaijan Technical University (1991-1992); head of the Department "Theory of mechanisms and machines" (1993-2001 and 2015-2021). Currently, he is a consultant Professor at the Department" Mechatronics and machine design". Professor R. I. Alizade developed his research areas at Columbia University, USA (1973-1974), University of Florida, USA (1981), Beijing University of Aeronautics and Astronautics, China (1989-1990). The results of scientific research were implemented in the Association "Energy", Moscow (1983-1988). Continuing research and teaching in the field of robotics was carried out at the Department of "Mechanical engineering" of the Izmir Institute of Technology, Turkey (2002-2013). The problems of kinematic synthesis of function generation, path generation and body guidance of spatial mechanisms by using the theory of screws and approximation kinematic geometry are solved. The problems of modular and system approach of structural, kinematic analysis and synthesis of manipulators with linear and angular constraints are solved. Create parallel structure manipulators with variable values for the mobility of closed loops of robotic systems are created. Subsequent scientific research is reflected in the problems of developing new models of Rovers with guiding mechanisms of P. Chebyshev, as well as in the work of structural synthesis of six-legs Euclidean manipulators of a parallel structure for docking space aggregates. Currently, new robotic machines are being created using the technology of manual carpet weaving. The results of scientific research are reflected in 8 authors' certificates and more than 120 scientific articles. The majority

of scientific research is published in International impact journals (Thomson and Scopus), reflected in the proceedings of the World Congresses "Theory of Mechanisms and Machines" (IFToMM), as well as in the proceedings of International Symposiums "Science of Mechanisms and Machines" (AzC IFToMM - 2010, 2013, 2017 - Azerbaijan-Turkey). Professor R. I. Alizade is well known in the field of "Theory of Mechanisms and Machines" with his publications on scientific areas of robotics. Under his leadership, 10 researchers from Azerbaijan and Turkey defended their "PhD" dissertations in the field of "Theory of Mechanisms and Machines". He is a member of the editorial Board of the international journal (IFToMM) "Problems of mechanics", the Republican journals "Machine science" and "Professional education and human capital", a member of the Technical Committee for Linkages and Mechanical Control, of the International Federation for the development of science Theory of Mechanisms and Machines (TC IFToMM).

Professor Alizade R.I. starting from 2014 continues also his scientific and pedagogical activity at the National Aviation Academy as a professor at the Department of Flight equipment and aviation engines.

On behalf of the editorial board and the entire team of the international scientific and technical journal Machine Science, we congratulate Prof. Rasim Alizadeh, we wish him good health and success in his scientific activities!
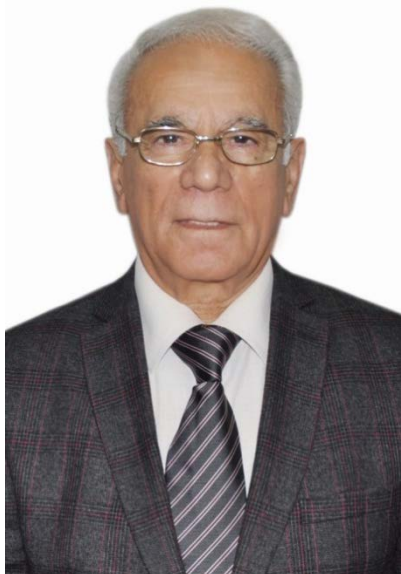
For the anniversary of prof., DSc (Technical) Vagif Movlazade!

Vagif Zahid Movlazade - Consultant-professor of department of "Machine Building Technology", doctor of technical sciences, Honored Engineer was born on November 7, 1941.

He graduated with honors diploma from the Azerbaijan Polytechnic Institute in 1963 and worked as a design engineer at the "Bakelektroshtamp" plant, then passed military service in 1963-1965, and continued his career as a junior researcher at the All-Union Petroleum Engineering Research Institute in 1965-1966. From 1966 he worked as an assistant, graduate student, senior teacher, associate professor at the departament of "Machine Building Technology" of the Azerbaijan Technical University (AzTU), from 1987 to November 18, 2016 he worked as the head of the department, and after that he became a consultant-professor of the department.

In 1977-1981 he was the head of department of "Engineering Graphics" of the Azerbaijan Polytechnic Institute, in 1981-1985 he was a professor at the Annaba University of the People's Democratic Republic of Algeria, in 1986-1990 he was the secretary of the party committee of AzTU, in 1992-1996 he served as Vice-Rector for Science and Technology.

In 1973 he defended his dissertation at the Kuibyshev Polytechnic Institute of Russia (now Samara State Technical University), in 1998 he defended his doctoral dissertation at AzTU on the specialty 05.02.08 - "Machine Building Technology". Under his supervision, 4 graduate students defended their dissertations. One of them is an Ethiopian citizen.

On 02.09.1988 by the decision of the Supreme Attestation Commission of the USSR he was awarded the title of associate professor of "Machine Building Technology", on 09.01.2004 by the decision of the Supreme Attestation Commission of the Republic of Azerbaijan he was awarded the title of professor of "Machine Building Technology".

He is the author of 2 textbooks, 14 teaching aids, 6 methodical instructions, 1 monograph, 5 inventions, 1 patent. His more than 180 scientific articles have been published in prestigious magazines in England, Germany, Algeria, Russia, Ukraine, Estonia and our republic.

In 1975, 1991, 1999, 2002 and 2006 he underwent internships through German Academic Exchange Service (DAAD) at the Technical Universities of Braunschweig, Dresden and the Freiberg Mountain Academy in Germany.

In 1999-2005 he was a member of the expert council of the Supreme Attestation Commission of the Republic of Azerbaijan. He was a member of the editorial board of the journal "Scientific works" of AzTU, Deputy Editor-in-Chief of the

international scientific-technical journal "Mechanics-Machine Building" of the Ministry of Education, Deputy Chairman of the Scientific-Methodical Commission "Machine Building - Metallurgy" of the Ministry of Education, D02.171 Specialized Dissertation Council, the Science and Education Commission.

In November 2011, by the decree of the President of the Republic of Azerbaijan, V.Z. Movlazade was awarded the honorary title of Honored Engineer.

Currently, V.Z. Movlazade is the chairman of the ED 2.32 Dissertation Council established under the AzTU by the order of the Supreme Attestation Commission under the President of the Republic of Azerbaijan No. F-33 dated February 3, 2020.

V.Z. Movlazade is the Deputy Chairman of the Council of Elders of AzTU, a member of the Public Council of AzTU, a member of the editorial board of the International Scientific and Technical Journal "Machine Science", a member of the Scientific Council of AzTU.

During his work at AzTU, V.Z. Movlazade paid special attention to the training of scientific and pedagogical staff at the department of "Machine Building Technology", created conditions for young researchers to work as interns at the department, helped to send them to various postgraduate studies in Russia. It is the result of his work that some of the employees of the department of "Machine Building Technology" are scientists who have worked in scientific centers in Germany and Russia.

Prof. Vagif Zahid oglu Movlazade will be 80 years old on November 7, 2021. We congratulate him on his 80th anniversary, thank him for his fruitful work in the field of education, wish him good health, good life in his family and success in his future career as a consultant-professor at AzTU.

On behalf of the editorial board and the entire team of the international scientific and technical journal Machine Science, we congratulate Prof. Vagif Movlazade, we wish him good health and success in his scientific activities!

FREE VIBRATION ANALYSIS OF THE SANDWICH COMPLETE CONICAL SHELL WITH FUNCTIONALLY GRADED MATERIALS FACINGS

Abdullah SOFIYEV

Department of Civil Engineering of Engineering Faculty,
Suleyman Demirel University, 32260, Isparta, Turkey

E-mail: abdullahavey@sdu.edu.tr

Abstract: The free vibration analysis of the sandwich complete conical shell with functionally graded materials (FGMs) facings based on the classical shell theory (CST) is studied. The basic equations of metal-rich truncated conical shells with FGMs facings are derived and solved by employing Galerkin method. The closed form solution for dimensionless frequency parameters of the sandwich complete conical shell with FGM facings is found. The effects of kinds of FGM facings and variation of thickness of facings on the magnitudes of dimensionless frequency parameters are studied in numerical analysis part.

Keywords: *Functionally graded materials, FGM facings, sandwich complete conical shell, metal-rich core, free vibration, frequency parameters*

Introduction. Aircraft, space vehicles, satellites and sensitive technologies, such as nuclear reactors, innovative high-performance carrier component design have always been at the forefront. Efforts to develop a new generation of composite materials in the form of coating or basic material, makes it possible to create new sandwich structures and makes it more popular. Such structures, good thermal and acoustic insulation, to reduce some resistance, light weight and long service life, high strength and hardness, both features, and also be easy to produce [1, 2].

One of the main drawbacks of conventional sandwich constructions is that delamination occurs due to strong stress concentration on the surfaces between the layers. For this reason, the designer needs to systematically expand the class of materials in order to select the best materials for the sandwich construction elements. In recent years, functional graded materials (FGMs) produced due to its wide range of applications belong to the new generation of composite materials [3-6]. Smooth and continuous change of FGM properties from one surface to another reduces stress concentration in layered composites and contributes to avoid interface problems. One of first studies on the design, vibration and stability of sandwich plates and shells with FDM layer is presented in the source [7, 8]. Following these studies, stability and vibration problems of sandwich construction elements are solved using different theories [9-14]. In this study, the closed-form solution is found for the dimensionless frequency of the FGM coated sandwich complete conical shells and the aforementioned drawbacks can be slightly overcome in the literature.

Basic relations. Figure 1a shows a sandwich truncated conical shell with a metal core and FGM coatings. This sandwich-truncated conical shell is transformed into a complete sandwich-conical shell (Figure 1b). A sandwich conical shell with

FGM coatings and enriched metal cores are formed in a triple system. The $OS\zeta\theta$ coordinate system is considered at the top of the complete cone and on the reference surface of the three-layer system. The axes and some sandwich conical shell parameters are explained on the figure (Fig. 1a). Length of complete and truncated conical shells are S_2 and L, the radii of small large bases are R_1 and R_2, respectively. The total thickness of sandwich conical shells are $h = 2h_{fg} + h_m$ in which h_m is thickness of metal core and h_{fg} is the thickness of FGM coatings (Fig. 1c).
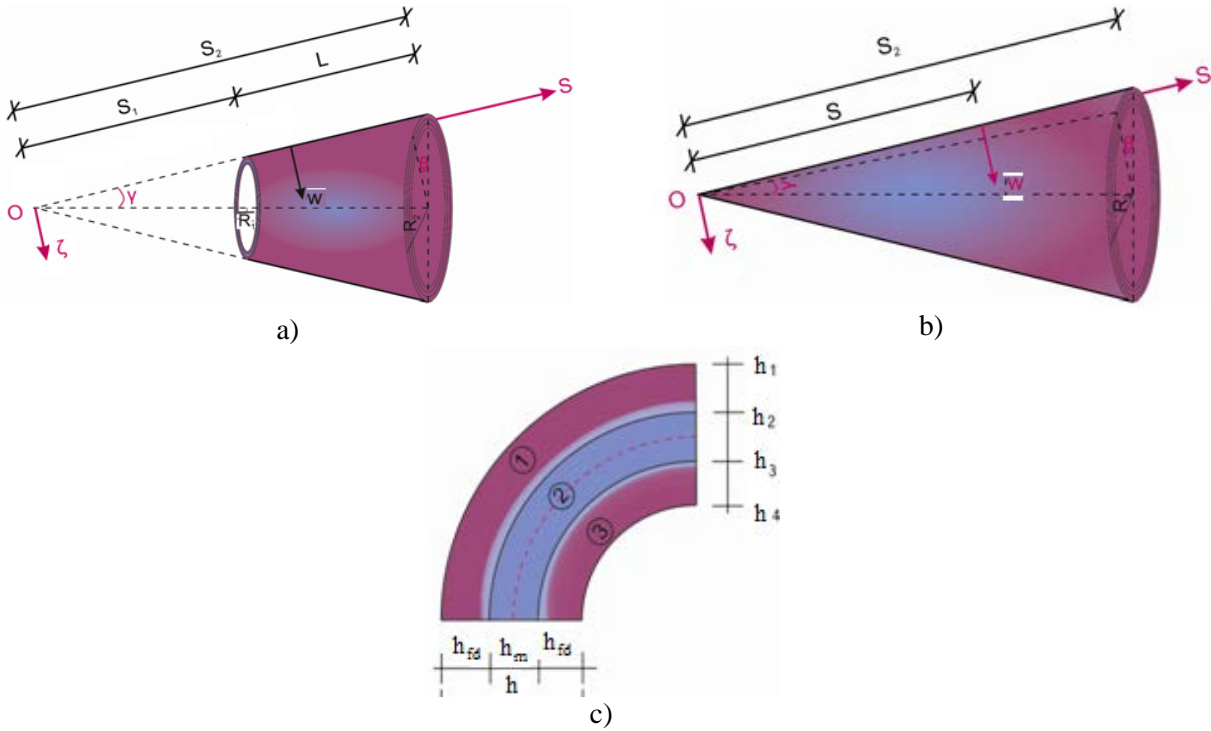
Figure 1. a) Coordinate system in the FGM sandwich truncated and b) complete conical shells, c) arrangement of layers; (1) FGM, (2) enriched metal, (3) FCM

The volume fractions of the materials in the layers of FGM coated sandwich conical shells are expressed as [11]:

$$V^{(1)} = (2\overline{\zeta} + 1)/(2\zeta_2 + 1), \quad 1.layer$$

$$V^{(2)} = 1 \qquad 1, \qquad\qquad 2.layer \qquad\qquad (1)$$

$$V^{(3)} = (2\overline{\zeta} - 1)/(2\zeta_3 - 1), \quad 3.\,layer$$

The mathematical models of the material properties of FGM coated sandwich conical shells are expressed as [11]:

$$E_{fd}^{(1)} = E_c e^{V^{(1)}\ln(E_m/E_{cs})}, \quad \nu_{fd}^{(1)} = \nu_c e^{V^{(1)}\ln(\nu_m/\nu_c)}, \quad \rho_{fd}^{(1)} = \rho_c e^{V^{(1)}\ln(\rho_m/\rho_c)}$$

$$(2)$$

$$E_{fd}^{(3)} = E_c e^{V^{(3)}\ln(E_m/E_c)}, \quad \nu_{fd}^{(3)} = \nu_c e^{V^{(3)}\ln(\nu_m/\nu_c)}, \quad \rho_{fd}^{(3)} = \rho_c e^{V^{(3)}\ln(\rho_m/\rho_c)}$$

where $E_{\mathrm{m}}, v_m, \rho_m$ and $E_{\mathrm{c}}, v_c, \rho_c$ are the Young's moduli, Poisson's ratios and densities of the metal and ceramic surfaces of the FGM coatings in the sandwich conical shells, respectively.

$$
\left[E_{sand}, v_{sand}\right] = \begin{cases} E_{fd}^{(1)}, v_{fd}^{(1)}, \ \rho_{fd}^{(1)} & -h_1 \le \zeta \le -h_2 \\[2mm] E_m, v_m, \ \rho_m & -h_2 < \zeta < h_3 \\[2mm] E_{fd}^{(3)}, v_{fd}^{(3)}, \ \rho_{fd}^{(3)} & h_3 \le \zeta \le h_4 \end{cases} \tag{3}
$$

Basic Equations. The force and moment components are defined as [7-12]:

$$
\left(T_{ij}, M_{ij}\right) = \sum_{k=1}^{3} \int_{h_k}^{h_{k+1}} \left[1, \zeta\right] \sigma_{ij}^{(k)} \, \mathrm{d}\zeta \quad (i, j = 1,2) \tag{4}
$$

where T_{ij} and $M_{\mathrm{ij}} (i = 1,2)$ are force and moment components, $\sigma_{ij}^{(k)} (i = 1,2; j = 2,3)$ are stresses on the layers of the sandwich conical shells with FGM coatings and $k = 1,2,3$ denotes number of layers.

The relations between the stress-deformation components of the FGM-coated sandwich conical shells can be written as:

$$
\begin{bmatrix} \sigma_{11}^{(k)} \\[3mm] \sigma_{22}^{(k)} \\[3mm] \sigma_{12}^{(k)} \end{bmatrix} = \begin{bmatrix} Q_{11}^{(k)} & Q_{12}^{(k)} & 0 \\[3mm] Q_{12}^{(k)} & Q_{11}^{(k)} & 0 \\[3mm] 0 & 0 & Q_{66}^{(k)} \end{bmatrix} \begin{bmatrix} \varepsilon_{11} \\[3mm] \varepsilon_{22} \\[3mm] \varepsilon_{12} \end{bmatrix} \tag{5}
$$

where $Q_{ij}^{(k)}, (i, j = 1,2,...,6; k = 1,2,3)$, are the coefficients in the layers that contain the quantities depending on the material properties [11-14].

The relations between the force components and the Airy function are as follows [6, 12-14]:

$$
T_{11} = h \frac{\partial^2 \Psi}{\partial y^2}, T_{22} = h \frac{\partial^2 \Psi}{\partial x^2}, T_{12} = -h \frac{\partial^2 \Psi}{\partial x \partial y} \tag{6}
$$

Substituting the relations (5) into integrals (4), then resulting equations with the relations (6), in motion and compatibility equations, after some mathematical operations we obtain the motion and compatibility equations for FGM sandwich truncated conical shells as

$$
\begin{bmatrix} L_{11} & L_{12} \\[3mm] L_{21} & L_{22} \end{bmatrix} \begin{bmatrix} \Psi \\[3mm] w \end{bmatrix} = 0 \tag{7}
$$

The contents of the above differential operators are explained as:

$$L_{11} = C_{02}e^{-4x}\left(\frac{\partial^4}{\partial x^4} - 4\frac{\partial^3}{\partial x^3} + 4\frac{\partial^2}{\partial x^2} + \frac{\partial^4}{\partial \varphi^4} + 2\frac{\partial^2}{\partial \varphi^2}\right)$$

$$+ (2C_{01} - C_{05})e^{-4x}\left(\frac{\partial^4}{\partial x^2 \partial \varphi^2} - 2\frac{\partial^3}{\partial x \partial \varphi^2} + \frac{\partial^2}{\partial \varphi^2}\right) + S_2 e^{-3x}\left(\frac{\partial^2}{\partial x^2} - \frac{\partial}{\partial x}\right)\cot\gamma$$

$$L_{12} = -C_{03}e^{-4x}\left(\frac{\partial^4}{\partial \varphi^4} + 2\frac{\partial^2}{\partial \varphi^2} + \frac{\partial^4}{\partial x^4} - 4\frac{\partial^3}{\partial x^3} + 4\frac{\partial^2}{\partial x^2}\right)$$

$$- (2C_{04} + C_{06})e^{-4x}\left(\frac{\partial^4}{\partial x^2 \partial \varphi^2} + 2\frac{\partial^3}{\partial x \partial \varphi^2} - \frac{\partial^2}{\partial \varphi^2}\right) - \rho_t S_2^4 \frac{\partial^2}{\partial t^2}$$

$$\left.\vphantom{\begin{array}{c}1\\1\\1\\1\\1\\1\\1\\1\\1\\1\\1\end{array}}\right\} (8)$$

$$L_{21} = B_{01}e^{-4x}\left(\frac{\partial^4}{\partial x^4} - 4\frac{\partial^3}{\partial x^3} + 4\frac{\partial^2}{\partial x^2} + \frac{\partial^4}{\partial \theta_1^4} + 2\frac{\partial^2}{\partial \varphi^2}\right)$$

$$+ (2B_{02} + B_{05})e^{-4x}\left(\frac{\partial^4}{\partial x^2 \partial \varphi^2} - 2\frac{\partial^3}{\partial x \partial \varphi^2} + \frac{\partial^2}{\partial \varphi^2}\right)$$

$$L_{21} = -B_{04}e^{-4x}\left(\frac{\partial^4}{\partial \varphi^4} + 2\frac{\partial^2}{\partial \varphi^2} + \frac{\partial^4}{\partial x^4} - 4\frac{\partial^3}{\partial x^3} + 4\frac{\partial^2}{\partial x^2}\right)$$

$$+ (B_{06} - 2B_{03})e^{-4x}\left(\frac{\partial^4}{\partial x^2 \partial \varphi^2} - 2\frac{\partial^3}{\partial x \partial \varphi^2} + \frac{\partial^2}{\partial \varphi^2}\right) + S_2 e^{-3x}\cot\gamma\left(\frac{\partial^2}{\partial x^2} - \frac{\partial}{\partial x}\right)$$

where $\phi = \theta \sin\gamma$ and $x = \ln(S/S_2)$ the new variable that used to facilitate the integration process and $C_{0i}, B_{0i} (i = 1,2,...,6)$, are parameters depending on the material properties of FGM sandwich conical shells [11].

Solution of Basic Equations. Since the FGM sandwich conical shell is the simply supported, the solution of the Eq. (7) is searched as follows [11, 12]:

$$\Psi(x,\theta,t) = \overline{\Psi}(t)S_2\, e^{(\lambda+1)x}\sin(m_1 x)\cos(m_2\phi), \quad w(x,\theta,t) = \overline{w}(t)e^{\lambda x}\sin(m_1 x)\cos(m_2\phi) \tag{9}$$

where $\overline{\Psi}(t)$ and $\overline{w}(t)$ time dependent functions and λ is a parameter which defined from minimum conditions of the frequency and it takes the value 2.4. In addition, $m_1 = \dfrac{m\pi}{x_0}, m_2 = \dfrac{n}{\sin\gamma}, x_0 = \ln\dfrac{S_2}{S_1}$ in which m is the meridional wave number and n is the circumferential wave number.

Substituting (9) into set of the Eq. (7) and taken into account $S_1 \to 0$, then applying Galerkin's method, after some mathematical operations we obtain the expression for he dimensionless frequency :

$$\omega_1 = \frac{S_2}{h}\sqrt{\frac{\Lambda_1 + \Lambda_2}{\Lambda_3 \Lambda_\rho}\frac{\rho_c}{E_c}} \tag{10}$$

where the following definitions apply:

$$\Lambda_1 = \Big[C_{02} \big(A_1 - 4A_2 + 4A_3 + m_2^4 A_5 - 2m_2^2 A_8 \big) + (2C_{01} - C_{05}) m_2^2 \big(2A_4 - A_3 - A_5 \big) + \big(A_{01} - A_{00} \big) S_2 \cot \gamma \Big] \times$$

$$\times [B_{03} \big(4B_{14} - m_2^4 B_9 + 2m_2^2 B_{12} - B_{13} - 4B_{15} \big) - (B_{06} - 2B_{03}) m_2^2 \big(B_{10} + 2B_{11} \big) + B_{00} S_2 \cot \gamma];$$

$$\Lambda_2 = \Big[C_{03} m \big(\beta_2^4 A_9 - 2m_2^2 A_{12} + A_{13} - 4A_{14} + 4A_{15} \big) + (2C_{04} + C_{06}) m_2^2 \big(2A_{11} - A_{10} - A_9 \big) \Big]$$

$$\times \Big[B_{01} \big(m_2^4 B_1 - 2m_2^2 B_4 + B_5 - 4B_6 + 4B_7 \big) - (2B_{02} + B_{05}) m_2^2 \big(B_2 + 2B_3 - B_4 \big) \Big];$$

$$\Lambda_3 = B_{01} \big(m_2^4 B_1 - 2m_2^2 B_4 + B_5 - 4B_6 + 4B_7 \big) - (2B_{02} + B_{05}) m_2^2 \big(B_2 + 2B_3 - B_4 \big);$$

$$\Lambda_\rho = 2\theta_{2\lambda+2} \rho_t S_2^4, \quad \theta_{2\lambda+i} = \frac{m_1^2}{\big[(2\lambda+i)^2 + 4m_1^2 \big] (2\lambda+i)}; \quad i = -2; \ -1; \ 0; \ 1; \ 2$$

(11)

In order to find the minimum values of the dimensionless frequency parameter of the FGM sandwich complete conical shells, the expression (10) is minimized according to the number of wave, n.

Results and discussion. In this section, the minimum values of the dimensionless frequency parameters of FGM sandwich complete conical shells are found numerically and the results obtained are analyzed. As the FGM facings, a mixture of SUS304/Si$_3$N$_4$, i.e., stainless steel and silicon nitrate, which is a metal-ceramic mixture, is used. The material properties of FGM facings are taken from Ref. [6]. Sandwich complete conical shells with FGM, ceramic and metal coatings are used and three types of sandwich cones are designed as follows: FMF, CMC and MMM.

In Table 1, the variation of the values of ω_1 for three types of FMF, CMC and MMM sandwich complete conical shells versus half-peak angle, γ, is presented. In Table 1, the geometric dimensions of the sandwich complete conical shells are as follows: $h_{core}/h_{coat} = 4$, $R_2/h = 25$ and $\lambda = 2.4$. Also, the values in parentheses indicate the number of circumferential wave number (n).

As can be seen in Table 1, the values of ω_1 decrease considerably in all three types of sandwich complete conical shells due to the increase of half-peak angle, γ, while the number of circumferential waves increases. When the values of the ω_1 for the FMF sandwich complete conical shell are compared with the values of CMC and MMM cones, the effects of FGM coatings are (-11%) and 29%, respectively, and approximately independent of the change of the half-peak angle, γ.

Table 1. Variation of the values of ω_1 for FMF, CMC and MMM complete conical shells versus the γ.

			ω_1		
γ	15°	30°	45°	60°	75°
FMF	44.061(2)	23.618(3)	13.643(3)	9.494(3)	6.790(3)
CMC	49.409(2)	26.578(3)	15.299(3)	10.640(3)	7.634(3)
MMM	38.200(2)	20.324(3)	11.826(3)	8.242(3)	5.854(3)

Fig. 2 presents the distribution of the values of ω_1 for three types (FMF, CMC and MMM) sandwich complete conical shells depending on the ratio of the coating thickness (h_{core}/h_{coat}) to the core thickness. The geometric dimensions of the sandwich complete conical shells are as follows: $R_2/h = 25$, $\gamma = 30^o$ and $\lambda = 2.4$.
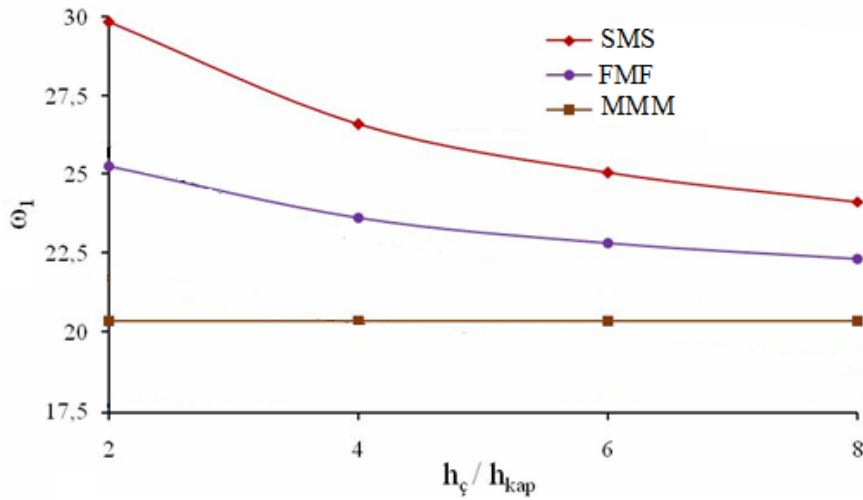
Figure 2. *Variations of the values of ω_1 for FMF, CMC and MMM sandwich complete conical shells versus the h_{core}/h_{coat}*

As shown in Figure 2, the values of ω_1 for FMF and CMC sandwich conical shells decrease when the ratio, h_{core}/h_{coat}, increases. When the values of ω_1 for FMF and CMC sandwich conical shells were compared, it was found that the effect of FMF coating profile on the values of ω_1 decreased significantly (- 15.4%) for $h_{core}/h_{coat} = 2$, even though it was approximately (-8%) for $h_{core}/h_{coat} = 8$. Thus, the effect of the FGM coatings on the values of ω_1 is reduced by the increase of the ratio, h_{core}/h_{coat}. When the values of the dimensionless frequency parameter of FMF sandwich conical shells were compared with the values of the MMM complete conical shell, the effect of FGM coatings was 23.61% for $h_{core}/h_{coat} = 2$, whereas this effect was reduced to 9%, when $h_{core}/h_{coat} = 8$. When the dimensionless frequency parameter values of CMC sandwich complete conical shells were compared to the values of the MMM complete conical shell, the effect of metal and ceramic coatings was 46% for $h_{core}/h_{coat} = 2$, while this effect was found to be 18.5%, when $h_{core}/h_{coat} = 8$.

Conclusions. The free vibration analysis of the sandwich complete conical shell with FGMs facings based on the CST is studied. The basic equations of metal-

rich truncated conical shells with FGMs facings are derived on the basis of CST and solved by employing Galerkin method. The closed form solution for dimensionless frequency parameters of the sandwich complete conical shell with FGM facings is found. The effects of kinds of FGM facings and variation of thickness of facings on the magnitudes of dimensionless frequency parameters are studied in numerical analysis part.

REFERENCES:

[1] Vinson, J.R. *Sandwich structures*. Applied Mechanics Reviews, 54:201–214, (2001).

[2] Librescu, L., Hause, T. *Recent developments in the modeling and behavior of advanced sandwich constructions: a survey*. Composite Structures, 48:1–17, (2000).

[3] Koizumi, M., *FGM activities in Japan*. Composites Part B: Engineering, 28:1–4, (1997).

[4] Ichikawa, K. *Functionally Graded Materials in the 21st Century*. A Workshop on Trends and Forecasts, Kluwer Academic Publisher, Boston, (2001).

[5] Müller, E., Drašar, C., Schilz, J., Kaysser, W.A. *Functionally graded materials for sensor and energy applications*. Materials Sciences Engineering A, 362:17–39, (2003).

[6] Shen, H.S. *Functionally Graded Materials, Nonlinear Analysis of Plates and Shells,* Florida, CRC Press, (2009).

[7] Zenkour, A.M. *A comprehensive analysis of functionally graded sandwich plates: Part 2. Buckling and free vibration*. International Journal Solids and Structures, 42:5243–5258, (2005).

[8] Sofiyev, A.H., Deniz, A., Akcay, I.H., Yusufoglu, E. *The vibration and stability of a three-layered conical shell containing a FGM layer subjected to axial compressive load*. Acta Mechanica, 183:129-144, (2006).

[9] Sobhy, M. *An accurate shear deformation theory for vibration and buckling of FGM sandwich plates in hygrothermal environment*. International Journal of Mechanical Sciences, 110:62-77, (2016).

[10] Sofiyev, A.H. *The vibration and buckling of sandwich cylindrical shells covered by different coatings subjected to the hydrostatic pressure*. Composite Structures, 117: 124–134, (2014).

[11] Sofiyev, A.H. Osmancelebioglu, E. *The free vibration of sandwich truncated conical shells containing functionally graded layers within the shear deformation theory*. Composites Part B: Engineering, 120:197-211, (2017).

[12] Sofiyev, A.H., Kuruoglu, N. *On the vibration analysis of FGM truncated and complete conical shells under various boundary conditions and resting on elastic foundations*. Journal of Engineering Mathematics, 77:131-145, (2012).

[13] Sofiyev, A.H. *Application of the FOSDT to the solution of buckling problem of FGM sandwich conical shells under hydrostatic pressure*. Composites Part B: Engineering 144:56-66, (2018).

[14] Sofiyev, A.H., Turan, F. *On the nonlinear vibration of heterogenous orthotropic shallow shells in the framework of the shear deformation shell theory*. Thin–Walled Structures, 161, 107181, (2021).

STRUCTURAL SYNTHESIS OF ROBOT MANIPULATORS BY USING SCREW WITH VARIABLE PITCH

Rasim ALIZADE

Department of "Mechatronic and machine design", Azerbaijan Technical University, Baku, Azerbaijan

Email: alizada_rasim@hotmail.com

Abstract: This paper focuses on the systematic type synthesis of parallel robot manipulators by using new structural formulas based on the screw theory. New structural formulas as a total number of screw in kinematic pairs ($\$$), number of screws with variable pitch ($\tilde{\$}$), total number of screws that represent the contact geometry of lower and higher joint elements (t), mobility equation for robot manipulators (M), dimension of the closed loop (λ), motion of end effector of parallel manipulator (m), number degree of freedom of kinematic pairs (f), refers to find the kinematic structure of robot manipulators realizing a specified motion requirement. Twenty kinematic pairs with structural parameters $\left(\$, \tilde{\$}, f, t\right)$ are introduced. History of six structural formulas using for structural synthesis of parallel robot manipulators from space and different subspaces are presented as a table with equations, authors, years and some commentaries. The structural synthesis approach is based on the elementary notions of screw theory. Using the proposed of structural formulas approach, families of platform manipulators are constructed from a set of structural units. This paper is appropriate for engineers with interest in robotics, rovers, space docking parallel manipulators and screw theory.

Keywords: Kinematic pair screws; Motion of end effector; Screws with variable pitch; Dimension of closed loop.

Introduction. Structural synthesis of robot manipulators is the fundamental concept in robot design. The mobility of robotic mechanical system indicates the number of independent input parameters to solve the configuration of robots. If mobility of the kinematic chain is equal to zero ($M = 0$) and can not be split into several structural groups, we will get a simple structural group. Combining the simple platform (with $n \geq 2$ kinematic pairs) type structural groups with given actuators, we can get parallel platform type robot manipulators needed to define the location (position and orientation) of end effectors. Serial platform manipulators control the motion of the platform, which are connected each others by hinges, branches, legs and other kinematic chains going from the platforms toward the frame. Complex robot manipulators consist of independent branches and legs loops with variable general constraints $\{\lambda_k\}_2^6$. Many platform type robot manipulators use legs with variable general constraints. Therefore structural formulas are used by engineers for design the parallel and serial platform Euclidean robot manipulators with variable general constraints. Structural synthesis of parallel Cartesian platform robot manipulators consists from connecting the simple structural groups constructed in the orthogonal planes to actuators and moving platform.

The history of formulas for structural analysis and synthesis of mechanisms and robotic mechanical systems during the second half of the 19th century, the first and second half of the 20th century and the beginning of 21st century had been

investigated and illustrated in the Table by 38 equations, authors, years and commentaries in the fundamental investigations [1] and in a critical review [2]. Several investigations are described a systematic approach of structural synthesis and analysis of mechanisms by using screw theory. First investigation was given by Mueller [3] , where in equations for simple structural group and for kinematic chains were used the number of screw in kinematic pairs. Voinea and Atanasiu [4] and Waldron [5] introduced mobility equation of mechanisms with rank parameter equivalent to screw system of the closed loops. The scientific investigations of structural synthesis and analysis of robot manipulators by using screw theory were more dedicated in the beginning of 21st century. Huang and Li [6] proposed a type synthesis of parallel manipulators with mobility $\{M_i\}_3^5$ by using screw theory. Fang and Tsai [7] developed a problem of structural synthesis and analysis by applying screw theory. They enumerated limb structures for parallel manipulators according to reciprocity of limb twist system and wrench system. Jin et.al. [8] are proposed the structural synthesis and analysis of parallel manipulators by using screw algebra. The design of parallel manipulators based on Plücker coordinates is examined by Gao et.al. [9]. An analytical method of using equivalent screw groups for structural synthesis of over constrained parallel manipulators is described in the study of Zhoo et.al. [10]. Kong and Gosselin [11 − 14] proposed a new way for the type synthesis of parallel manipulators with different type of end effector motions by using screw theory and virtual chain approach.

History of formulas for structural synthesis and analysis of robot manipulators given by author at.al. are presented as 6 several equations (formulas 1-6 in Table 1) with the unique key controlling parameters. In investigation [15] the mobility number, λ, is a characteristic of an independent loop of robot manipulator. In Table 1 (formulas ♯ 1) we have been considered mobility equation which contain mixed independent loops with variable general constraint. The history of new formula [16] about the number of independent loops was done in Table 1(formulas ♯ 2). The number of independent loops in platform manipulators is described by the number of mobile platforms (B), the total number of joints on the mobile platforms (j_b) and the total number of branches between mobile platforms (c_b). In the paper [17] and in the Table 1.1 (formulas ♯ 3) the number of independent loops is described as $L = C − B$, where $C = c_l + c_b$ is sum of legs and branches. A classification of parallel manipulators based on the number of mobile platforms, number of joints on the mobile platforms, number of legs and branches, and types of kinematic pairs are also presented. A new structural formulas for robots (formulas ♯ 4 in the Table 1), working in Cartesian space, having three legs in orthogonal planes, introducing simple structural groups in space $\lambda = 6$ and in subspaces $\{\lambda\}_3^5$, and connected to actuators and to the end effector are introduced. Simple serial platform type structural groups in $\lambda = 3$ and $\lambda = 6$ are presented also in [1]. In the study [18] new structural formulas (formulas ♯ 5 $in\ the\ Table$1) for parallel and serial platform Euclidean robot manipulators with variable general constraints of branch loops and legs were presented. Selecting the legs of the robot manipulators as moving dyads on Euclidean

planes the direct and inverse task will become easier to solve. The new proposed Euclidean manipulators have several legs, which create Euclidean motions on their own Euclidean planes.

Table 1. Structural formulas for synthesis and analysis of robot manipulators.

№	Equations	Authors	Commentary
1	2	3	4
1.	1. $M = \sum_{i=1}^{j} f_i - \sum_{k=1}^{L} \lambda_k$ 2. $M = \sum_{i=1}^{j} f_i - \lambda L$ 3. $d = 6 - \lambda$ $\{d\}_0^4$ – general constraint for motion of rigid body in space; L – the number of independent loops; λ – the loop motion parameters; f_i – the DoF of kinematic pairs; j – the number of joints.	F. Freudenstain and R.I. Alizade [15] 1975	1. Mobility equation for mechanisms which contain mixed independent loops with variable general constraint. 2. Mobility equation of mechanisms with the same number of independent, scalar loop closure equations in each independent loop. M is the mobility of mechanisms. λ_k is the dimension of the active motion space.
2.	1. $L = j_b - B - C_B$ 2. $M = \sum_{i=1}^{j} f_i - \lambda(j_B - B - C_B) + q - j_p$ 3. $\sum_{i=1}^{j} f_i = \lambda(j_B - B - C_b)$ B – the number of mobile platforms; j_B – the total number of joints on the mobile platforms; C_b – the total number of branches between mobile platforms.	R.I. Alizade [16] 1988	1. L is the number of independent loops. 2. M is mobility of mechanisms and platform manipulators. 3. Equation for simple structural groups $\{\lambda\}_2^6$, q is excessive over closing constraints, j_p is number of passive DoF in kinematic pairs.
3.	1. $L = C - B$ 2. $M = \sum_{i=1}^{j} f_i - \lambda(C - B)$ 3. $\sum_{i=1}^{j} f_i = \lambda(C - B)$ $C = C_l + C_b$, parameter C is the sum of legs and branches. $C_l = j_B - 2C_b$ C_l – the total number of legs.	R.I. Alizade and C. Bayram [17] 2003	1. New formula for the number of independent loops. 2. Mobility equation of platform robot manipulators. 3. Equation for simple structural groups.
4.	1. $M = (B - C)\lambda + \sum_{i=1}^{j} f_i + q - j_p$ 2. $M = (\lambda + 3) + \sum_{l=1}^{C_l} (d_l - D)$ $\qquad + \sum_{l=1}^{C_l} (f_l - \lambda_l) + q - j_p$ $C = C_l + C_b + C_h$	R.I. Alizade, C. Bayram and E. Gezgin [1] 2007	1. Mobility equation for robotic systems. 2. A structural formula of mobility loop–legs equation for parallel Cartesian platform manipulators. d is the constraint parameter of independent loop. D is the number of dimensions of vectors in

	C_h – the number of hinges; $\lambda = 6 - d$; λ – the number of independent location parameters of rigid body in the independent loop; d_l – the number of dimensions of vectors in subspaces of legs. f_l – DoF of the kinetic pairs on the leg.		Cartesian space.
5.	1. $M = \lambda + j_h + \sum_{L=1}^{n}(f_L - \lambda_L)$ $+ \sum_{l=1}^{c_l}(f_l - \lambda_l) + q - j_p$ 2. $m = \lambda + c_l + j_h + \sum_{l=1}^{c_l}(d_l - D) + \sum_{L=1}^{n}(f_L - \lambda_L)$ j_h – the number of hinges between platforms; f_L – DoF of kinematic pair on the branch-loop. λ_L – the motion of rigid body in branch-loop.	Rasim Alizade, Fatih Cemal Can, Erkin Gezgin [18] 2008	1. The general structural formula of serial-parallel Euclidean robot manipulators with variable general constraints. 2. The general formula for motion of platforms. D – dimensions of vectors ($D = 3$ for space R^3, $d = 2$ for plane R^2)
6.	1. $\$ = f - \tilde{\$} + t$ 2. $M = \sum_{f=1}^{\lambda-1} fP_f - \sum_{k=1}^{L} \lambda_k + q$ 3. $M = \sum_{f=1}^{\lambda-1} fP_f - \lambda(C - B) + q$ 4. $M = \lambda + \sum_{l=1}^{c_l}\left(\sum_{f=1}^{\lambda-1} fP_f - \lambda_l\right)$ $+ \sum_{b=1}^{L_b}\left(\sum_{f=1}^{\lambda-1} fP_f - \lambda_b\right) + j_h$ 5. $m = \lambda + c_l + j_h + \sum_{l=1}^{c_l}(d_l - D)$ $+ \sum_{b=1}^{L_b}\left(\sum_{f=1}^{\lambda-1} fP_f - \lambda_b\right)$ 6. $M = \lambda + \left(\sum_{f=1}^{\lambda-1} fP_f - \lambda_l\right)c_l + \sum_{f=1}^{\lambda-1}(fP_f - \lambda_b)L_b$ $+ j_h$ 7. $m = \lambda + c_l + j_h + (d_l - D)c_l$ $+ \left(\sum_{f=1}^{\lambda-1} fP_f - \lambda_b\right)L_b$ t – represents the number of screws that describe the contact geometry of joint elements. $t = 2$ – contact elements on surface; $t = 3$ – contact elements on line; $t = 4$ – contact elements on points;	Rasim Alizade 2017	1. Total screws in kinematic pair. 2. Mobility equation for robot manipulators with variable loop motion parameters. 3. Mobility equation with the same dimension in each independent loop. 4. Structural formula for Euclidean platform type robot manipulators with variable general constraints. 5. Structural formula that describe the motions of end effector on the parallel robot manipulators. 6. Mobility equation for Euclidean manipulators with constant general constraint. 7. Motion of end effector of Euclidean manipulator with constant general constraint.

The motion of the platform is defined by three independent curves of three

platform points moving on three Euclidean reference planes. The general formula for motion of platforms is given also. To create new robot manipulators, simple platform structural groups with variable general constraints were considered.

This study enunciates screw system with variable pitch for the prismatic and cylindrical joints. Applying concepts the number of independent screw, number of screw with variable pitch, number of screws and motions for lower and higher kinematic pairs (Table 1.6.1) become possible to provide the structural characteristics of 20 kinematic pairs (Table 2). Two new general mobility equations for robot manipulator with mixed and the same dimension of closed loop are presented in the work (Table1.6.2 and 1.6.3).

Applying above mobility equations for structural synthesis problem the new wheeled robot that are called as "Rover" had been designed. This rover consists from moving platform and two suspensions with six wheels connected to the platform. Each suspension consist from paired two Chebyshev lambda mechanisms called bogie and one dyad called rocker. Two parallel suspensions are connected by a differential gear mechanism (Fig.2).

The problem of structural synthesis of parallel wheeled rover was solved by using structural formulas 3 and 5 from Table 1.6. In current study, new structural formulas are introduced for parallel Euclidean plaform robot manipulators (Table1.6) with variable and fixed general constraints. Structural synthesis task of four new design Eucilidean docking parallel manipulators with three, four, five and six legs were solved for spacecraft (Table 3). Furthermore, new 6DoF Euclidean docking manipulators of Spacecraft and their structural classification with the same general constraints of each legs are presented. Also, in the Table 3 were depicted the structural parameters, kinematic structures, motion of platform, number of legs and 3D drawing of new docking parallel manipulator of Spacecraft. It is clear that the 6DoF Euclidean parallel manipulator with different number of legs will better generate the given position and orientation of moving platform.

Introduction to screw with variable pitch. The structural and kinematic analysis and synthesis problem have been studying with the goal of identified new methods for composing robot manipulators capable of performing various prescribed positions and orientations of the end effectors. Screw with variable pitch can represent the prismatic joint, P, with the variable pitch parameter $\mu_P = \infty$, and also the cylindrical joint $C(RP)$ with variable pitch $\mu_C = (\infty; 0)$ that describe a rotation motion ($\mu_R = 0$) and translation motion $\mu_P = \infty$.

As shown in Fig. 1, the location of a rigid body (RB) of the cylindrical joint can be described by the three parameters for position (x, y, z) and three independent parameters (d, α, θ) for orientation. Let coordinate system A and was then translated parallel to the point B_1 (Fig. 1a). The position of point B_1 is described by vector $\bar{r}(x, y, z)$. Next, the system B_2 that is initially aligned with system B_1 is rotated by the twist angle α about the x_{B_1} axis. Following this the coordinate system B_2 of rigid body is translated along the z_{B_2} axis by a distance d. Lastly the coordinate system B

that was firstly aligned with the system B_2 is rotated by the angle θ around z_B, so we will get orientation of the coordinate system $Bx_B y_B z_B$.

Transformation of one coordinate system B to a reference coordinate system A correspond to the transformation of screw $\$$, when the relative position and orientation of the pair of screws are known (Fig. 1a). By using homogeneous coordinates the transformation of the system will be represented by 4×4 matrix as:

$$
{}_B^A T = \begin{bmatrix} 1 & 0 & 0 & x \\ 0 & 1 & 0 & y \\ 0 & 0 & 1 & z \\ 0 & 0 & 0 & 1 \end{bmatrix} \begin{bmatrix} 1 & 0 & 0 & 0 \\ 0 & c\alpha & -s\alpha & 0 \\ 0 & s\alpha & c\alpha & 0 \\ 0 & 0 & 0 & 1 \end{bmatrix} \begin{bmatrix} 1 & 0 & 0 & 0 \\ 0 & 1 & 0 & 0 \\ 0 & 0 & 1 & \tilde{d} \\ 0 & 0 & 0 & 1 \end{bmatrix} \begin{bmatrix} c\tilde{\theta} & -s\tilde{\theta} & 0 & 0 \\ s\tilde{\theta} & c\tilde{\theta} & 0 & 0 \\ 0 & 0 & 1 & 0 \\ 0 & 0 & 0 & 1 \end{bmatrix} =
$$

$$
= \begin{bmatrix} c\tilde{\theta} & -s\tilde{\theta} & 0 & x \\ s\tilde{\theta}c\alpha & c\tilde{\theta}c\alpha & -s\alpha & y - \tilde{d}s\alpha \\ s\tilde{\theta}s\alpha & 0 & c\alpha & z + \tilde{d}c\alpha \\ 0 & 0 & 0 & 1 \end{bmatrix} \tag{1}
$$

where: $S\theta$ and $C\theta$ represent the sine and cosine of θ, and $S\alpha$ and $C\alpha$ represent the sine and cosine of α.

Knowledge of these six parameters $(x, y, z, \alpha, d, \theta)$ completely defines the position and orientation of the B coordinate system attached to the rigid body of the cylindrical joint and measured with respect to the A coordinate system as shown in Eq.(1). The location of rigid body reduce a single vector $\bar{S}//\bar{Z}_B$ and a couple moment $\bar{U}//Z_{B_1}$ at point B_1 with a twist angle α (Fig. 1b). The couple moment $\bar{U} = \bar{r} \times \bar{S}$ may be resolved into two components: one $\bar{U}_{//}$collinear with joint vector $\bar{S}$ in the direction by twist angle α. The perpendicular component $\bar{U}_{\perp}$ will rotate rigid body around cylindrical joint vector $\bar{S}$ by rotation angle θ, so $\bar{\theta} = \theta\bar{S}$.

The twist angel α was defined between vectors $\bar{S}$ and $\bar{U}$ (Fig. 1b) mesured in a right-hand sense about $\bar{x}_{B_1}$. The rotation angle θ was defined between $\bar{x}_{B_2}$ and $\bar{x}_B$ measured in a right hand sense about $\bar{S}$ (Fig. 1a). It is known that, there are two distinct angles between 0 and 2π that will have the same cosine value. So, the expressed for the cosine and sine of α and θ can be expressed by Eqs. (2):

$$
\begin{cases} \cos\alpha = \bar{U} \cdot \bar{S} \\ \sin\alpha = (\bar{U} \times \bar{S}) \cdot \bar{x}_{B_1} \end{cases} \quad \begin{cases} \cos\theta = \bar{x}_B \cdot \bar{x}_{B_2} \\ \sin\theta = (\bar{x}_B \times \bar{x}_{B_2}) \cdot \bar{Z}_B \end{cases} \tag{2}
$$

As shown in Fig. 1, the axes of the cylindrical joint $\bar{S}$ and a couple moment $\bar{U}_{//}$ has the same line. Thus the combination of a collinear vector $\bar{S}$ and a couple moment $\bar{U}_{//}$ is called a screw or wrench.

So, the screw with variable pitch has both a translation d and rotation θ about the axis $\bar{S}$ described by twist angle α. Parameters d, θ and α are independent parameters of rigid body motion respect to screw $\tilde{\$}$ with variable pitch.

Two collinear vectors $\bar{S}$ and $\bar{U}_{//}$ uniquely determine the position and orientation of the screw with variable pitch.
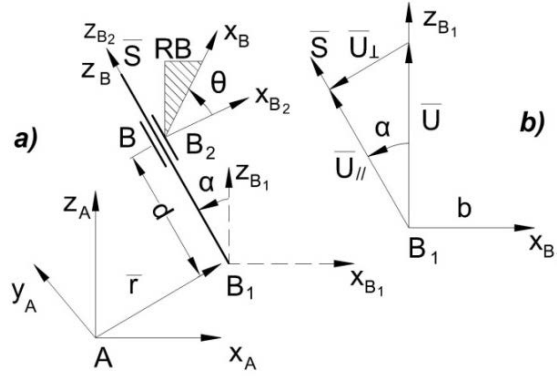
Fig. 1. Kinematic model of cylindrical joint

$\bar{S}$ is an axis vector and $\bar{U}_{//}$ is moment of screw $\tilde{S}$, where $\bar{S}$ defines the direction of motion of screw $\tilde{\$}$ and moment $\bar{U}_{//}$ determines the rotation around the axis. Unit vector $\bar{S}$ and moment $\bar{U}_{//}$ can be introduced as dual vector that is called a screw with variable pitch:

$$\tilde{\$} = \bar{S} + \varepsilon\left(\bar{U}_{//} + \tilde{\mu}\bar{S}\right) \tag{3}$$

where $\varepsilon^2 = 0$ is operator of Clifford.

The ratio of joint position d and joint rotation θ in cylindrical joint reduce to the following variable pitch:

$$\tilde{\mu} = \frac{d}{\theta} \tag{4}$$

As shown in Fig. 1b the rotation moment in cylindrical joint reduce to expression as follow:

$$\bar{U}_{//} = \bar{U} \cdot \cos\alpha = (\bar{r} \times \bar{S})\cos\alpha \tag{5}$$

Hence, using Eqs. $(3 \div 5)$ the vectors $\bar{S}$ and resultant couple moment $\bar{U}$ describing location of a rigid body with cylindrical joint can be descried as a screw with variable pitch:

$$\tilde{\$} = \begin{bmatrix} \bar{S} \\ (\bar{r} \times \bar{S})\cos\alpha + \tilde{\mu}\bar{S} \end{bmatrix} \tag{6}$$

So, as shown in Eq. (6), six independent components $(x, y, z, \alpha, d, \theta)$ describe the location of screw with variable pitch. As shown in Eq. (7) the couple moment $\bar{U}$ of the screw with variable pitch is:

$$\bar{U} = (\bar{r} \times \bar{S})\cos\alpha + \tilde{\mu}\bar{S} \tag{7}$$

Since the screw axis and its moment are in orthogonal planes and unit of screw with variable pitch $|\tilde{\$}| = 1$, so

$$\bar{S} \cdot (\bar{r} \times \bar{S}) = 0 \quad \text{and} \quad \bar{S} \cdot \bar{S} = 1 \tag{8}$$

Multiplying both side of Eq.(7) to the vector $\bar{S}$ we get the following equation:

$$\bar{S} \cdot \bar{U} = (\bar{r} \times \bar{S}) \cdot \bar{S}\cos\alpha + \tilde{\mu}\bar{S} \cdot \bar{S} \quad \text{or} \quad \tilde{\mu} = \frac{\bar{S} \cdot \bar{U}}{\bar{S} \cdot \bar{S}} \tag{9}$$

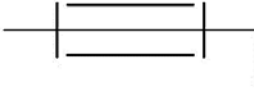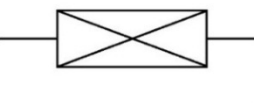For revolute, prismatic, screw and cylindrical joints the parameters of pitch to Eq.(8) can be described as follows:

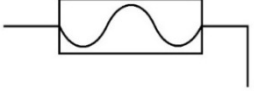$$\mu_R = 0, \quad \mu_\$ = \frac{d}{\theta}, \quad \tilde{\mu}_p = \infty, \quad \tilde{\mu}_C = \{0, \infty\}.$$

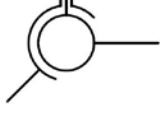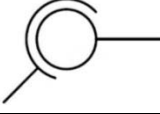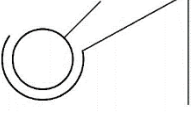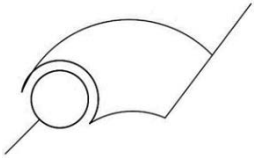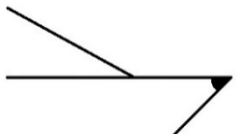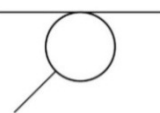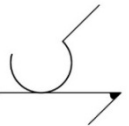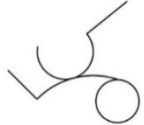**Structural formulas for robot manipulators by using screw theory.** The design problem of robot manipulators are a valuable task for structural synthesis. It is known that over constraint robot manipulator must satisfy the geometry of angular and linear constraints that correspond to the geometry of kinematic pairs moving in subspaces. The goal of structural synthesis by using screw theory are identified new methods for composing robot manipulators capable of performing various prescribed functions, position and orientations of end effectors. It is required to form a new structural formula for robot manipulators by using screw theory allows to solve the structural synthesis with variable general constraints including platforms, hinges, legs and branch loops with different ranks, that is introduced from different subspaces and spaces.
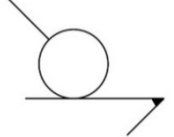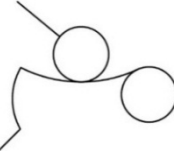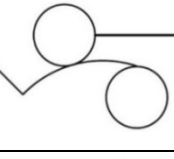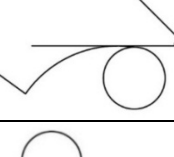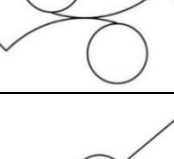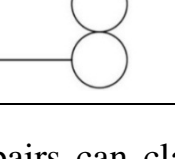
It is known that two rigid bodies attached to each other by surfaces are formed lower kinematic pairs, otherwise if contact geometry of two rigid bodies is line or a point are formed higher kinematic pairs. Due to the fact that the unconstraint space has dimension $\lambda = 6$ with independent motions 3R3P, but dimension of over constraint subspaces is $\lambda = 2 \div 5$ with different angular and linear or just angular conditions in the loops of robot manipulators. Usually kinematic pairs need constraints $c = 1 \div 5$ in order to be defined properly degree of freedom $f = \lambda - c$. Each kinematic pair has input and output link screws and joint independent screws \$ with constant pitch μ, however some joints with translation motions has additional variable screws $\tilde{\$}$ with variable pitch $\tilde{\mu}$.

The simple planar surface can be represented by two parallel screws $\underline{\$_1 \$_2}$ or two orthogonal screws $\$_1^{\perp} \$_2$, so for lower kinematic pairs number of screws $t = 2$. The intersection of two planar surfaces $\underline{\$_1 \$_2}$ and $\underline{\$_2 \$_3}$ will be result in a line represented by $\$_1 \overline{\$_2 \$_3}$ or as $\$_1^{\perp} \$_2^{\perp} \$_3$ so for higher kinematic pair with line contact of elements the number of screws $t = 3$. The intersection of three planar surfaces that will be result in a point can be represented by four screws $\$_1 \overline{\$_2 \$_3} \rightarrow \$_2^{\perp} \$_4$ or as $\$_1^{\perp} \$_2^{\perp} \$_3^{\perp} \$_4$, so for higher kinematic pair with point contact of elements the number of screws $t = 4$. Elements of the structural bonds can be illustrated as "‗" describe the parallel of screws and " $\perp$ " describe the perpendicular of screws.

Table 2 Joints kinematic parameters.

№	Name	Symbol	Kinematic parameters				Diagram
			t	f	$\tilde{\$}$	\$	
1	2	3	4	5	6	7	8
1	Revolute	R	2	1	0	3	
2	Prismatic	P	3	1	1	3	

3	Screw	H	2	1	0	3	
4	Cylindrical	C	2	2	1	3	
5	Sphere with finger	S_f	2	2	0	4	
6	Spherical	S	2	3	0	5	
7	Sphere in cylinder slot	S_{cs}	3	4	1	6	
8	Sphere in torus slot	S_{ts}	3	4	0	7	
9	Plane to slope line	$F_{/L}$	4	4	1	7	
10	Plane to perpendicular line	$F_{\perp L}$	4	3	1	6	
11	Plane to parallel lines	$F_{//L}$	3	4	2	5	
12	Line to Sphere	L_S	4	4	1	7	
13	Cylinder to plane	C_F	3	4	2	5	
14	Cylinder to torus	C_t	4	4	1	7	

15	Sphere to plane	S_F	4	5	2	7	
16	Hyperboloid to Sphere	H_s	4	5	2	7	
17	Sphere to Torus	S_t	4	5	2	7	
18	Torus to plane	T_F	4	5	2	7	
19	Torus to torus	T_t	4	5	2	7	
20	Sphere to sphere	S_s	4	5	2	7	

The usage of recurrent screws in the study of kinematic pairs can clarify the motion concept easily. From this point of view the number of independent screws in kinematic pairs can be introduced as follow:

$$\$ = f - \tilde{\$} + t \tag{9}$$

where:

$\tilde{\$}$ = number of screws with variable pitch;

t = number of screws of lower ($t = 2$) or higher kinematic pairs ($t = 3$ for line and $t = 4$ for point contact of elements);

f = degrees of freedom of relative motion permitted at joint.

The twenty kinematic pairs of robot manipulators in all types, symbols, kinematic parameters and their diagrams are shown in Table 2. Using Eq.(9) and (1.1) from Table 1 we can introduce a new general mobility equation for mechanisms with mixed dimensions of closed loops as:

$$M = \sum_{f=1}^{\lambda-1} f P_f - \sum_{k=1}^{L} \lambda_k + q \tag{10}$$

where: λ_k = number of independent, scalar, loop closure equations associated with k-th independent loop;

P_f is the number of f mobility joints. $f = \$ + \tilde{\$} - t$ is DoF at joint;

q = number of depended constraint equations.

As show in Table 1, the number of independent loops $L = c - B$, so mobility Eq. (10) can be introduced as mobility equation for robot manipulators with the same number of independent, scalar loop closure equation in each independent loop:

$$M = \sum_{f=1}^{\lambda-1} fP_f - \lambda(C - B) + q \qquad (11)$$

where: $C = c_l + c_b$ is the sum of legs and branches;

B = number of mobile platforms.

The overall performance of robots and rovers are usually constructed from the multiple platforms, hinges leg and branch loops with variable general constraint parameters, describing the location of rigid body. These robots and rovers can be affected by the topology of their possible mechanical structures. The motions (rotation and translation) of rigid links and platforms of the manipulators could be described in space R^3 and in plane R^2 with dimensions of vectors $D = 3$ and $D = 2$ in reference frame respectively. The location of rigid body in the three dimensional space R^3 can be obtain by Euclidean motions of the two dimensional subspaces R^2. It is known that the location of rigid body in space R^3 can be determined minimum by three independent curves of the three points of moving rigid body. Let there are dyads kinematic chains on each Euclidean "$3 \leq planes \leq 6$". If these kinematic chains of Euclidean planes are joined to the moving rigid body by spherical or spherical-torus kinematic pairs, so we will attain location of the rigid body in the three dimensional space R^3.

The general structural formula for parallel-serial Euclidean platform type manipulators with variable general constraints [18] including hinges (j_h), leg (l) and branch (L_b) loops can be also formulated in the form as (Table 1):

$$M = \lambda + \sum_{l=1}^{c_l}\left(\sum_{f=1}^{\lambda-1} fP_f - \lambda_l\right) + \sum_{b=1}^{L_b}\left(\sum_{f=1}^{\lambda-1} fP_f - \lambda_b\right) + j_h \qquad (12)$$

where: λ is the dimension parameter of moving platform; λ_l and λ_b are dimension parameters of leg and branch loops; j_h is the number of hinges between platforms.

The structural formula for motion [18] of platforms that are created by mechanical system from different Euclidean planes can be introduced in the following form (table 1):

$$m = \lambda + c_l + j_h + \sum_{l=1}^{c_l}(d_l - D) + \sum_{b=1}^{L_b}\left(\sum_{f=1}^{\lambda-1} fP_f - \lambda_b\right) \qquad (13)$$

where d_l is the number of dimensions of vectors of the legs in Euclidean planes;

D is the number of dimensions of vectors in the reference frame.

If the number of independent scalar leg-closure equations identical in each Euclidean planes and identical in each branch loops, the general structural formula (12) for Euclidian manipulators can be defined as

$$M = \lambda + \left(\sum_{f=1}^{\lambda-1} fP_f - \lambda_l \right) c_l + \sum_{f=1}^{\lambda-1} (fP_f - \lambda_b) L_b + j_h \qquad (14)$$

The general formula for motion of end effector of manipulator (13) with the same dimensions of Euclidean manipulator legs and branch-loops can be given in the following from:

$$m = \lambda + c_l + j_h + (d_l - D)c_l + \left(\sum_{f=1}^{\lambda-1} fP_f - \lambda_b \right) L_b \qquad (15).$$

Structural Synthesis of 6DoF Parallel Docking Manipulator of Spacecraft. In space flights the orbital docking system is used. The use of an orbital station with two docking units ensures a rigid connection with the formation of a hermetically sealed tunnel. A large number of interacting mechanisms are concentrated in the docking aggregates. The multi-functionality of the working bodies requires the solution of the problem of the structural synthesis of spatial manipulators of coupling aggregates. Since the mechanisms operate in open space, it is therefore necessary to develop new manipulators, nodes and elements of kinematic pairs. Structural parameters, kinematic structure, motion of platform and 3D drawing of the spaces docking manipulators $6RRS_t$ is depicted in Table 3. Controllable space vehicles are brought to a touch with a certain speed and position, after which the process of docking with a spatial manipulator of a parallel structure begins, which ends with a rigid connection of two docking units. After the end of the flight, an undocking takes place by releasing the mechanical connections of the docking device of the platform manipulator from the orbital station (Table 3.1).

When docking it is required that the coaxial position of the docking assemblies and the zero linear and angular velocities be maintained. The possible values of the relative coordinates and their first derivatives in the case of mechanical contact are called the initial conditions of the docking. Deviations from the co-axial position (Table 3.2) are determined by the linear coordinates δ_y, δ_z and planar angles δ_ψ, δ_φ, δ_θ. The total deviations of the docking units from the co-axial position are added from the errors: unit settings, measurements and control dynamics. Electromechanical docking devices have been created to reduce errors based on electromechanical dampers. With the damping, the brake robot can accelerate in a unit of millisecond to a speed of several thousand revolutions per minute.

The new four proposed Euclidean docking manipulators have identical legs as plane dyads RR as shown in Table 3.3a. Each end of dyads connect to the moving platform by spherical-tours pairs. Kinematic pair with 4DoF is introduced as sphere in torus slot pair S_{ts} that perform three rotations and one circular translation (Table 3.3 b). Note that, end points of each dyads respect to the fixed reference frame (Table 3.3 c) define the curve of one point of the platform in the reference Euclidean plane. Three legs RRS_{ts} of the moving platform defines the three reference Euclidean planes (Table 3.3 c) that are located under an angle of $120°$. It is known that the location of

the moving rigid body in space can be defined by minimum three independent curves of three rigid body points moving on three Euclidean reference planes.

Since the Euclidean parallel docking manipulator consist of a movable platform and legs, then the number of branch-loops $L_b = 0$, hinges $j_h = 0$ and $\lambda_l = const$, so Eq. (14) takes the form:

$$M = \lambda + \left(\sum_{f=1}^{\lambda-1} fP_f - \lambda_l \right) c_l \qquad (16)$$

In the same way when $L_b = 0$, $j_h = 0$ and $d_l = const$, then the formula (15) for motion of platform of Euclidean docking manipulator can be written in the form

$$m = \lambda + (1 + d_l - D)c_l \qquad (17)$$

Example 1. Design a parallel Euclidean docking robot manipulator with $\lambda = 6$, $\lambda_l = 6$, $c_l = 6$, $M = 6$. Find both the number and kind of kinematic pairs on each leg. Also, find the motion of docking platform.

By using Eq.(16) total DoF and kind of kinematic pairs of the legs can be calculated as

$$(M - \lambda)c_l^{-1} + \lambda_l = \sum_{f=1}^{5} fP_f \quad or$$

$$6 = P_1 + 4P_4, \quad or \quad P_1 = 2 \ and \ P_4 = 1$$
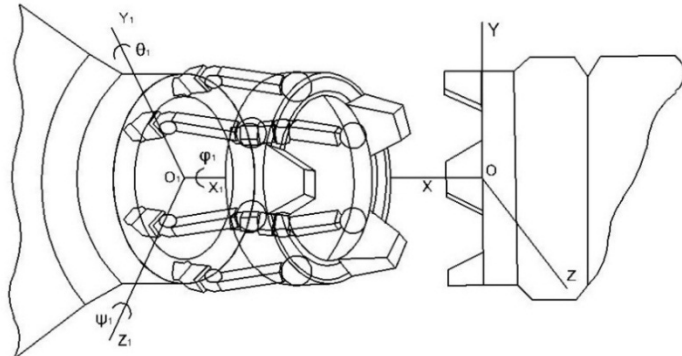
so that, in the designed docking manipulator, each leg will consist of two kinematic pairs with one degrees of freedom (revolute pairs RR) and one kinematic pair with four degrees of freedom (sphere in torus slot pair S_{ts}). By using Eq.(17), the motion of the docking platform will be $m = 6$, it means motion of platform will R_x, R_y, R_z, P_x, P_y, P_z.

Kinematic structure with different structural parameters of Euclidean docking robot manipulator with six legs is shown in Table 3.1.

The above procedure can be used for Euclidean docking robot manipulators with three, four and five legs.

The result of the new Euclidean docking robot manipulators are shown in Table 4. Elements of the structural bonds can be illustrated as: Restangle ($\square$):

Table 3. Parallel Euclidean Platform Spacecraft Docking Manipulator.

№	The new Spatial Docking Manipulator of Spacecraft.
1	

	$R_x, R_y, R_z,$ P_x, P_y, P_z	α 60°	λ_l 6	c_l 6	leg. $P_1 = 2$ $P_4 = 1$	d_l 2,2,2 2,2,2	m_p 6	M 6
1	2	3	4	5	6	7	8	9

The Deviations of the Docking Units.								
2								
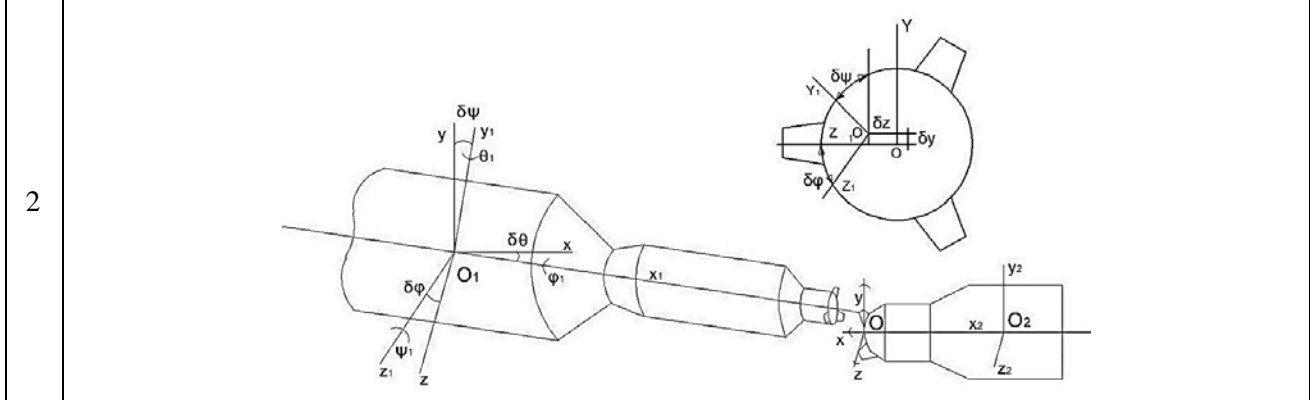
a	Dyad in reference Euclidean plane.	b	Sphere in torus slot pair	c	The three platform points on three Euclidean planes.
3	RR		S_t		$3RRS_t$
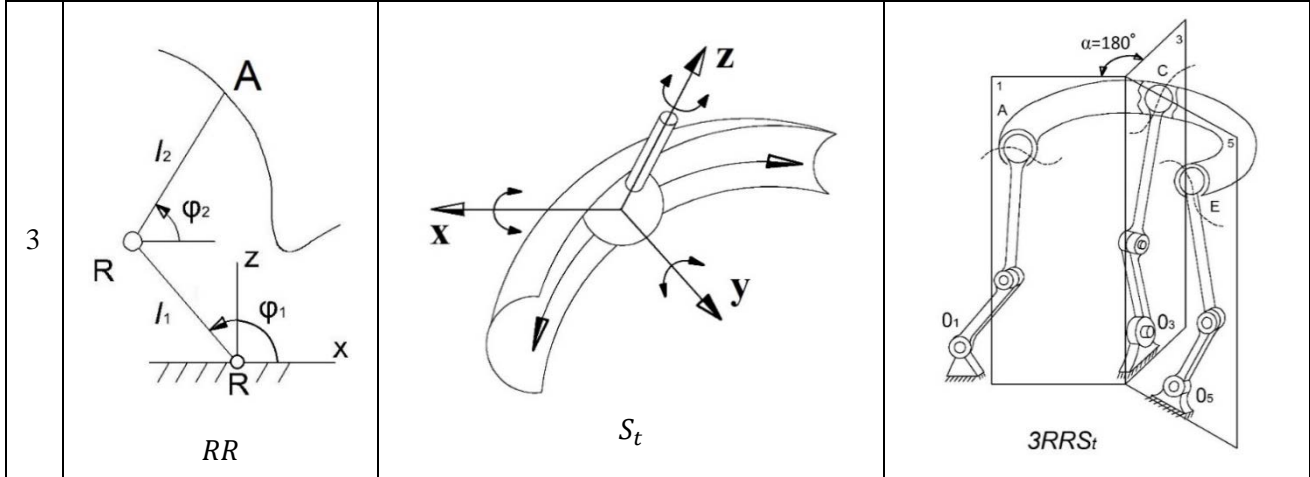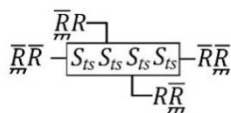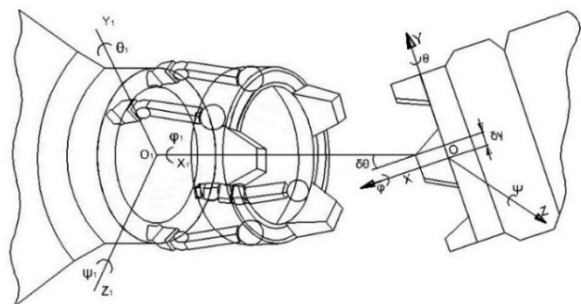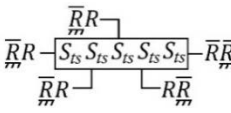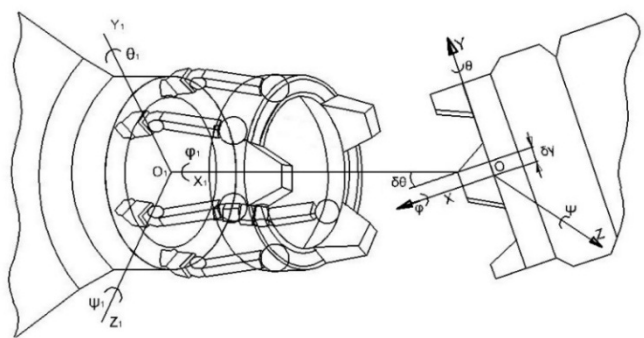
Table 4. New 6DoF Parallel Docking Manipulators of Spacecraft.

Structural bonding		Illustration						
	Motion of platform	Angle between Euclidean planes	λ_l	c_l	leg. $\sum fP_f$	d_l	m_p	M
1	2	3	4	5	6	7	8	9
	$R_x, R_y, R_z, P_x,$ P_y, P_z	120°	6	3	$P_1 = 2$ $P_4 = 1$	2,2,2	6	6
1	2	3	4	5	6	7	8	9
1								

1	2	3	4	5	6	7	8	9
$\overline{R}R$ — $\overline{\overline{R}}R$ — $[S_{ts}\,S_{ts}\,S_{ts}\,S_{ts}]$ — $R\overline{R}$ — $R\overline{\overline{R}}$	$R_x, R_y, R_z, P_x, P_y, P_z$	90°	6	4	$P_1 = 2$ $P_4 = 1$	2,2,2, 2	6	6

| 2 | |

1	2	3	4	5	6	7	8	9
$\overline{R}R$ — $\overline{\overline{R}}R$ — $[S_{ts}\,S_{ts}\,S_{ts}\,S_{ts}\,S_{ts}]$ — $R\overline{R}$ — $\overline{\overline{R}}R$ — $R\overline{\overline{R}}$	$R_x, R_y, R_z, P_x, P_y, P_z$	72°	6	5	$P_1 = 2$ $P_4 = 1$	2,2,2, 2,2	6	6

| 3 | |

describes moving platform with spherical-torus pairs S_t.

Platform leg $(-, \llcorner)$: connection of the spherical-torus pairs on the moving platform with pairs of the legs.

$\overline{\overline{R}}$: input joint on fixed frame.

$\overline{R}$: input joint on moving frame.

Structural Synthesis of Wheeled Robots. It is obvious that wheeled robot have been developed for Mars and Moon surface. First we consider the definition of wheeled robot: "A wheeled robot is an autonomous system capable of traveling a terrain with natural or artificial obstacles". As shown in Fig. 2.1 kinematic structure of wheeled robot has six wheels with symmetric structure for both sides. Each side has three wheels which are connected to each other by the main linkage and two loops kinematic chain. Main linkage called rocker that has two joints, where first joint connected to back wheel and second joint assembled to platform. The rocker is kinematic chain where the second path of link connected rigidly to another linkage system with two wheels. The second linkage system is called bogie (Fig. 2.2). So, rocker-bogie kinematic chain is called suspension system. Wheeled rough terrain mobile robots are called as "Rover". Rovers can carry more weight with high-speed, easy novigation and more precisely can be calculated position and orientation. First rover was "Lunakhod" and second rover was six wheeled syspension system, which

connects the wheels to the platform. This connection are linkage mechanisms, damping and complex spring.

The new bogie mechanism consists of two Chebyshev lambda mechanisms which are connected symmetrically. Paired two lambda mechanisms are used as motion generation mechanisms, where couplers are input links. To move the coupler points M_1 and M_2 along a line sufficiently and necessary to fulfil the design relation: $3d - a = 2b$. The length of parametre d can be changed according to relation $1,55a \leq d \leq 3a$ (Fig. 2.1). The same second suspension kinematic chains are assembled in opposite side of moving platform. Right and left suspensions are connected to each other by a differential gear mechanism (Fig. 2). When one side climbing over obstacle, this mechanism rotates the platform around the rocker joints by average angle of two sides (Fig. 2.1). So, the wheeled robot is equipped with six wheels and possibly a manipulator setup mounted on the platform for handling of work pieces, tools or special devices. On inclined surface the moving rover can hold the main plarform horizontal. Navigation gets easier by this feature of rover. Rovers are driven by commands which are sent from ground operators after tested in $3D$ computer simulation. Some of the critical motions such as climbing high slope, new rover designs are needed to more flexible duaring field operation.

Example 2. Design a parallel wheeld rover with six legs $c_l = 6$, three branch $c_b = 3$ and one moving platform $B = 1$ (Fig. 2.1). The dimension parameter of each independent loops on the left and right suspensions $\{\lambda_k\}_1^8 = 3$ (Fig. 2.2). The number of kinematic pairs with one DoF in the left and right suspensions $P_1 = 30$. Two suspensions kinematic chains are connected by differential gear mechanism. Find the number of motors for parallel whelled rover. Also, find the motion of the rover's platform.

First, we define the number of independent loops (Table 1.3):
$$L = C - B = c_l + c_b - B = 6 + 3 - 1 = 8.$$
Using Eq. (11) total DoF of parallel wheeled rover can be calculated as
$$M = \sum_{f=1}^{5} f P_f - \lambda(C - B) = P_1 - \lambda(c_l + c_b - B) =$$
$$= 30 - 3(6 + 3 - 1) = 6.$$
By using Eq.(17), the motion of the moving rover's platform can be defined as
$$m = \lambda + (1 + d_l - D)c_l = 6 + (1 + 2 - 3) = 6.$$
Thus, the problem of the structural synthesis of the wheeled rocker-bogie mechanism is solved and it is introduced in Fig.2. Spring and damper application to double lambda bogie good solution for high-speed off-road vehicles.

Rocker-Bogie suspensions can be used also for vehicles with a larger number of wheels. An example of a layout for an 8-wheeler each suspension will consist from four motion generation Chebyshev lamda mechanisms with the four given wheels. İn this case the vehicle may be summetrical and it can run in both direction without any difference.

№			
1			
	1	2	3
2			
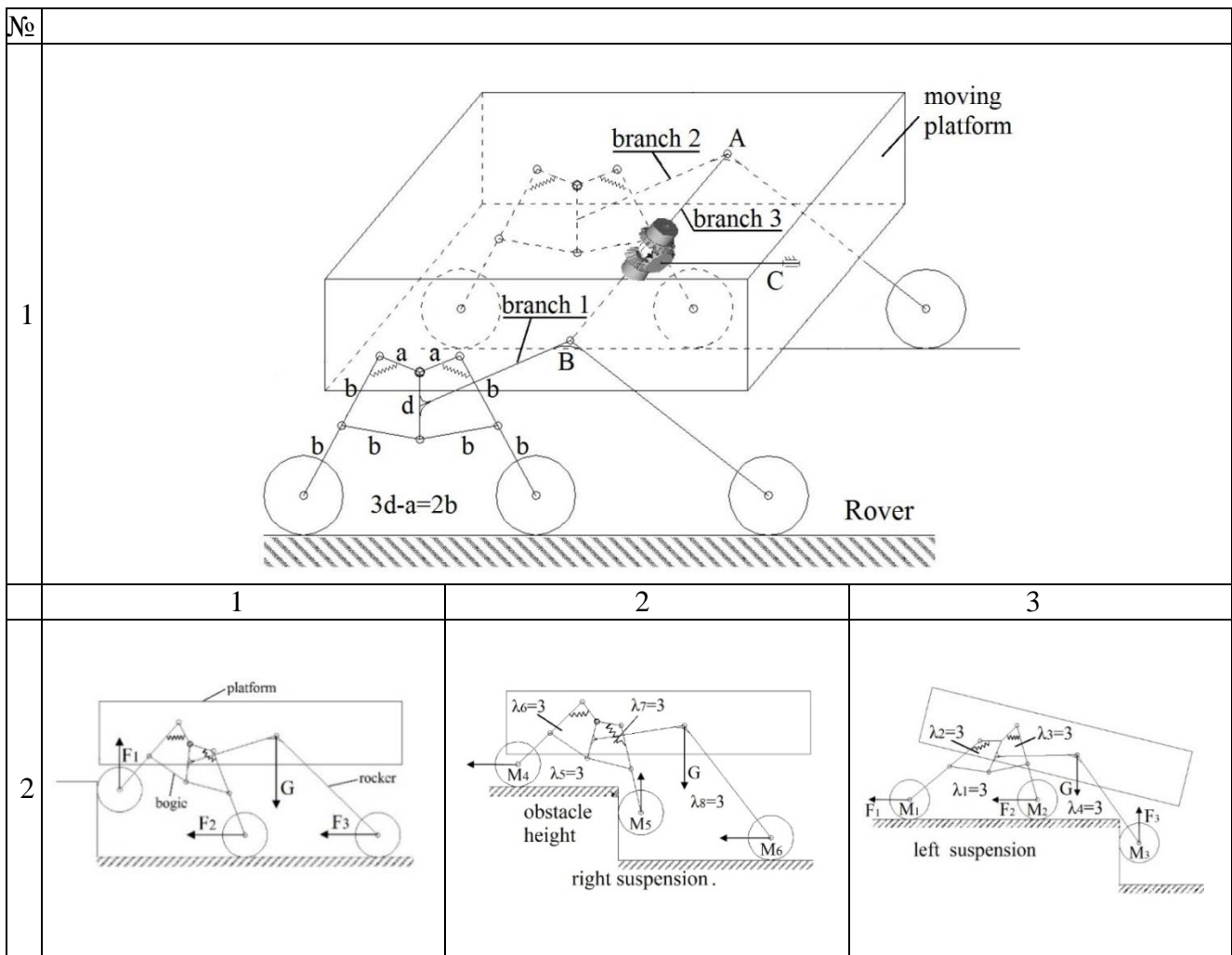
Fig. 2. Kinematic model of rocker-bogey mechanism.

Conclusion. The problem of structural synthesis of the robot manipulators with variable general constraint of the legs and closed loops can be difficult and complex task depends on the DoF and motion of an end-effector concept. It is described a new structural formula of kinematic pairs for robot manipulators by using screw with variable pitch. From this point the twenty kinematic pairs are shown with types, simbols, kinematic screw parameters and their diagrams. It were introduced two new general mobility equations for mechanisms with mixed or fixed dimensions of close loops. The general structural formula for Euclidean manipulators with variable or identical general constraints are introduced. The new structural formula for motion of end effector of robot with legs from different Euclidean planes were considered. Four new Euclidean 6DoF parallel docking manipulators of Spacecraft were reviewed and synthesized. Funally, by using sistematic process of structural synthesis by using for mobility of robot and motion of moving platform were developed to create new structure of wheeled robot-rover for Mars and Moon surface.

REFERENCES:

[1]. Alizade R.I., Bayram C., Gezgin E., *Structural Synthesis of serial platform manipulators, IFToMM J*., Mechanism and Machine Theory 42, 580-599, (2007).

[2]. Gogu G., *Mobility of mechanisms: a critical review*, IFToMM J.Mech. Mach. Theory 40, 1068-1097, (2005).

[3]. Muller R., *Die zwanglanfigkeit kinematische ketten*, Unpublished dissertation (1920), as quoted in K. Federhofer: Graphische Kinematic and Kinetostatic, Springer, Berlin, (1932).

[4]. Voinea R., Atanasiu M., *Contributions a la theorie geometrigue des vis*, Bull. Inst. Politech. Bucuresti XXI (3) (1959).

[5]. Waldron K.J., *The constraint analysis of mechanisms*, J. Mech. 1, pp. 101-114, (1966).

[6]. Huang Z., Li Q.C., *General methodology for type synthesis of symmetrical lower-mobility parallel manipulators and several novel manipulators*, Int. J. Robot. Res. 21, pp. 131-145, (2002).

[7]. Fang Y., Tsai L.W., *Structure synthesis of a class of 4-DoF and 5-DoF parallel manipulators with identical limb structures*, Int. J. Robot. Res. 21, pp. 799-810, (2002).

[8]. Jin Y., Chen I.M., Yang G., *Structure synthesis and singularity analysis of a parallel manipulator based on selective actuation*. Proceeding of the International Conference on Robotics and automation (2004) 4533-4538.

[9]. Gao F., Li W., Zhao X., Jin Z., Zhao H., New Kinematic structures for 2-5 DoF parallel manipulator designs, IFToMM J, Mechanism and Machine Theory 37, pp. 1395-1411, (2002).

[10]. Zhao T. S., Dai J. S., Huang Z., *Geometric analysis of over constrained parallel manipulators with 3-4 DoF*, ASME Journal Series C, Vol. 45, No. 3, pp. 730-740, (2002).

[11]. Kong X., Gosselin C. M., *Type Synthesis of 3T1R 4-DoF parallel manipulators based on screw theory*, IEEE Transactions on Robotics and Automation, Vol. 20, No. 2, pp. 181-190, (2004).

[12]. Kong X., Gosselin C. M., *Type synthesis of 4-DoF SP-equivalent parallel manipulators: A virtual chain approach*, IFToMM J., Mechanism and Machine Theory, 41, pp. 1306-1329, (2006).

[13]. Kong X., Gosselin C. M., *Generation of parallel manipulators with three translational degrees of freedom based on screw theory*, Proceedings of Symposium on Mechanisms, Machines and Mechatronics, Montreal, Canada (2001).

[14]. Kong X., Gosselin C. M., *Type synthesis of parallel mechanisms*, Springer (2007).

[15]. Freudenstein F., Alizade R.I., *On the degree of freedom of mechanisms with variable general constraint*, IV World IFToMM Congress, England, pp. 51-56, (1975).

[16]. Alizade R.I., *On the degree of freedom of kinematic chain,* Az. Pol. Inst., Automation design of mechanisms, manipulator and robots, Baku, pp. 3-14, (1988).

[17]. Alizade R.I. , Bayram C., *Structural synthesis of parallel manipulators*, IFToMM J. Mech. Mach. Theory 39, pp. 857-870, (2004).

[18]. Alizade R.I., Can F.C., Gezgin E., *Structural synthesis of Euclidean platform robot manipulators with variable general constraints*, IFToMM J. Mech. Mach. Theory 43, pp. 1431-1449, (2008).

STUDY OF THE EFFICIENCY FACTOR OF SLIDING BEARINGS OF THE NEW CONSTRUCTIVE SOLUTION OF MULTISTAGE REDUCER

Isa KHALILOV[1], Beyali AHMEDOV[2], Anar HAJIYEV[3]

[1,2,3]Department of "Mechatronic and machine design", Azerbaijan Technical University, Baku, Azerbaijan

E-mail: _khalilov@aztu.edu.az[1]_, ahmedov.beyali@mail.ru[2], anar_hajiyev_1991@mail.ru[3]

Abstract. The article deals with the issues of quantitative assessment of the internal resistance of oil in sliding bearings of the new constructive solution of two-line three-stage reducer intended for use in transmission mechanisms of machines and devices. Based on the analysis of possible kinematic diagrams of the new constructive solution of reducer, it was determined that the directions of rotation of the driving and driven shafts coincide with the directions of rotation of block gears mounted on sliding bearings. In this case, the resistance in the sliding bearings becomes a useful driving force, which becomes a useful factor characterizing the internal driving force of the oil. This improves the reliability of the mechanism, as well as significantly reduce the energy consumption of the mechanical transmission. Based on the results of calculations, it was determined that the efficiency factor of the new constructive solution of a three-stage reducer is about 2% higher than in classic reducers.

Keywords: _new constructive solution, sliding bearings, double gear, block, driving force, efficiency factor, oil layer, angular velocity, resistance force._

Introduction. The economic indicators of machines and devices largely depend on the correct choice of kinematic schemes of their constituent mechanisms. Usually 70% of the cost of machines and equipment is the material from which its structural elements are made. One of the components of machines and devices are their transmission mechanisms – reducers (which also known as gearbox) or multipliers [1].

Gear reducers used as a transmission mechanism are widely used in almost all areas of modern technology. The production of reducers that can transmit up to 10 000 kW is estimated at several million pieces per year. Currently, new designs of reducers are being developed in mechanical engineering, as well as methods for calculating the strength of their structural elements are being refined and improved.

At present, in order to save metal used in the production of three-stage gearboxes and to reduce their overall dimensions, the main direction of the development of this mechanical system is the placement of an intermediate shaft under its drive shaft. With this design, the length of the gearbox is reduced and this to some extent affects its price (Figure 1).

Based on research, it was determined, that at designing of machines and devices, including multi-stage reducers (gearboxes), the main geometric dimensions of their constituent structural elements are determined by the existing operating criteria in a chaotic manner without taking into account the influence of exciting factors. And this in turn, leads to different values of the reliability of structural elements, an increase in their metal consumption (and dimensions), as a result of which the technical level of

Isa KHALILOV, Beyali AHMEDOV, Anar HAJIYEV.
Study of the efficiency factor of sliding bearings of the new
constructive solution of multistage reducer

the mechanical system decreases. Therefore, at designing of modern multi-stage gearbox (multiplier) that is resistant to market competition, along with the constructive changes introduced into them, it is necessary to take into account the provisions of the principles of the system approach.
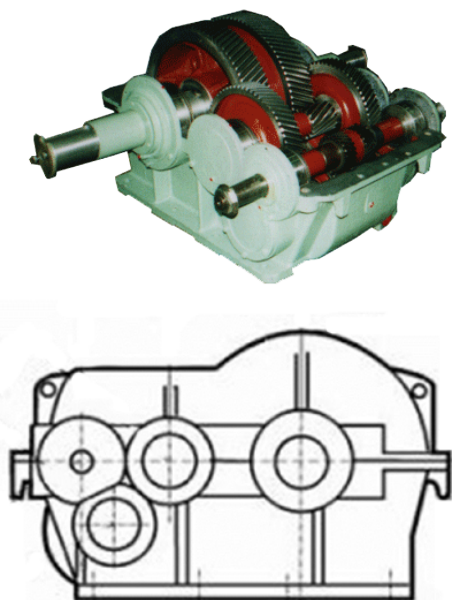
Figure 1. Improved two-line
three-stage reducer
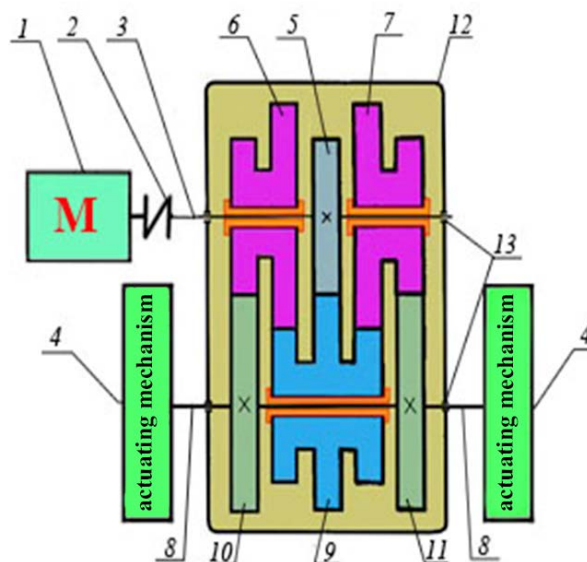
Figure 2. New constructive solution of two-line
three-stage reducer which has only two shafts

Formulation of the problem. Increasing the number of stages in classic multi-stage helical gear reducers increases the number of gears, countershafts, and accordingly the number of bearings. In turn, increasing the number of structural elements of the reducer leads to a reduction of its reliability and efficiency, and to increase overall dimensions. To effectively solve this problem, at the department of "Mechatronic and machine design" of Azerbaijan Technical University developed, researched and tested a new principle of designing structural elements of the multistage one- and two-line cylindrical gear reducer system, the novelty of which was approved by the Eurasian Patent (№017053) [2].

Fig. 2 shows a kinematic diagram of a new two-line three-stage reducer. The drive shaft 3 of the gearbox is rigidly connected to the electric motor 1 by coupling 2, and the driven shaft 8 is rigidly connected to effector (disks) 4 of the machine. The drive gear 5 is rigidly attached to the drive shaft 3, the double gear blocks 6 and 7 rotate freely around the axis of the drive shaft. The driven gears 10 and 11 are rigidly attached to the driven shaft 8, and the three-gear block 9 rotates freely around the axis of the driven shaft. The drive and driven shafts are mounted on 15 rolling bearings mounted on the housing 16.

The reducer is equipped with double and triple gear blocks, which are located along the length of the driving and driven shafts, which freely rotate around the axes of these shafts and form the following stages, excluding the intermediate shafts from the design, and their supports (bearings). The principle of operation of the proposed

Isa KHALILOV, Beyali AHMEDOV, Anar HAJIYEV.
Study of the efficiency factor of sliding bearings of the new
constructive solution of multistage reducer

gearbox is as follows: the movement from the drive shaft, which receives rotary motion from the electric motor 1, with the help of the drive gear 5 rigidly mounted on it, is transmitted to the three-crown block gear 9 freely mounted on the driven shaft.

Operation principle of proposed reducer is follows: the movement from the drive shaft, which receives a rotational movement from the electric motor 1, with the help of the drive gear 5 rigidly installed on it, is transmitted to the triple gear block 9, which freely mounted on the driven shaft. In this case, although the angular velocities of the block gears and the corresponding drive and driven shafts are different, their directions coincide and give a push to each other. Triple-gear block 9 with the clutch transmits rotational motion to double-gear blocks 6, 7 which are mounted on the drive shaft. And the double-gear blocks 6, 7 freely rotating around the axis of the drive shaft transmit the rotary motion to the gears 10, 11, rigidly fixed to the driven shaft.

In this case, the direction of their rotational speeds is the same, since both the driven gears 10, 11 and the drive shaft 8, as well as the drive gear 5 and the drive shaft 3 are rigidly connected.

To carry out a comparative analysis of classical multistage gearboxes with a new constructive solution of multistage gearbox, the kinematic characteristics of each of them are preliminarily determined.

Total transmission number for a classic multi-stage reducer [4;5]:

$$u_\Sigma = u_1 \cdot u_2 \cdot u_3, \cdots u_k = \frac{z_2 \cdot z_3 \cdots z_k}{z_1 \cdot z_2' \cdots z_{k-1}'} \tag{1}$$

Since new constructive solution of the multi-stage gearboxes $u_1 = u_2 = u_3 = \ldots = u_k$, the total transmission number for them is expressed as follows

$$u_\Sigma = u_p^k = \left(\frac{z_2}{z_1} \right) \tag{2}$$

there u_1, u_2, u_3, u_k - gear ratio of the respective stages;

k_p – number of stages.

The new constructive solution of the three stage reducer consists of a drive shaft, a drive gear, two double-gear and one triple-gear blocks and driven shaft. The small gear of the first stage is rigidly fixed to the drive shaft. And double-gear and triple-gear blocks are mounted on sliding bearings on the shaft. These double-gear and triple-gear blocks rotate in the rotation direction of the drive and driven shafts, which in turn, to some extent, reduces the value of the resistance moment.

The proposed new constructive solution of the three stage reducer is suitable in length and height to fit with coaxial three-stage spur gearboxes. The symmetrical arrangement of the stages in the new construction allows for a more compact design than in the classic three-stage gearboxes. This gearbox has a drive shaft that acts as an axle for the second stage. In this version, the mechanical system excludes two shafts, two "shaft-hub" connections and four rolling bearings, which reduces the number of structural elements and increases the reliability of the gearbox.

Isa KHALILOV, Beyali AHMEDOV, Anar HAJIYEV.
Study of the efficiency factor of sliding bearings of the new
constructive solution of multistage reducer

The new constructive solution of the gearbox with five or more single stages differs in that even in these gearboxes, despite the increase in the number of double-gear blocks, its previous length and height remain unchanged, but the width increases.

Depending on the number of stages K_p, the number of double-gear blocks K_b is determined as follows:

$$K_b = K_p - 1 \tag{3}$$

As can we see, the proposed new constructive solution of the gearboxes are more compact than classical gearboxes, and in all cases they allow to form more successful gearboxes for a given mechanical system. One of the important tasks to reduce the cost of repair and downtime of a new multi-stage gearboxes is to increase their reliability.

Solution of the problem. Due to structural and economic considerations, sliding bearings are used instead of rolling bearings as supports for the double-gear blocks of the new constructive solution of the gearboxes.

These bearings are embedded under the gear blocks which are placed on the shaft and rotate freely around its axis.

Based on the analysis of possible kinematic diagrams of the new constructive solution of reducer, it was determined that the directions of rotation of the driving and driven shafts coincide with the directions of rotation of block gears mounted on sliding bearings. In this case, the resistance in the sliding bearings becomes a useful driving force, which becomes a useful factor characterizing the internal driving force of the oil. It improves the reliability of the mechanism, as well as significantly reduces the energy consumption of the mechanical transmission.

The pressure created in the fluid layer by friction of one surface against another is determined according to the Reynolds equation as follows [6]:

$$\frac{\partial}{\partial x}\left(h^3 \frac{\rho}{\mu}\frac{\partial p}{\partial x}\right) + \frac{\partial}{\partial z}\left(h^3 \frac{\rho}{\mu}\frac{\partial p}{\partial z}\right) =$$
$$= 12\rho V + 6\frac{\partial}{\partial x}(\rho U h) + 6\frac{\partial}{\partial z}(\rho W h) + 12h\frac{\partial \rho}{\partial t} \tag{4}$$

there U, V, W - components of the velocities of one surface on the other surface along the axes OX, OY and OZ, respectively; μ_0 - dynamic viscosity of oil; ρ_y - oil density; h - the thickness of the oil layer in the area under consideration.

If we apply this expression to a normal cylindrical sliding bearing, the expression will be much simpler. Thus, if the lubrication process is carried out by an incompressible oil, then at $t = const$ its density is equal to $\rho_y = const$ and $\frac{\partial \rho_y}{\partial t} = 0$. In addition, if the temperature and pressure of the liquid change insignificantly along the length of the liquid, then the value of μ_0 can be averaged and considered constant. In steady-state operation at a constant rotation of journal, the rotational speed V in the direction of the OX axis will be constant: $V = const$. On the other hand, since the center of the journal does not change its position $e = const$, then the rotation speed V in the direction of the OY axis will be zero. Since the fluid flow velocity is directed

Isa KHALILOV, Beyali AHMEDOV, Anar HAJIYEV.
**Study of the efficiency factor of sliding bearings of the new
constructive solution of multistage reducer**

along the bearing end surfaces, its velocity in the direction of the OZ axis is less than in the direction of rotation, therefore, $W = 0$ can be taken.
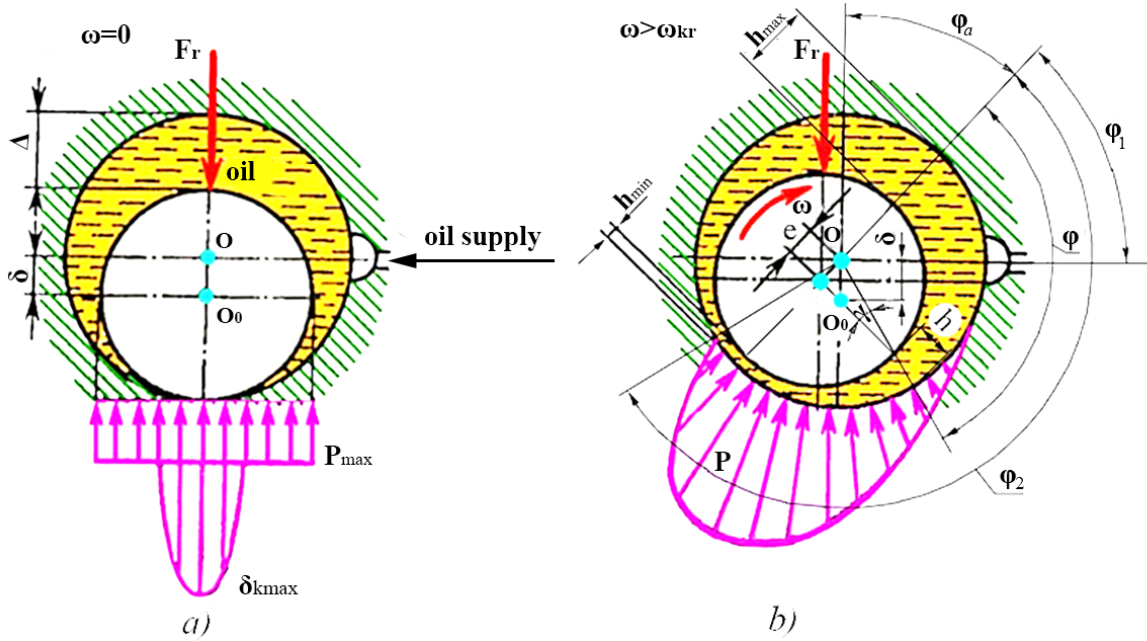
Figure 3. Scheme for determining the pressure at any arbitrary section of the oil layer.

If we take these conditions into account in expression (4), then Reynolds's expression will be greatly simplified as follows [6]:

$$\frac{\partial}{\partial x}\left(h^3 \frac{\partial p}{\partial x}\right) = 6\mu_0 Uh \tag{5}$$

Let's integrate this expression, then:

$$h^3 \frac{dp}{dx} = 6\mu_0 Uh + C \tag{6}$$

To determine the integral constant, it is assumed that at a given thickness of the oil layer ($h = h_m$) the pressure takes its maximum value and becomes $\frac{dp}{dx} = 0$ when $p = p_{max}$ (Figure 3). Then from the expression (6):

$$C = -6\mu_0 Uh_m$$

If we consider this expression in (6), then [9]:

$$\frac{dp}{dx} = 6\mu_0 U \frac{h - h_m}{h^3} \tag{7}$$

To make it easier to determine the pressure (p) in an arbitrary section, we substitute $dx = rd\varphi$ and $U = \omega r$.

The thickness of the fat layer between the journal and the backing is determined by the following expression [6]:

$$h = \delta - e\cos(180^0 - \varphi) \tag{8}$$

there $\delta = 0{,}5s$- radial bearing clearance; $s = D - d$ - diametral clearance; D, d - respectively the diameters of the bearing and the journal.

If we change $\frac{e}{\delta} = \chi^*$ in this formula, then

$$h = \delta(1 + \chi^* cos\varphi) \tag{9}$$

Isa KHALILOV, Beyali AHMEDOV, Anar HAJIYEV.
Study of the efficiency factor of sliding bearings of the new
constructive solution of multistage reducer

there χ^*- relative eccentricity.

For the minimum thickness of the oil layer:

$$h_{min} = \delta(1 + \chi^* cos\varphi_m) \tag{10}$$

there φ_m- angle corresponding to maximum pressure.

If we consider these expressions in (7), then we get

$$\frac{dp}{d\varphi} = 6\frac{\mu_0\omega}{\psi^2}\frac{\chi^*(cos\varphi - cos\varphi_m)}{(1 + \chi^* cos\varphi)^3} \tag{11}$$

there $\psi = \frac{s}{d} = \frac{\delta}{r}$ - relative clearance.

If we integrate the expression (11) from φ_1 to φ' to determine the specific pressure in the section forming the angle φ' with the center lines, then

$$P_{\varphi'} = 6\frac{\mu_0\omega}{\psi^2}\int_{\varphi_1}^{\varphi'}\frac{\chi^*(cos\varphi - cos\varphi_m)}{(1 + \chi^* cos\varphi)^3}d\varphi \tag{12}$$

The pressure per unit area in the section under consideration is determined by the following expression:

$$\Delta P_{\varphi'} = P_{\varphi'}lr\Delta\varphi' = P_{\varphi'}\frac{ld}{2}\Delta\varphi'$$

In steady-state operation, the external load acting on the bearing unit is defined by the following expression [6; 8]:

$$F_r = \frac{3\mu_0\omega}{\psi^2}ld\int_{\varphi_1}^{\varphi_2}cos[\pi - (\varphi' + \varphi_a)]d\varphi'\int_{\varphi_1}^{\varphi'}\frac{\chi^*(cos\varphi - cos\varphi_m)}{(1 + \chi^* cos\varphi)^3}d\varphi \tag{13}$$

If we make a substitution in this formula

$$\Phi_F = 3\int_{\varphi_1}^{\varphi_2}cos[\pi - (\varphi' + \varphi_a)d\varphi']\int_{\varphi_1}^{\varphi'}\frac{\chi^*(cos\varphi - cos\varphi_m)}{(1 + \chi^* cos\varphi)^3}d\varphi \tag{14}$$

then the load acting on the bearing unit is defined as follows: [4;7]:

$$F_r = \frac{\mu_0\omega dl}{\psi^2}\Phi_F \tag{15}$$

there Φ_F- bearing load factor; $l = (0,5 \div 1,5)d$- length of bearing; ω – summary angular velocity of corresponding shaft (journal) and sliding bearing.

As already noted, the rotation directions of the drive and driven shafts at new constructive solution of the gearboxes coincide with the rotation directions of gear blocks mounted on sliding bearings. Consequently, the total angular velocity will be equal to the sum of the angular velocities of the shaft and the sliding bearings.

In the total angular velocity of the sliding bearings integrated under the gear blocks of the new constructive solution of three-stage two-line reducer that we are studying (Figure 4):

Isa KHALILOV, Beyali AHMEDOV, Anar HAJIYEV.
Study of the efficiency factor of sliding bearings of the new
constructive solution of multistage reducer

$$First\ gear\ block\ \omega_{21} = \omega_2 + \frac{\omega_1}{u} = \frac{\omega_1}{u_1^3} + \frac{\omega_1}{u_1} = \omega_1 \left(\frac{1+u_1^2}{u_1^3}\right)$$

$$Second\ gear\ block\ \omega_{11} = \omega_1 + \frac{\omega_1}{u_2^2} = \omega_1 \left(\frac{1+u_2^2}{u_2^2}\right)$$

(16)

There - u_1 and u_2 - corresponding gear ratios of the first and second stages of reducer.

Before designing a new multi-stage gearbox taking into account the full use of the permissible load of the high-speed stage and proper lubrication of the gears it is usually assumed that the gear ratio of each stage of the gearbox is $u_1 = u_2 = u_3 = \cdots = u_n$.
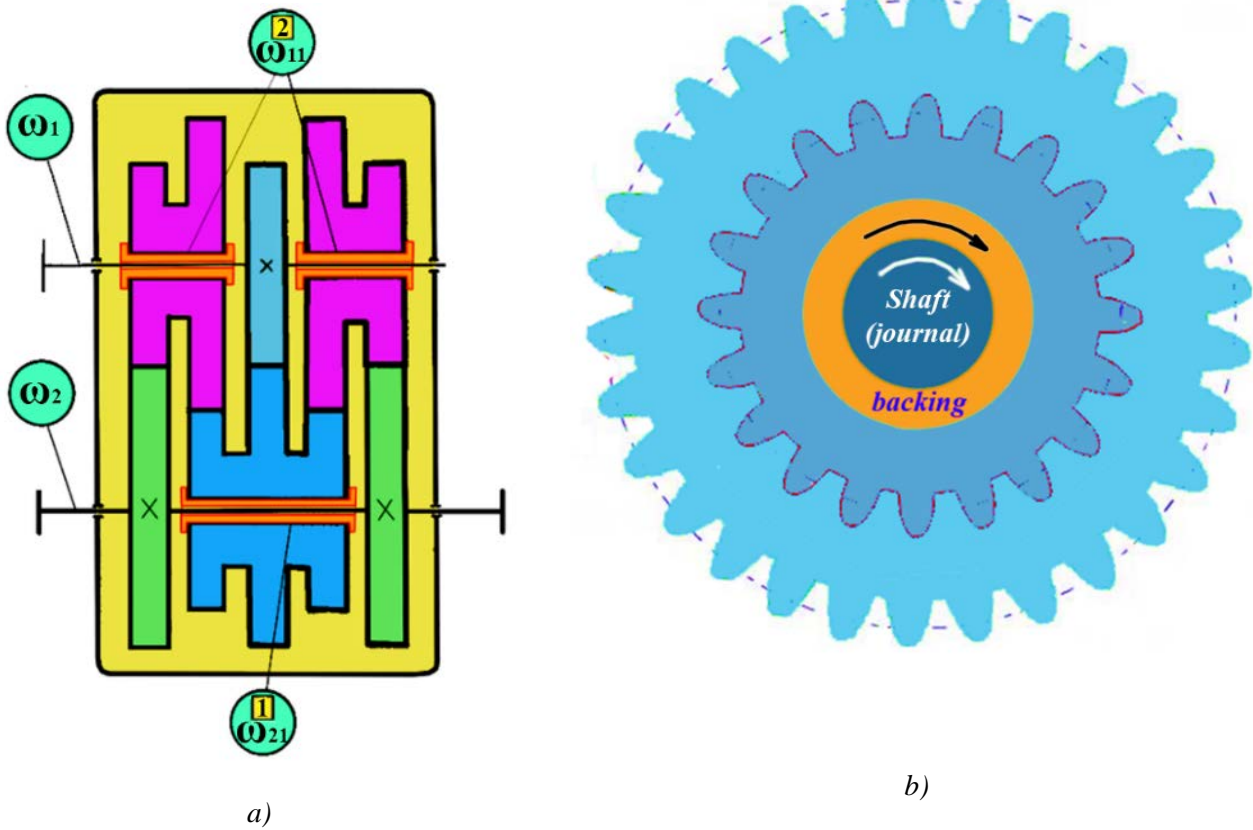
Figure 4. The new constructive solution of multistage reducer
a - kinematic diagram; b – gear block

According to the expression (15) the relationship between Φ_F and the main parameters of the bearing under constant load can be determined by the following expression:

$$\Phi_F = \frac{F_r}{ld}\frac{\psi^2}{\mu_0\omega} = \frac{p\psi^2}{\mu_0\omega}$$

(17)

The load factor of the corresponding sliding bearings of the reducer:

Isa KHALILOV, Beyali AHMEDOV, Anar HAJIYEV.
Study of the efficiency factor of sliding bearings of the new
constructive solution of multistage reducer

$$\left.\begin{array}{l}\Phi_{F1} = \dfrac{(F_{r1} + F_{r2})\psi_1^2}{\mu_0\omega_{21}d_1l_1} = \dfrac{(F_{r1} + F_{r2})\psi_1^2 u_1^3}{(1 + u_1^2)\mu_0\omega_1 d_1 l_1} \\[4mm] \Phi_{F2} = \dfrac{(F_{r2} + F_{r3})\psi_2^2}{\mu_0\omega_{11}d_2l_2} = \dfrac{(F_{r2} + F_{r3})\psi_2^2 u_2^2}{(1 + u_2^2)\mu_0\omega_1 d_2 l_2}\end{array}\right\} \tag{18}$$

Then the total load factor of the sliding bearings of the reducer:

$$\Phi_F = \Phi_{F1} + \Phi_{F2} =$$

$$= \frac{1}{\mu_0\omega_1}\left(\frac{(F_{r1} + F_{r2})\psi_1^2 u_1^3}{(1 + u_1^2)d_1 l_1} + \frac{(F_{r2} + F_{r3})\psi_2^2 u_2^2}{(1 + u_2^2)d_2 l_2}\right) \tag{19}$$

According to Newton's law, the frictional force that slides the oil layer in sliding bearings:

$$\left.\begin{array}{l}F_{f1} = \pi dl\mu_0\dfrac{v}{\delta} = \pi d_1 l_1\dfrac{\mu_0\omega_{21}}{\psi_1} = \pi d_1 l_1\dfrac{\mu_0\omega_1}{\psi_1}\left(\dfrac{(1 + u_1^2)}{u_1^3}\right) \\[4mm] F_{f2} = \pi dl\mu_0\dfrac{v}{\delta} = \pi d_2 l_2\dfrac{\mu_0\omega_{11}}{\psi_2} = \pi d_2 l_2\dfrac{\mu_0\omega_1}{\psi_2}\left(\dfrac{(1 + u_2^2)}{u_2^2}\right)\end{array}\right\} \tag{20}$$

Total force used to repel friction in the sliding bearings of reducer:

$$P_f = \frac{\pi\mu_0}{2}\omega_1^2\left(\frac{l_1 d_1^2}{\psi_1}\left(\frac{(1 + u_1^2)}{u_1^3}\right)^2 + \frac{l_2 d_2^2}{\psi_2}\left(\frac{(1 + u_2^2)}{u_2^2}\right)^2\right) \tag{21}$$

The moment of frictional forces under the condition of integration of the driving force of the oil on the journal surface:

$$T_f = \frac{\pi\mu_0}{2}\omega_1\left(\frac{l_1 d_1^2}{\psi_1}\left(\frac{(1 + u_1^2)}{u_1^3}\right) + \frac{l_2 d_2^2}{\psi_2}\left(\frac{(1 + u_2^2)}{u_2^2}\right)\right) \tag{22}$$

Total efficiency factor of new constructive solution of reducer [2]:

$$\eta_\Sigma = \frac{P_2}{P_1} = \frac{P_1 - P_f}{P_1} = 1 - \frac{P_{d\varsigma} + P_{dy} + P_f}{P_1} =$$

$$= 1 - \left(\psi_{ge}^* + \psi_{rb}^* + \psi_{sb}^*\right) \tag{23}$$

there ψ_{ge}^*- the factor coefficient taking into account the losses in the clutch; ψ_{rb}^* - coefficient taking into account the losses in the rolling bearings; ψ_{sb}^* - the total useful ratio, which characterizes the internal resistance force of the oil in the sliding bearings.

$$\psi_{sb}^* = \frac{P_f}{P_1} = \frac{\pi\mu_0\omega_1^2}{2P_1}\left(\frac{l_1 d_1^2}{\psi_1}\left(\frac{(1 + u_1^2)}{u_1^3}\right)^2 + \frac{l_2 d_2^2}{\psi_2}\left(\frac{(1 + u_2^2)}{u_2^2}\right)^2\right) \tag{24}$$

If the power in the drive shaft of the new multi-stage reducer is P_1, and the power in the outlet shaft without the sliding bearings is P_2, then the power in the outlet shaft of the reducer will be as follows, taking into account the positive effect of the internal resistance of the oil in the sliding bearings:

Isa KHALILOV, Beyali AHMEDOV, Anar HAJIYEV.
Study of the efficiency factor of sliding bearings of the new
constructive solution of multistage reducer

$$P_2^* = P_2 - \psi_{sb}^* P_2 = P_2(1 - \psi_{sb}^*) \tag{25}$$

If we take into account the friction loss when the gears are engaged (ψ_{ge}) and the friction loss in the roller bearings (ψ_{rb}), then the efficiency factor of the current mechanical system:

$$\eta^* = \frac{P_2^*}{P_1} = \frac{P_2(1 - \psi_{sb}^*)}{P_1} \tag{26}$$

$$\frac{\eta^*}{(1 - \psi_{sy}^*)} = \frac{P_2}{P_1} = 1 - \psi_{ge} - \psi_{rb}$$

from there

$$\eta^* = (1 - \psi_{ge} - \psi_{rb})(1 - \psi_{sb}^*) \tag{27}$$

Formulas (26) and (27) allows us to estimate the performance of the new three-stage reducer, as well as the energy loss in the transmission.

It is known that

$$1 - \psi_{ge} - \psi_{rb} = \eta_{ge} \cdot \eta_{rb} \tag{28}$$

$$(1 - \psi_{sb}^*) = \eta_{sb} \tag{29}$$

Then the efficiency factor of the new three-stage reducer:

$$\eta^* = \eta_{ge}^3 \eta_{rb}^2 \eta_{sb} \tag{30}$$

To quantify the internal resistance of the oil in the sliding bearings, we assume that the new constructive solution of reducer uses industrial oil И-30, and for this oil the dynamic viscosity at $60^0 C$ is $\mu_0 = 0,014\,Pa \cdot sec$. The power of the electric motor of the converting mechanism of the pumping unit is $P_M = 7,5kVt$, the rotational speed of its shaft is $n_M = 750\,min^{-1}$, so the angular velocity of the drive shaft of the reducer:

$$\omega_1 = \frac{\omega_M}{u_b} = \frac{\pi \cdot n_M}{30 \cdot u_b} = \frac{3,14 \cdot 750}{30 \cdot 1,6} = 49,06\,sec^{-1}$$

there $u_b = 1,6$ - is the transmission number of the belt drive applied in the converting mechanism of the pumping unit.

Assuming that the efficiency factor of the belt drive is $\eta_b = 0,96$, then the force on the gear shaft of the reducer:

$$P_1 = P_M \cdot \eta_b = 7,5 \cdot 0,96 = 7,2\,kVt$$

The new constructor assumes the diameter of the gear shaft under the bearing $d_1 = 50mm$, its length $l_1 = 50mm$, relative distance $\psi_1 = 0,002$, diameter of the drive shaft under the bearing $d_2 = 50mm$, its length $l_2 = 100mm$ and relative distance $\psi_2 = 0,003$. The coefficient of the total internal resistance of the oil in the sliding bearings is as follows:

$$\psi_{sy}^* = \frac{P_f}{P_1} = \frac{\pi \mu_0 \omega_1^2}{2P_1} \left(\frac{l_1 d_1^2}{\psi_1} \left(\frac{(1 + u_1^2)}{u_1^3} \right)^2 + \frac{l_2 d_2^2}{\psi_2} \left(\frac{(1 + u_2^2)}{u_2^2} \right)^2 \right) =$$

Isa KHALILOV, Beyali AHMEDOV, Anar HAJIYEV.
Study of the efficiency factor of sliding bearings of the new
constructive solution of multistage reducer

$$= \frac{3,14 \cdot 0,014 \cdot 49,06^2}{2 \cdot 7,2 \cdot 10^3} \left(\frac{0,05 \cdot 0,05^2}{0,002} \left(\frac{(1+4^2)}{4^3} \right)^2 + \frac{0,1 \cdot 0,05^2}{0,003} \left(\frac{(1+4^2)}{4^2} \right)^2 \right) =$$
$$= 0,007348(0,00441 + 0,0941) = 0,000724$$

If we take into account efficiency factor of gear drive $\eta_{ge} = 0,98$, efficiency factor of a pair of rolling bearing $\eta_{rb} = 0,99$, then the efficiency factor of new three-stage reducer:

$$\eta^* = \eta_{ge}^3 \eta_{rb}^2 (1 - \psi_{sb}^*) = 0,98^3 \cdot 0,99^2 (1 - 0,000724) = 0,9218$$

efficiency factor of reducer with classic construction:

$$\eta = \eta_{ge}^3 \eta_{rb}^4 = 0,98^3 \cdot 0,99^4 = 0,9041$$

Comparison of the efficiency of the new three-stage reducer with the efficiency of the classic three-stage reducer as a percentage:

$$\Delta\eta = \frac{\eta^* - \eta}{\eta} 100\% = \frac{0,9218 - 0,9041}{0,9041} 100\% = 1,96\%$$

Conclusions. As we can see, since in the new constructive solution of the gearbox the rotation direction of the sliding bearings and the rotation of the shafts coincide, the mutual displacement of the oil layers in the clearances of the sliding bearings, the partial contact of the roughness of the surfaces in contact with each other, and the displacement forces associated with the viscosity of the oil have a positive effect on the movement shafts and the efficiency factor of the mechanical system. Based on the results of calculations, it was determined that the efficiency factor of the new constructive solution of a three-stage reducer is about 2% higher than in classic reducers.

REFERENCES:

[1]. Vodeyko V.F., Efros D.G., Gear reducers (Russian). Moscow, MADI, 48 p., (2014).

[2]. Abdullaev A.H., Najafov A.M., Three-stage double-flow cylindrical gear, Patent №: 017053 B1, F16H 1/20 The Eurasian Patent Organization (EAPO), Moscow/Russia, Bulletin № 9, 4 p., (2012)

[3]. Najafov A.M., Abdullaev A.I., *About results of industrial testing of a three-stage double-flow reducer of the СКД 3-1,5-710 pumping unit.* Bulletin of NTU "KhPI". № 40, pp. 89-93, (2013).

[4]. Ivanov M.N., Finogenov V.A. Machine Elements (Russian). Moscow/Russia: "Visshaya shkola", 408 p., (2008).

[5]. Matlin M.M., Mozgunova A.I., Lebskiy S.L., Shandybina I.M., Basics of calculating parts and units of transport machines. Volgograd: VOLGTU, 251 p, (2010).

[6]. Chernavsky S.A., Sliding bearings. MASHGIZ, Moscow, 245 p., (1963).

[7]. Aristov A.I., Malysheva E.B., et al. Calculation of landings with a clearance (by the example of sliding bearings). MADI, 28 p., (2015).

[8]. Nazarenko Y.B., Hydrodynamics of sliding bearings and critical rotor speeds. Science, №3 (111), pp.16-18, (2017)

[9]. Balyakin V.B., Vasin V.N., Machine parts. Samara, 151 p., (2004)

THE INFLUENCE OF DELAYS IN ELASTICITY AND DAMPING ON AUTO-PARAMETRIC OSCILLATIONS

Alishir ALIFOV[1], Mikhail MAZUROV[2]

[1]Mechanical Engineering Research Institute of the Russian Academy of Sciences,
Moscow, Russia,
[2]Plekhanov University of Economics, Moscow, Russia

E-mail: a.alifov@yandex.ru[1], mazurov37@mail.ru[2]

Abstract. The interaction of self-oscillations and parametric oscillations under the influence of delayed elastic and damping forces in the presence of a limited power energy source in the system is considered. To construct solutions to a nonlinear system of equations, the direct linearization method was used, which contains the linearization accuracy parameter. Using this method, equations of non-stationary and stationary motions are obtained to determine the amplitude, phase of oscillations and the speed of the energy source. Based on the Routh-Hurwitz criteria, the stability of stationary modes of motion is considered and the stability conditions are derived. In order to obtain information about the effect of elastic delays and damping on the dynamics of the system, calculations were performed for various combinations of their values. The corresponding amplitude-frequency characteristics and a graph of the load on the energy source from the side of the oscillatory system are constructed.

Keywords: *self-oscillations, parametric oscillations, energy source, limited power, delay, elasticity, damping, method, linearization.*

Introduction. In many problems [1-9, etc.], it becomes necessary to take into account the phenomenon of hysteresis (delay). Among them, hysteresis can be noted: plastic in mechanics, ferromagnetic and dielectric in physics, in control problems, in biology, in automatic control, etc. The carriers of hysteresis are part of a more complex system and therefore should be considered together. At cyclically changing stresses, the maximum amplitude of which is significantly lower than the elastic limit, dynamic hysteresis is observed, which is caused by inelasticity or viscoelasticity. "In case of inelasticity, in addition to purely elastic deformation (corresponding to Hooke's law), there is a component that completely disappears when stress is removed, but with some delay, and with viscoelasticity, this component does not completely disappear with time" [Wikipedia]. The retardation effects appear depending on the yield and discontinuous deformation, specimen geometry, loading conditions and modes, as well as on the properties of the loading system. Hysteresis also occurs as a result of thermoelasticity, magnetoelastic phenomena, changes in the position of point defects, etc. The delay has a significant effect on the control process and the stability of the system, it can lead to oscillations in it, which arise, for example, in servo systems, regulators, rolling mills, etc. Therefore, the study of the effects caused by the influence of the delay is of great practical interest.

For the analysis of nonlinear systems with delay, approximate methods are used (Bogolyubov-Mitropol'skiy averaging, harmonic linearization, energy balance, etc.

[10-19]), which are characterized by significant labor and time costs depending on the type of nonlinearity characteristics. Large expenditures of labor and time are one of the main problems in the analysis of the dynamics of nonlinear systems. With reference to works [20-23], this is indicated in [24], where it is noted that this problem exists for the study of coupled oscillatory networks that play an important role in chemistry, biology, physics, electronics, neural networks, etc. The method of direct linearization (MDL), described in [25-31, etc.], is fundamentally different from these methods. The advantages of the MDL over the well-known methods of analyzing nonlinear systems are simplicity and the associated low (several orders of magnitude less) labor and time costs, the absence of laborious and complex approximations of various orders, the possibility of obtaining final design relations regardless of the specific type and degree of nonlinearity. Using the MDL, below we consider the effect of delays in elasticity and damping on mixed parametric and self-oscillations in the presence of a limited power source in the system that supports the functioning of the system.

Model. Consider the well-known model (Fig.1) of a mechanical frictional self-oscillating system [32-35]. Nonlinear differential equations describing its motion, taking into account the delays in elasticity and damping, have the form

$$m\ddot{x} + k_0\dot{x} + c_0 x = T(U) - bx\cos\nu t - k_\eta\dot{x}_\eta - c_\tau x_\tau \tag{1}$$

$$I\ddot{\varphi} = M(\dot{\varphi}) - r_0 T(U)$$

where $k_0 = const$, $c_0 = const$, $T(U)$ is a nonlinear friction force that depends on the relative velocity $U = V - \dot{x}$ and causes self-oscillations, $V = r_0\dot{\varphi}$, $\dot{x}_\eta = \dot{x}(t-\eta)$, $x_\tau = x(t-\tau)$, $\eta = const$, $\tau = const$, η and τ are delays, $r_0 = const$ is the radius of the point of application of the friction force $T(U)$, I is the total moment of inertia rotating parts, $M(\dot{\varphi})$ is the difference between the torque of the power source and the torque of the forces of resistance to rotation, $\dot{\varphi}$ is the speed of rotation of the engine.
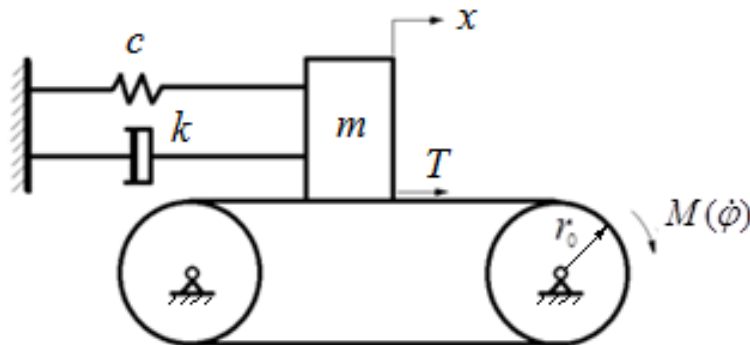

Fig.1. System model.

Let us imagine the friction force $T(U)$ with a widely used in practice falling characteristic of the coefficient of friction from the sliding speed, which was also

observed when considering the problem of measuring friction forces in space conditions [36]:

$$T(U) = T_0 \left[\operatorname{sgn} U + f(\dot{x}) \right], \qquad f(\dot{x}) = \sum_{n=0}^{3} \delta_n \dot{x}^n \qquad (2)$$

$$\operatorname{sgn} U = \begin{cases} 1 & \text{at} \quad U > 0 \\ -1 & \text{at} \quad U < 0 \end{cases}$$

Here T_0 is the normal reaction force, $T_0 \leq T(0) \leq T_0$, $\delta_0 = -\alpha_1 V + \alpha_3 V^3$, $\delta_1 = \alpha_1 - 3\alpha_3 V^2$, $\delta_2 = 3\alpha_3 V$, $\delta_3 = -\alpha_3$, α_1 and α_3 are constants.

Using the MDL [25-31], replace the nonlinear function $f(\dot{x})$ with a linear

$$f_*(\dot{x}) = B_T + k_T \dot{x} \qquad (3)$$

where B_T and k_T are the linearization coefficients.

The B_T and k_T coefficients are determined by the expressions

$$B_T = \delta_0 + N_2 \delta_2 \upsilon^2, \qquad k_T = \delta_1 + \delta_3 \bar{N}_3 \upsilon^2 \qquad (4)$$

Here $N_2 = (2r+1)/(2r+3)$, $\bar{N}_3 = (2r+3)/(2r+5)$, $\upsilon = \max|\dot{x}|$ and the r symbol represent the *linearization accuracy parameter*. As shown in [25], it can be selected from the interval (0, 2).

Taking into account (2) and (3), equations (1) take the form

$$m\ddot{x} + k_0 \dot{x} + c_0 x = T_0 (\operatorname{sgn} U + B_T + k_T \dot{x}) - bx \cos \nu t - k_\eta \dot{x}_\eta - c_\tau x_\tau \qquad (5)$$

$$I\ddot{\varphi} = M(\dot{\varphi}) - r_0 T_0 (\operatorname{sgn} U + B_T + k_T \dot{x})$$

The solution of the equation with linearization can be constructed by the *method of change of variables with averaging* [25], which makes it possible to consider stationary and non-stationary processes. In [25], for a linearized general equation, a standard form of relations for these processes was obtained. In accordance with this standard form, we can immediately write out the results of solving the first equation of (5), and for the second equation we use the averaging procedure described in [29].

Equation solutions. Note that there are two fundamentally different cases, determined by the characteristic of the friction force $T(U)$ at $U > 0$, $u \geq ap$ and $U < 0$, $u < ap$, where $u = r_0 \Omega$ and Ω is the average value of the speed $\dot{\varphi}$ of the energy source. To derive the relations for $u < ap$, we use the technique described in [34].

By the method of change of variables with averaging noted above, we have

$$x = a \cos \psi, \quad \dot{x} = -\upsilon \sin \psi, \quad \psi = pt + \xi \qquad (6)$$

where $\upsilon = ap$, $p = \nu/2$.

Taking into account $x_\tau = a \cos(\psi - p\tau)$, $\dot{x}_\eta = -\upsilon \sin(\psi - p\eta)$, we obtain from (5) the following equations for determining the non-stationary values of the amplitude a, phase ξ and velocity u:

a) $u \geq ap$:

$$\frac{da}{dt} = -\frac{1}{4pm}(2aA - ba \sin 2\xi)$$

$$\frac{d\xi}{dt} = \frac{1}{4pma}(2aE + ab\cos 2\xi) \tag{7,a}$$

$$\frac{du}{dt} = \frac{r_0}{I}\left[M(\frac{u}{r}) - r_0 T_0(1 + B_T)\right];$$

b) $u < ap$:

$$\frac{da}{dt} = -\frac{1}{4pm}\left[2aA - ba\sin 2\xi - \frac{8T_0}{\pi ap}\sqrt{a^2 p^2 - u^2}\right]$$

$$\frac{d\xi}{dt} = \frac{1}{4pma}(2aE + ab\cos 2\xi) \tag{7,b}$$

$$\frac{du}{dt} = \frac{r_0}{I}\left[M(\frac{u}{r}) - r_0 T_0(1 + B_T) - \frac{r_0 T_0}{\pi}(3\pi - 2\psi_*)\right]$$

Here $A = p(k_0 + k_\eta \cos p\eta - T_0 k_F) - c_\tau \sin p\tau$, $\quad E = m(\omega_0^2 - p^2) + c_\tau \cos p\tau$, $\quad \omega_0^2 = c_0/m$,
$\psi_* = 2\pi - \arcsin(u/ap)$.

Under the conditions $\dot{a} = 0$, $\dot{\xi} = 0$, $\dot{u} = 0$, equations of stationary motions are obtained from (7). In the case of $u < ap$, the amplitude of stationary oscillations is determined by the approximate expression $a \approx u/p$.

In the case of $u \geq ap$, the amplitude and phase of stationary oscillations are determined by the following expressions

$$A^2 + E^2 = 0.25b^2, \qquad tg\, 2\xi = -A/E \tag{8}$$

The stationary values of the velocity are found from the condition $\dot{u} = 0$, which gives the relation

$$M(u/r_0) - S(u) = 0 \tag{9}$$

Here the function $S(u)$ represents the load on the energy source and has the form

a) $u \geq ap \quad \rightarrow \quad S(u) = r_0 T_0(1 + B_T)$

b) $u < ap \quad \rightarrow \quad S(u) = r_0 T_0\left[(1 - B_T) + \pi^{-1}(3\pi - 2\psi_*)\right]$

The calculated stationary values of the amplitude are used to construct the $S(u)$ curve. The point (s) of intersection of the curves $M(u/r_0)$ and $S(u)$ determines the stationary value of the velocity u. In the case of $u < ap$, the expression of the load on the energy source $S(u)$ is simplified by taking into account the approximate equality $ap \approx u$ for the amplitude.

Stability of stationary oscillations. To test the stability of stationary motions, we compose equations in variations for (7), use the Routh-Hurwitz criteria, and obtain

$$D_1 > 0, \quad D_3 > 0, \quad D_1 D_2 - D_3 > 0 \tag{10}$$

where $D_1 = -(b_{11} + b_{22} + b_{33})$,

$D_2 = b_{11}b_{33} + b_{11}b_{22} + b_{22}b_{33} - b_{23}b_{32} - b_{12}b_{21} - b_{13}b_{31}$

$D_3 = b_{11}b_{23}b_{32} + b_{12}b_{21}b_{33} - b_{11}b_{22}b_{33} - b_{12}b_{23}b_{31} - b_{13}b_{21}b_{32}$

For $u \geq ap$, we have:

$$b_{11} = \frac{r_0}{I} \left[Q + r_0 T_0 (\alpha_1 - 3\alpha_3 u^2 - 3\alpha_3 N_2 a^2 p^2) \right] ; \quad b_{12} = -\frac{r_0^2}{I} 6\alpha_3 T_0 N_2 u a p^2 ; \quad b_{13} = 0$$

$$b_{21} = -\frac{1}{m} 3\alpha_3 T_0 a u ; \quad b_{22} = -\frac{1}{m} \alpha_3 T_0 \bar{N}_3 a^2 p^2 ; \quad b_{23} = -\frac{Ea}{pm}$$

$$b_{31} = 0 ; \quad b_{32} = 0 ; \quad b_{33} = -\frac{A}{pm}$$

where $h = 3(u_0^2 - u^2)/\bar{N}_3$; $u_0^2 = \alpha_1/3\alpha_3$; $N_2 = (2r+1)/(2r+3)$; $\bar{N}_3 = (2r+3)/(2r+5)$ and $Q = \frac{d}{du} M(\frac{u}{r})$.

In the case of $u < ap$, the coefficients b_{11}, b_{12}, b_{21}, b_{22} take the form:

$$b_{11} = \frac{r_0}{I} \left[Q + r_0 T_0 (\alpha_1 + 3\alpha_3 u^2 + 3\alpha_3 N_2 a^2 p^2) - \frac{2 r_0 T_0}{\pi \sqrt{a^2 p^2 - u^2}} \right]$$

$$b_{12} = -\frac{2 r_0^2 T_0 u}{I} \left[3 N_2 \alpha_3 a p^2 + \frac{1}{\pi a \sqrt{a^2 p^2 - u^2}} \right]$$

$$b_{21} = -\frac{T_0 u a}{m} \left[3\alpha_3 - \frac{2}{\pi a^2 p^2 \sqrt{a^2 p^2 - u^2}} \right]$$

$$b_{22} = -\frac{T_0}{m} \left[\alpha_3 \bar{N}_3 a^2 p^2 + \frac{2 u^2}{\pi a^2 p^2 \sqrt{a^2 p^2 - u^2}} \right]$$

Calculations. In order to obtain information about the effect of the delay on the oscillation modes, calculations were carried out with the parameters: $\omega_0 = 1 c^{-1}$, $m = 1 \text{kgf} \cdot c^2 \cdot \text{cm}^{-1}$, $b = 0.07 \text{kgf} \cdot \text{cm}^{-1}$, $c_0 = 0.05 \text{kgf} \cdot \text{cm}^{-1}$, $k_0 = 0.02 \text{kgf} \cdot c \cdot \text{cm}^{-1}$, $c_\tau = 0.05 \text{kgf} \cdot \text{cm}^{-1}$, $k_\eta = 0.06 \text{kgf} \cdot c \cdot \text{cm}^{-1}$, $T_0 = 0.5 \text{kgf}$, $\alpha_1 = 0.84 \text{ c} \cdot \text{cm}^{-1}$, $\alpha_3 = 0.18 \text{ c}^3 \cdot \text{cm}^{-3}$, $r_0 = 1 \text{cm}$, $I = 1 \text{kgf} \cdot c \cdot \text{cm}^2$. For the delays $p\eta$ and $p\tau$, the values from the interval $(0, 2\pi)$ were used, and in the linearization coefficients $N_2 = 3/5$, $\bar{N}_3 = 3/4$.

The amplitude-frequency curves $a(p)$ in Fig.2-4 were obtained at a speed $u=1.2$. The horizontal portions of the curves in Fig.4 reflect the dependence of $ap \approx u$. Curve *1* in all figures corresponds to the absence of delays ($k_\eta = 0$, $\eta = 0$, $\tau = 0$) and is shown for comparison. Oscillations with amplitudes are stable within the shaded and black-filled sectors for the steepness of the $Q = \frac{d}{du} M(u/r_0)$ characteristic of the power source. These sectors should be shown on the $S(u)$ load curve, but are shown on the amplitude curves for brevity. In the parts of the sectors filled with black, there is a rather weak stability, i.e. criteria (criterion) of stability (10) are fulfilled in the form $0.000X > 0$, where $X \leq 9$.
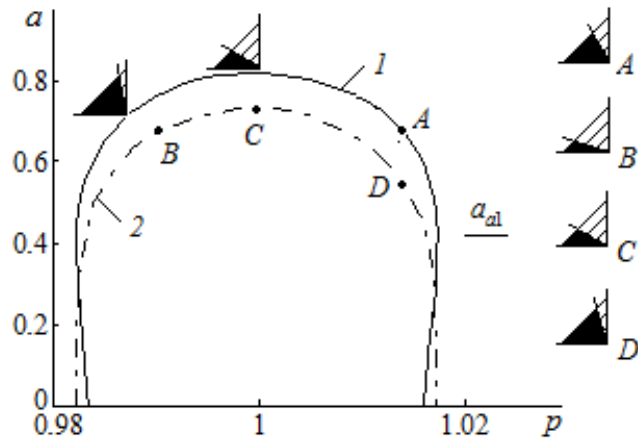
Fig.2. Amplitude-frequency curves at $\eta = 0$:
curve 1 – $\tau = 0$, curve 2 – $\tau = \pi/2$
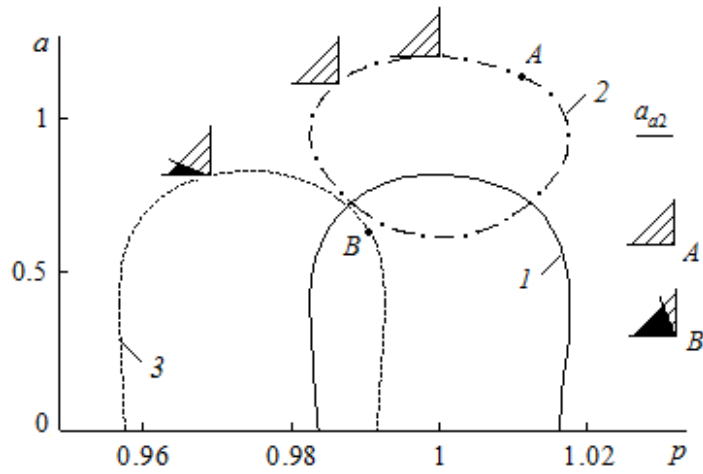

Fig.3. Amplitude-frequency curves at $\eta = \pi/2$:
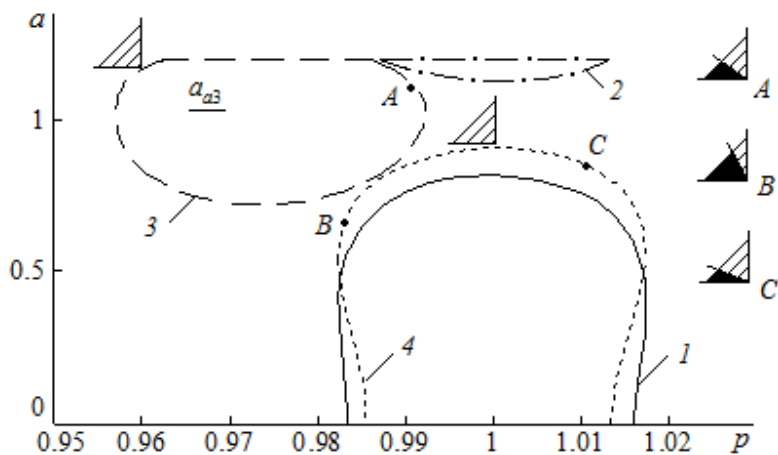*curve 2 – $\tau = \pi/2$, curve 3 – $\tau = \pi$*

Fig.4. Amplitude-frequency curves at $\eta = \pi$:
curve 2 – $\tau = \pi/2$, curve 3 – $\tau = \pi$, curve 4 – $\tau = 3\pi/2$

48

Conclusion. Containing the linearization accuracy parameter, the method direct linearization allows you to easily obtain solutions to a nonlinear system of differential equations and derive relationships for calculating the values of the amplitude and phase of oscillations, as well as the speed of the energy source. The calculations performed show that the combined action of various combinations of elasticity retardation and damping can strongly influence resonant oscillations. Under such action, the resonant region can shift in frequency. Depending on various combinations of lag values, the amplitude of the oscillations increase/decrease, the stability of the oscillations increase/decrease.

REFERENCES:

[1]. N.A.Babakov, A.A.Voronov, A.A.Voronova and others. *Theory of automatic control: Textbook for universities on spec. "Automation and telemechanics".* Part I. Theory of linear automatic control systems. Higher school, Moscow, Russia, (1986) (in Russian).

[2]. Encyclopedia of mechanical engineering. – URL: https://mash-xxl.info/info/174754/

[3]. Rubanik, V.P. *Oscillations of Quasilinear Systems with Time Lag.* Nauka, Moscow (1969) (in Russian).

[4]. Astashev V.K., Hertz M.E. *Self-oscillation of a visco-elastic rod with limiters under the action of a lagging force.* Mashinovedeniye, No.5, pp. 3-11, (1973) (in Russian).

[5]. Zhirnov B.M. *On self-oscillations of a mechanical system with two degrees of freedom in the presence of delay.* Journal of Applied Mechanics. Vol.9. No.10, pp. 83-87, (1973) (in Russian).

[6]. Abdiev F.K. *Delayed Self-Oscillations of a System with an Imperfect Energy Source.* Izv. Academy of Sciences of the Azerbaijan SSR. Series of physical, technical and mathematical Sciences, No.4, 134-139 (1983).

[7]. Semenov M.E. *Mathematical modeling of dynamical systems with hysteresis phenomena.* Dissertation by Doctor of Phys.-Math. Sciences. Voronezh (2003) (in Russian).

[8]. Zhou B. *Input delay compensation of linear systems with both state and input delays by adding integrators.* Systems and Control Letters. Vol.82, pp. 51-63, (2015).

[9]. Padhan D.G., Reddy B.R. *A new tuning rule of cascade control scheme for processes with time delay.*/ In Conference on Power, Control, Communication and Computational Technologies for Sustainable Growth, pp. 102-105, (2015).

[10]. Bogolyubov N.N., Mitropolsky Yu.A. *Asymptotic methods in the theory of nonlinear oscillations.* Nauka, Moscow, (1974) (in Russian).

[11]. I.I.Blekhman. *Oscillations of nonlinear mechanical systems.* Vibrations in technology: directory. Vol. 2. Engineering, Moscow (1979) (in Russian).

[12]. Zhuravlev V.Ph. and Klimov D.M. *Applied Methods in the Theory of Oscillations.* Nauka, Moscow (1988) (in Russian).

[13]. Migulin, V.V., Medvedev, V.I., Mustel E.R., Parygin V.N.; Ed. Migulin V.V. *Fundamentals of the theory of oscillations: Textbook. Management - 2nd ed.*, Nauka, Moscow, (1988) (in Russian).

[14]. Hayashi Ch. Nonlinear oscillations in physical systems. Princeton University Press, New Jersey (2014).

[15]. Moiseev N.N. *Asymptotic methods of nonlinear mechanics.* Nauka, Moscow, (1981) (in Russian).

[16]. Butenin, N.V., Neymark, Yu. I., Fufaev, N.A. *Introduction to the theory of nonlinear oscillations.* Nauka, Moscow, (1976) (in Russian).

[17]. Andronov A.A., Vitt A.A., Khaikin S.E. *Oscillation theory.* Nauka, Moscow, (1981) (in Russian).

[18]. Biderman, V.L. *The theory of mechanical vibrations: Textbook for universities.* High School, Moscow (1980) (in Russian).

[19]. Veretennikov V.G. *Stability and oscillations of nonlinear systems.* Nauka, Moscow (1984) (in Russian).

[20]. Acebrón J.A., et al. *The Kuramoto model: A simple paradigm for synchronization phenomena.* Reviews of Modern Physics, 77(1), 137-185 (2005).

[21]. Bhansali P., Roychowdhury J. *Injection Locking Analysis and Simulation of Weak-ly Coupled Oscillator Networks*, In: Li, P., et al., (eds.) Simulation and Verification of Electronic and Biological Systems, Springer Science+Business Media B.V., pp. 71-93 (2011).

[22]. Ashwin P., Coombes S., Nicks R. J. *Mathematical Frameworks for Oscillatory Network Dynamics in Neuroscience.* Journal of Mathematical Neuroscience, 6(2), 1-92 (2016).

[23]. Masoud Taleb Ziabari, Ali Reza Sahab, Seyedeh Negin Seyed Fakhari. *Synchronization New 3D Chaotic System Using Brain Emotional Learning Based Intelligent Controller.* International Journal of Information Technology and Computer Science (IJITCS), Vol.7, No.2, pp. 80-87 (2015). DOI: 10.5815/ijitcs.2015.02.10.

[24]. Gourary M.M., Rusakov S.G. *Analysis of Oscillator Ensemble with Dynamic Couplings.* AIMEE 2018. The Second International Conference of Artificial Intelligence, Medical Engineering, Education, 150-160 (2018).

[25]. Alifov A.A. *Methods of Direct Linearization for Calculation of Nonlinear Systems RCD.* Moscow (2015) (in Russian).

[26]. Alifov A.A. *Method of the Direct Linearization of Mixed Nonlinearities.* Journal of Machinery Manufacture and Reliability, Vol.46. No.2, 128-131 (2017). DOI: 10.3103/S1052618817020029 .

[27]. Alifov A.A., Farzaliev M.G., Dzhafarov Je.N. *Dynamics of a Self-Oscillatory System with an Energy Source.* Russian Engineering Research, Vol.38. No.4, pp. 260-262 (2018). DOI: 10.3103/S1068798X18040032.

[28]. Alifov A.A. *Calculating Mixed Forced and Self-Oscillations for Delayed Elastic Constraint and a Limited Power Energy Source.* Journal of Machinery Manufacture and Reliability, Vol.49, No.2, pp. 105-109, (2020). DOI: 10.3103/S1052618820020053.

[29]. Alifov A.A. *On the calculation of oscillatory systems with limited excitation by the methods of direct linearization.* Engineering and Automation Problems, No.4, 92-97 (2017).

[30]. Alifov A.A. *About Direct Linearization Methods for Nonlinearity.* Advances in Artificial Systems for Medicine and Education III. AIMEE 2019. Advances in Intelligent Systems and Computing. Vol. 1126. – P.105-114. Eds. Hu Z., Petoukhov S., He M. – Springer, Cham. (2020), DOI**:** https://doi.org/10.1007/978-3-030-39162-1_10 .

[31]. Alifov A.A. *Self-Oscillations in Delay and Limited Power of the Energy Source.* Mechanics of Solids, Vol.54, No.4, 607-613 (2019). DOI: doi.org/10.3103/S0025654419040150.

[32]. Kononenko V.O. *Excitation Limited Oscillation Systems.* Nauka, Moscow (1964) (in Russian).

[33]. Kononenko V.O. *Vibrating Systems with Limited Power-Supply.* Iliffe Books, London, (1969).

[34]. Alifov A.A., Frolov K.V. *Interaction of Nonlinear Oscillatory Systems with Energy Sources.* Hemisphere Publishing Corporation, New York, Washington, Philadelphia, London, (1990).

[35]. Tondl A. *On the interaction between self-exited and parametric vibrations.* Monographs and Memoranda, № 25. National Research Institute for Machine Design, Prague, (1978).

[36]. Bronovec M. A., Zhuravljov V.F. *On self-oscillations in systems for measuring friction forces.* Izv. Ros. Akad. Nauk, Mekh. Tv. Tela. No.3, 3-11, [Mech. Sol. (Engl. Transl.) 47 (3), 261-268 (2012)], (2012).

ANALYSIS AND MANUFACTURING OF 6 DoF HYBRID ROBOT MANIPULATOR FOR TELEOPERATION IN MEDICAL APPLICATIONS

Erkin GEZGIN

Izmir Katip Celebi University
Department of Mechatronics Engineering, Turkey

Email: erkin.gezgin@ikc.edu.tr

Abstract: Parallel to the rapidly developing technology, robot manipulators, whose areas of usage have continuously been expanded from the last periods of past century, have taken part in many different successful applications. Thanks to its increasing significance, nowadays medical science is one of the primary areas of those applications. Thus, this study targets mainly the field of medical science. Within the scope of this paper, six degrees of freedom hybrid robot manipulator with large workspace and adequate precision was introduced and equipped with dual actuators in its two Cartesian axes for possible haptic integration for the future. Target hybrid manipulator was designed in such a way that it can be used in various related medical applications such as teleoperations in robotic surgery, surgical navigation, dental and laparoscopic simulations. After the structural design part was completed, direct and inverse kinematic analysis procedures were carried out and by using rapid prototyping techniques the manipulator was manufactured.

Keywords: Hybrid Robot Manipulators, Teleoperation, Kinematic Analysis

1. Introduction. With the help of robot manipulators, wide range of robotic applications that are capable of haptic feedback from virtual or distant environments are continuously increasing in many areas for various user profiles. While utilizing novel algorithms in haptic control provide life like feedbacks, new manipulator designs offer larger workspaces and increased manipulation precision. Although related studies in the literature are mostly focused on control parts of the issue, design of a capable robot manipulator with sufficient degrees of freedom for predefined workspaces with respect to the given tasks and constraints should not be left unattended as it constitutes the most important part in this research area.

Wayne et al. [1] surveyed three different control algorithms that are related to the haptic manipulators in terms of interactions between humans and robotic devices and introduced their comparisons with each other. In their study authors created a bridge between the old and current developing control algorithms to emphasize the rapid development in the related literature. Hyung et al. [2] started their study by considering the negative effects of singularities in parallel manipulators on the haptic systems. In the light of their research, they proposed four task based and redundant control algorithms for the singularity problems of six degrees of freedom parallel haptic manipulator with four sub chains that was also designed by them. Also they compared the results of their algorithms in a simulation environment. Erwin et al. [3] designed force controlled haptic planar manipulator for the movement control analysis of human arm. In their study they reduced the contact instability problem by using servo based control system on the lightweight but stiff manipulator. Their manipulator and the controller design were tried on a subject that performs a position based task and

Erkin GEZGIN.
Analysis and Manufacturing of 6 DoF Hybrid Robot
**Manipulator for Teleoperation in Medical Applications**

the results were introduced. Schouten et al. [4] designed a torque controlled manipulator with haptic controller to specify the dynamics of human wrist joint. In their study the dynamics of the human wrist joint and effects due to neurological dysfunctions were measured under virtual conditions. Dede et al. [5] designed six degrees of freedom haptic hybrid robot manipulator that is capable of displaying point type contact. Authors reconfigured the R-Cube manipulator for the translational part of the system in terms of dimensions and orientations in order to comply with the requirements of the haptic system design criteria. The most important merits of the system are introduced as its compactness and high stiffness. In their study authors also presented the integration of the hybrid manipulator mechanism with control interface. Ryu et al. [6] designed six degrees of freedom modular manipulator in order to control a mobile system by means of teleoperation. Their introduced design has dual parallel manipulators with individual three degrees of freedom that are attached each other to form six degrees of freedom modular manipulator system. The system is capable to be used in the control of both planar and spatial tasks in various applications by utilizing only the necessary actuators and the manipulator section to reduce the CPU loads during calculations. Pinskier et al. [7] proposed a flexure based haptic enabled modular manipulator for micromanipulation tasks. In their study they investigated and verified the performance of an experimental 2 degrees of freedom configuration. Tian et al. [8] introduced the design of six degrees of freedom precision positioning system that was formed by the assembly of dual three degrees of freedom individual systems operated by piezoelectric actuators. In their study motion with high precision capability was obtained.

After the investigation of brief literature survey, it can be easily seen that, usage of robot manipulators for various fields are increasing. Throughout the literature, each study has tried to overcome the mechanical and software constraints by proposing new manipulator designs along with new control schemes to achieve precise, comfortable and efficient manipulation. Considering the advances in the field, this study tries to introduce six degrees of freedom new hybrid manipulator design that is formed by the assembly of three degrees of freedom serial spherical and three degrees of freedom parallel Cartesian manipulators for the medical applications. Cartesian part of the manipulator is modified by considering R-Cube [9] Cartesian parallel manipulator design in order to decrease the total number of dyads to achieve small footprint and comfortable manipulation in its workspace. While the semi-decoupled nature of the manipulator renders kinematic analysis problems to be solved easier, it also provides easy solutions to control problems. Although the study does not cover haptic feedback control, the manipulator is equipped with two actuators for future haptic integration. Throughout the study, structural design of the manipulator was introduced along with its direct and inverse kinematic analysis tasks. Also the manufacturing steps were shown along with the first manipulator prototype.

2. Structural Design and Synthesis. As mentioned in previous section the main aim of this study is to design a robot manipulator that will be used for the teleoperation tasks in medical applications such as robotic surgery, surgical navigation, dental

Erkin GEZGIN.
Analysis and Manufacturing of 6 DoF Hybrid Robot
Manipulator for Teleoperation in Medical Applications

and laparoscopic simulations. In the light of this aim, prior to the structural synthesis, design constraints of the task were specified as below.

• The end effector of the robot manipulator should be capable of mimicking all of the rigid body motions in space to ensure adequate teleoperation control.

• In order to utilize the robot manipulator for various different tasks, its overall workspace should be large and singularity free.

• Kinematic structure of the robot manipulator should be able to adapt various different applications without any modifications.

• Structure of the manipulator should be as simple as possible to render the kinematic analysis and control tasks easier.

• As the manipulator will be utilized for medical applications, it should have a structure that provides an adequate precision.
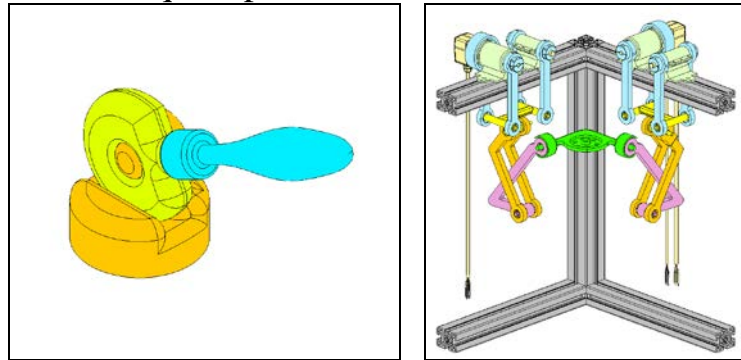
Fig. 1. a) Three Degrees of Freedom Serial Spherical Manipulator Responsible for Orientations,
b) Three Degrees of Freedom Cartesian Manipulator Responsible for Orientations
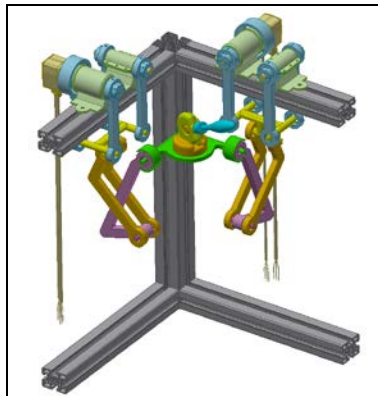

Fig. 2. Designed Six Degrees of Freedom Hybrid Robot Manipulator

Considering the criterions above, structure of the manipulator was determined to be hybrid. The overall system was decided to be designed in a way that three degrees of freedom Cartesian parallel manipulator section is responsible for translations while its three degrees of freedom serial spherical manipulator section is responsible for orientations. Thus the overall degrees of freedom become six. In order to fulfil the design constraints in Cartesian space, structure of the R-Cube parallel manipulator was modified so that Cartesian part of the final manipulator has two dyads instead of three. Although removing the dyad that is responsible for the z translation from the manipulator cancelled its decoupled motion in z axis, the hybrid manipulator gained a larger workspace and a smaller footprint (Figure 1-2). In accordance with the possi-

Erkin GEZGIN.
Analysis and Manufacturing of 6 DoF Hybrid Robot
Manipulator for Teleoperation in Medical Applications

ble haptic integration for future, the manipulator was equipped with dual actuators that are responsible for decoupled x and y translations. Moreover to be able to inspect z translation, single encoder was attached to one of the dyads.

While it is clear that, the serial part of the hybrid manipulator is three degrees of freedom, the mobility of the Cartesian section can be calculated by using the formulation [10] introduced below for the Cartesian manipulators.

$$M = (\lambda + 3) + \sum_{i=1}^{c_i}(d_i - D) + \sum_{i=1}^{c_i}(f_i - \lambda_i) + q - j_p \qquad (1)$$

Where in equation 1, λ is the space or subspace number, D is the dimension of the vectors in Cartesian space, d_i represents the dimensions of the vectors on the subspaces of the structural groups on the related leg, f_i is the total degrees of freedom of all joints in related leg, q is the number of excessive links, j_p is the number of passive degrees of freedoms, and c_i is the total number of legs. If the variables of this mobility equation are evaluated with respect to the designed manipulators Cartesian section, the mobility will be calculated as three.

$$M = (4+3) + (2-3) + (2-3) + (7-5) + (7-5) + 0 - 6 = 3$$

When the overall hybrid manipulator is considered, it can easily be seen that the kinematic structure of the manipulator consists of three closed loops, 17 revolute joints, and 15 links including the ground (Figure 3).
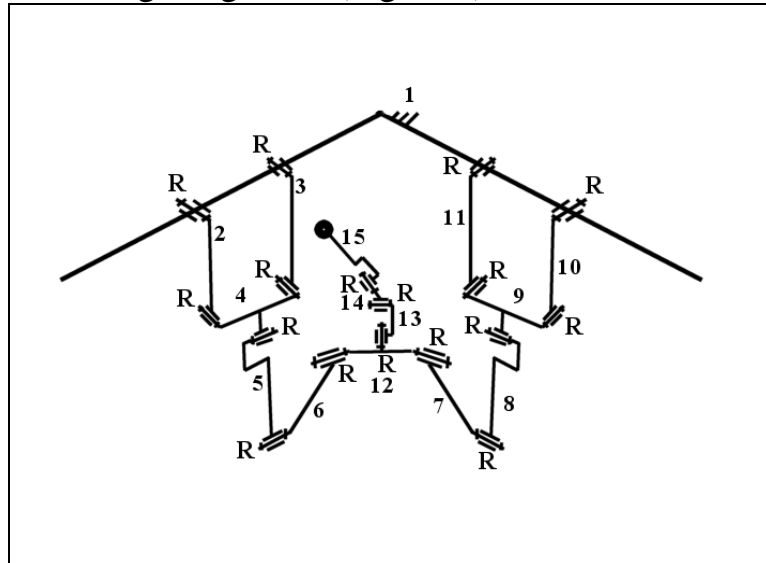

Fig. 3. Simple Kinematic Structure of Designed Hybrid Manipulator

3. Kinematic Analysis. This section is devoted to the direct and inverse kinematic analysis of the proposed hybrid manipulator. As the kinematic analysis of serial spherical section is straight forward and known, only Cartesian part of the manipulator will be considered.

3.1. Direct Task. Section view of the Cartesian part of the hybrid manipulator from the x-z plane is shown in figure 4 by revealing all its construction parameters and variables. Point P on the platform is taken so that it locates at the intersection of the three revolute axis of the serial spherical manipulator section.
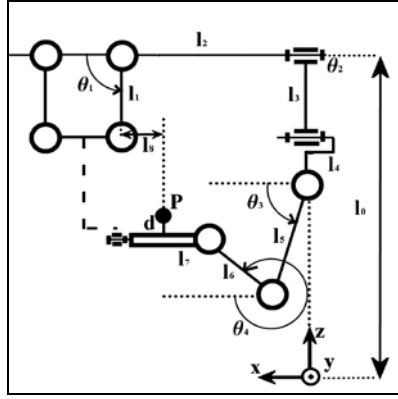
Erkin GEZGIN.
Analysis and Manufacturing of 6 DoF Hybrid Robot
Manipulator for Teleoperation in Medical Applications

Fig. 4. Section View of the Cartesian Part of The Hybrid Manipulator from the x-z Plane

As the translations on x and y axes are decoupled, the x and y coordinates of the P point on the platform can be easily calculated by the equations below.

$$P_x = l_2 + l_1 \cos \theta_1 - l_8$$
$$P_y = l_2 - l_3 \cos \theta_2 - l_8$$
(2)

It can be easily seen from the equation 2 that x and y coordinates of the point P on the platform depends only the variable angles θ_1 and θ_2 respectively. However, due to the modified Cartesian part, z coordinate of point P should be calculated in a more complex manner.

$$P_z = l_0 - (l_3 \sin \theta_2 + l_4 + l_5 \sin \theta_3 + l_6 \sin \theta_4 - d)$$
(3)

As seen in equation 3, z coordinate of the point P on the platform depends on four individual variable angles (θ_1, θ_2, θ_3, θ_4), yet as the Cartesian section of the manipulator has three degrees of freedom, one of the dependent variables should be eliminated from the equation. From this point of view in order to eliminate the selected parameter θ_4 from the equation 3, x coordinate of the point P will be written in another form.

$$P_x = l_5 \cos \theta_3 + l_6 \cos \theta_4 + l_7$$
(4)

When the x coordinates of point P in equation 2 and 4 are equalized,

$$\cos \theta_4 = K_1, \ K_1 = \frac{(l_2 + l_1 \cos \theta_1 - l_8 - l_5 \cos \theta_3 - l_7)}{l_6}$$
(5)

equation 5 will be obtained. Also by using equation 3,

$$\sin \theta_4 = A_1 - K_2, \ A_1 = -\frac{P_z}{l_6},$$

$$K_2 = \frac{(-l_0 + l_3 \sin \theta_2 + l_4 + l_5 \sin \theta_3 - d)}{l_6}$$
(6)

equation 6 can be written as above. If the squares of the equation 5 and 6 are taken and added together side by side,

$$A_1^2 - 2K_2 A_1 + K_3 = 0, K_3 = K_1^2 + K_2^2 - 1$$
(7)

equation 7 without the dependent variable θ_4 will be obtained. If the quadratic equation is solved for the parameter A_1,

Erkin GEZGIN.
Analysis and Manufacturing of 6 DoF Hybrid Robot
Manipulator for Teleoperation in Medical Applications

$$A_{1.1}, A_{1.2} = \frac{2K_2 \pm \sqrt{4K_2^2 - 4K_3}}{2} \tag{8}$$

two solutions will be found. Using these solutions, two distinct solutions for the z coordinate of point P can be calculated.

$$P_{z1} = -l_6 A_{1.1}$$
$$P_{z2} = -l_6 A_{1.2} \tag{9}$$

At this point it should be noted that, if the system is being used in the upper section of the workspace, the z coordinate of point P should be taken from the solutions that has the larger value and if the system is being used in the lower section of the workspace, the z coordinate of point P should be taken from the solution that has the smaller value.

3.2. Inverse Task. Similar to the direct task as the translations on x and y axes are decoupled, variable angles θ_1 and θ_2 can be easily calculated by using the given values of x and y coordinates of point P.

$$\theta_1 = \cos^{-1} \frac{P_x - l_2 + l_8}{l_1}$$

$$\theta_2 = \cos^{-1} \frac{P_y - l_2 + l_8}{l_3} \tag{11}$$

In order to find the variable angle θ_3 by using the given value of z coordinate of point P, θ_4 should be eliminated by utilizing the equations 3 and 4.

$$l_6 \sin \theta_4 = R_1 - l_5 \sin \theta_3, \quad R_1 = l_0 + d - l_3 \sin \theta_2 - l_4 - P_z \tag{12}$$

$$l_6 \cos \theta_4 = R_2 - l_5 \cos \theta_3, \quad R_2 = P_x - l_7 \tag{13}$$

When the squares of equation 12 and 13 are taken and added side by side, a single equation is obtained that is dependent on the variable θ_3.

$$R_1 \sin \theta_3 + R_2 \cos \theta_3 = R_3, \quad R_3 = \frac{R_1^2 + R_2^2 + l_5^2 - l_6^2}{2l_5} \tag{14}$$

If $\cos \theta_3$ is replaced with $\sqrt{1 - \sin^2 \theta_3}$ in equation 14, equation below will be formed.

$$(R_1^2 + R_2^2) \sin^2 \theta_3 - 2R_1R_3 \sin \theta_3 + (R_3^2 - R_2^2) = 0 \tag{15}$$

Utilizing equation 15, value of $\sin \theta_3$ can be calculated easily.

$$(\sin \theta_3)_{1.2} = \frac{2R_1R_3 \pm \sqrt{4R_1^2R_3^2 - 4(R_1^2 + R_2^2)(R_3^2 - R_2^2)}}{2(R_1^2 + R_2^2)} \tag{16}$$

Finally using equation 16, θ_3 can be calculated.

$$(\theta_3)_{1.2} = \sin^{-1} \frac{2R_1R_3 \pm \sqrt{4R_1^2R_3^2 - 4(R_1^2 + R_2^2)(R_3^2 - R_2^2)}}{2(R_1^2 + R_2^2)} \tag{17}$$

4. Prototype Manufacturing. After the completion of the kinematic analysis and simulation runs, manufacturing of the hybrid robot manipulator was carried out. All of the links of the designed manipulator was printed by using rapid prototype that uti-

Erkin GEZGIN.
Analysis and Manufacturing of 6 DoF Hybrid Robot
Manipulator for Teleoperation in Medical Applications

lizes ABS-Plus material. Also the manipulator frame was constructed by aluminum profiles to reduce the overall weight of the system (Figure 6).
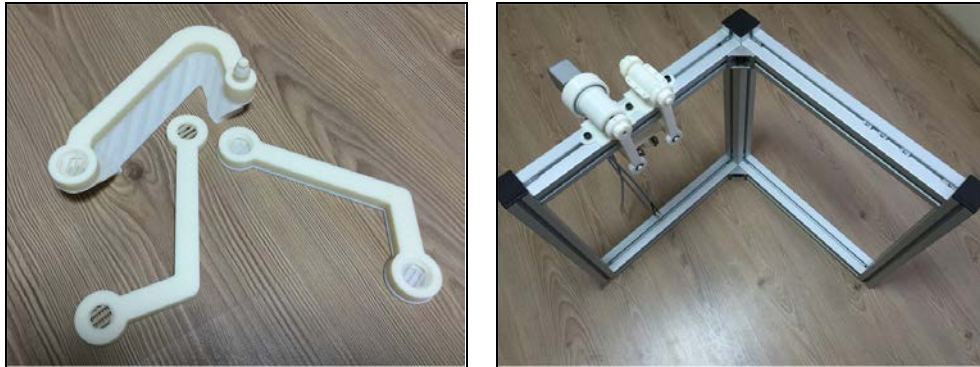

Fig. 6. Manipulator Links that are Printed oh Rapid Prototyper and the Aluminum Manipulator Frame

As mentioned before due to possible haptic feedback integration to the manipulator for future, two of its translation axes were equipped with brushless Maxon actuators with hall effect sensors and encoders (Figure 7).

Fig. 7. Brushless Maxon Actuators and the Detail of the Passive Revolute Joint

In order to be able to inspect the z translation of the system single Maxon HEDL-5540 encoder was attached to a joint located on one of the dyads of the manipulator (Figure 8) to measure the variable θ_3 (Figure 4).

Fig. 8. Maxon HEDL-5540 encoder

Overall prototyped hybrid manipulator can be seen in Figure 9 with its Cartesian Part and the attached serial part on the platform.

Erkin GEZGIN.
Analysis and Manufacturing of 6 DoF Hybrid Robot
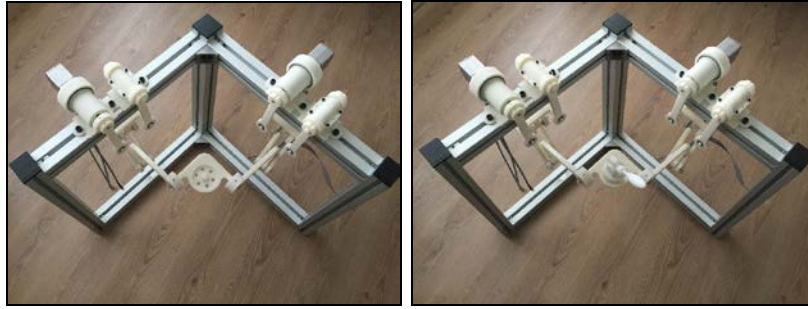**Manipulator for Teleoperation in Medical Applications**

Fig. 9. Prototype of the Hybrid Manipulator

5. Conclusions. Throughout this paper six degrees of freedom hybrid manipulator with large workspace and low footprint was proposed and manufactured for medical applications. Hybrid structure was formed by using three degrees of freedom modified R-Cube Cartesian manipulator for translations and attached on its platform, three degrees of freedom serial spherical manipulator for orientations. The direct and inverse tasks of the Cartesian part of the proposed manipulator were introduced along with the equations. As the manipulator was equipped with dual brushless actuators in its Cartesian part, possible haptic integration will be considered in future studies.

REFERENCES:

[1]. Wayne J.B., Davin K.S., *Reach out and touch someone: controlling haptic manipulators near and fa*r, Annual Reviews in Control 28, 87-95, (2004).

[2]. Hyung W.K., Jae H.L., Il H.S., Byung-Ju Y., *Comparative study and experimental verification of singular-free algorithms for a 6 DOF parallel haptic device*, Mechatronics 15, 403-422, (2005).

[3]. Erwin de V., Alfred C.S., Frans C.T. van der Helm, Piet C.T., Guido G.B., *A force-controlled planar haptic device for movement control analysis of the human arm*, Journal of Neuroscience Methods 129, 151-168, (2003).

[4]. Alfred C.S., Erwin de V., Bob van H., Frans C.T. van der H., *Design of a torque-controlled manipulator to analyse the admittance of the wrist joint*, Journal of Neuroscience Methods 154, 134–141, (2006).

[5]. Bilgincan T., Gezgin E., Dede M.I.C., *Integration of the hybrid-structure haptic interface: HIPHAD v1.0.* In Proceedings of the International Symposium of Mechanism and Machine Theory, 267-284, (2010).

[6]. Dongseok R., Jae-Bok S., Changhyun C., Sungchul K., Munsang K., D*evelopment of a six DOF haptic master for teleoperation of a mobile manipulator*, Mechatronics 20, 181-191, (2010).

[7]. Pinskier J., Shirinzadeh B., Clark L., Design, development and analysis of a haptic-enabled modular flexure-based manipulator, Mechatronics, http://dx.doi.org/10.1016/j.mechatronics.2016.10.004

[8]. Kunhai C., Yanling T., Fujun W., Dawei Z., Xianping L., and Shirinzadeh B., *Design and control of a 6-degree-of-freedom precision positioning system*, Robotics and Computer-Integrated Manufacturing 44, 77-96, (2017).

[9]. Weimin L., Gao F., Zhang J., R-CUBE, *a decoupled parallel manipulator only with revolute joints*, Mechanism and Machine theory 40.4, 467-473 (2005).

[10].Alizade R.I, Bayram C., Gezgin E., *Structural synthesis of serial platform manipulators*, Mechanism and Machine Theory 42.5, 580-599, (2007).

ENERGY EFFICIENT AUTONOMOUS LOWER LIMB EXOSKELETON FOR HUMAN MOTION ENHANCEMENT

Nazim MIR-NASIRI[1], Hudyjaya SISWOYO JO[2]

[1]Electrical and Electronic Engineering Department,
Nazarbayev University, Astana, Republic of Kazakhstan,
[2]H.Siswoyo Jo: Swinburne University of Technology, Sarawak, Malaysia

E-mail: nazim.mir-nasiri@nu.edu.kz[1], hsiswoyo@swinburne.edu.my[2]

Abstract: The paper describes conceptual design, control strategies and partial simulation for a new fully autonomous lower limb wearable exoskeleton system for human motion enhancement that can support its weight and increase strength and endurance. During the last decade, researchers have focused on the development of lower limb exoskeletons for power augmentation for military or medical assistance. Various problems remain to be solved where the most important is the creation of a power and cost efficient system that will allow an exoskeleton to operate for extended periods without being frequently recharged. The designed exoskeleton is enabling to decouple the weight/mass carrying function of the system from the forward motion function which reduces the power and size of propulsion motors and thus the overall weight, cost of the system. The decoupling takes place by blocking the motion at knee joint by placing passive air cylinder across the joint. The cylinder is actuated when the knee angle has reached the minimum allowed value to bend. The value of the minimum bending angle depends on usual walk style of the subject. The mechanism of the exoskeleton features a seat to rest the subject's body weight at the moment of blocking the knee joint motion. The mechanical structure of each leg has six degrees of freedom: four at the hip, one at the knee and one at the ankle. Exoskeleton legs are attached to subject legs using flexible cuffs. The operation of all actuators depends on the amount of pressure felt by the feet pressure sensors and knee angle sensor. The sensor readings depend on actual posture of the subject and can be classified in three distinct cases: subject stands on one leg, subject stands still on both legs and subject stands on both legs but transit its weight from one leg to other. This exoskeleton is power efficient because electrical motors are smaller in size and did not participate in supporting the weight like in all other existing exoskeleton designs.

Keywords: Energy efficient system, exoskeleton, motion enhancement, robotics.

Introduction. EXOSKELETON for human performance enhancement are wearable devices that can support and assist the user besides increasing their strength and endurance. The lower limb exoskeletons are now applied to several fields, including power augmentation for the military [1] or medical assistance [2], and rehabilitation [3]-[5]. In such devices human provides control signals while the exoskeleton actuators provide required power for performing the task. A distinctive characteristic of exoskeletons compared to other robotic interfaces with haptic feedback is their close physical and cognitive coupling between the robot and the user [6]. In such design, the physical human-robot interfaces were developed, i.e. the mechanical and sensory components that mediate the transfer of physical interaction between the user and the exoskeleton [7].

On lower extremity exoskeletons, most previous researchers paid their attention to developing walking aid systems for gait disorder persons or aged people [8],[9]. One of those systems is HAL (Hybrid Assistive Leg) developed by Yoshiyuki Sankai of University of Tsukuba was aimed at assisting human leg muscles during walking [10]. The system was based on electromyography (EMG) sensing of human muscles

as the primary drive signals. The development resulted in several versions of HAL with the latest HAL-5 in 2009 [11]. The exoskeleton was motor powered on the hip and knee joints, leaving other joints free. The significance of their design is the implementation of EMG sensing which detects muscle activities before actual limb movement. Motor driven joints approach was taken by other researches as well [12]. The developed Berkeley Lower Extremity Exoskeleton (BLEEX) was aimed at enhancing human strength and endurance for payload transport [13], [14]. The exoskeleton incorporates hydraulic actuation on all three sagittal joints and two coronal joints on the hip with all others joints free. The overall control design of BLEEX was to minimize interface between human and machine. Therefore, there was no sensor in direct measurement of human leg but includes all required sensors for determining the dynamics of the exoskeleton. The control system monitors the dynamics of the exoskeleton to determine operator's intention of motion. The significance of BLEEX is of the complex control network distributed throughout the exoskeleton and a custom designed onboard engine to power the hydraulic actuation system. Hydraulic actuation was implemented by various researchers. The ECUST Leg Exoskeleton Robot (ELEBOT) designed at East China University of Science and Technology (ECUST) shares the similar design goal as BLEEX but with a simplified system [15]. ELEBOT has the same approach of using hydraulic system as joint actuation. However, it was identified that only the knee joints would require substantial actuation support and therefore leaving all other joints free. The control of ELEBOT also came close to that of BLEEX by only monitoring stance phase and torque generated on the hydraulic actuators.

While the above exoskeleton designs require substantial power for operation on low efficiency, an exoskeleton design at Massachusetts Institute of Technology (MIT) attempted to lower the power requirement for load carrying [16]. The exoskeleton has only series elastic actuation at hip sagittal joints, variable damper at the knee joints and spring at ankle sagittal joints. The control is based on a state machine and monitors forces and orientation of the exoskeleton to determine the states. The Walking Assist Device designed at Honda Research and Development aims at increasing the lower extremity endurance of the elderly and those with weak legs [17]. By partially supporting the upper body weight, the user bears less weight on the lower limbs and requires less energy for motion. The device was a pair of non-anthropomorphic mechanical limbs attached to a seat. The whole device was fixed between the user's legs during operation. The walking assist device was only powered by electric motor at each of the knee joints and incorporates only pressure sensors beneath the shoes of the device. The control monitors user's weight applied on the pressure sensors and provides required force on both knees to achieve the predetermined weight reduction on both of the user's legs.

Various problems remain to be solved, the most daunting being the creation of a power and cost efficient system that will allow an exoskeleton to operate for extended periods without being frequently plugged into external power. The paper presents a conceptual design and partial simulation of a new exoskeleton that will enable to decouple the weight/mass carrying function of the system from the forward motion

control which will reduce the power and size of propulsion motors and thus reduce the overall weight, cost and required electrical power for the system. Such lighter and cheaper devices are currently important engineering research area in medicine and military [18].

Mechanical structure of the exoskeleton. Fig. 1 shows the conceptual sketch of the proposed exoskeleton structure in Solid Works. In the figures seat 1 is there to rest subject's body and support its weight. Each exoskeleton leg has four degrees of freedom: two at the hip 2, one at the knee 3 and one at the ankle 4 to allow legs forward and lateral motions. Cushioned seat 1 in between subject crotch is connected to two parallel rigid pipes 5 at the back the object. A back panel 6 mounted onto the rigid pipes serves as a platform for control and power supply mounting. At hip level, the two parallel rigid pipes extend out to the two hip coronal joints. The link then continues to both sides of the hip 2 where sagittal and transverse joints are located, subsequently to the knee joints 3 and through the ankle joints 4 to the ground. Both exoskeleton legs are attached to subject legs using flexible cuffs 7. Single degree four-bar linkage mechanism 8 with rotary joints at the hip level provides hip-centered lateral rotation of the exoskeleton leg around vertical axis. The remaining three single-degree parallel axes rotary joints at the hip 2, knee 3 and ankle 4 provide freedom of flexion at the joints. Pneumatic cylinders 9 are used to block the motion at the knee joints 3 when necessary to support the weight.
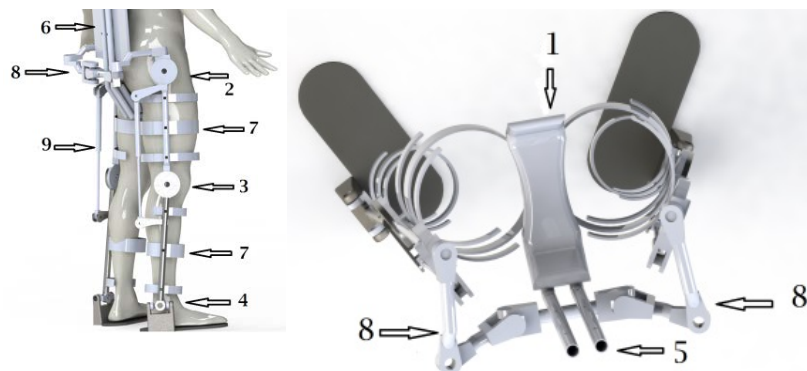

Fig. 1. Components of the exoskeleton

Fig. 2 shows schematic diagrams of the exoskeleton. In these figures 1 are adjustable telescopic members of the exoskeleton; 2 are dummy pneumatic cylinders that are able to inhibit the motion at the knee joints; 3 and 4 are the sensors to detect motion of subject thigh and shank; 5 are springs to support feet 6 of the exoskeleton; 7 and 8 are flexible belts to fasten exoskeleton to the subject thigh and shank. In the figures M_1 and M_2 are motors driving the hip and knee joints of each leg; C_1 and C_2 are solenoid valves of the pneumatic cylinders 2 that are able to inhibit motions at the knee joints; S_1 and S_2 are flexible strips 3 and 4 with bonded strain gages that are able to sense the tiny motions of subject limbs; F_1 and F_2 are foot pressure sensors to sense the amount of pressure applied by the ground on the exoskeleton sole 6 during the walk. The pressure at the exoskeleton sole is generated due to the transmission of the weight forces via mechanical structure to the ground while the subject is resting on the seat.
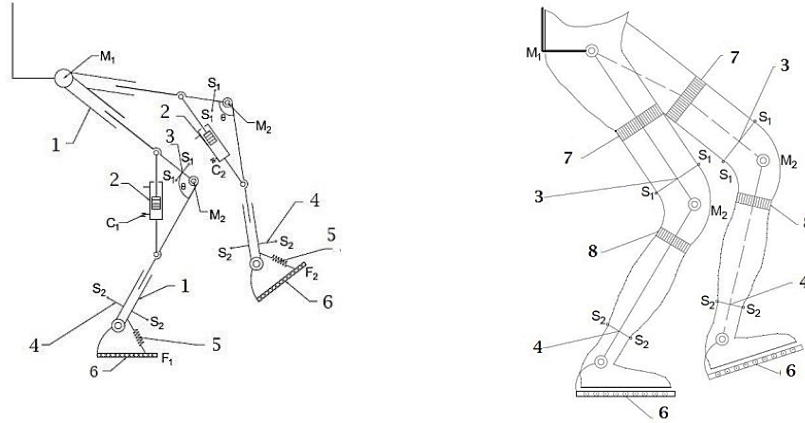
Fig. 2. Schematic drawing of the exoskeleton

Human-Machine Interfacing and Control. The operation of all actuators, i.e. hip joint motors M1, Knee joint motors M2 the knee motion inhibiting cylinders of solenoid valves C1 and C2, depends on the amount of pressure felt by the feet pressure sensors F1 and F2 (Fig. 2). The pressure on the feet depends on actual posture of the subject and can be classified in three distinct cases. If (case 1, Fig.3b) the subject is standing on one leg and the knee motion is inhibited, then the total subject body weight P_b *is resting on the seat 1 (Fig.1) and* the weight is fully transmitted via stationary leg structure to the ground. The expected pressure reading from the corresponding foot sensors F (Fig. 4) will be at its maximum possible value $P=P_b$. However, the reading from other foot pressure sensor will be at zero value because it is not in touch with the ground. If (case 2, Fig. 3a) the subject stands still on both legs then the total subject body weight is almost equally shared by both leg structures and the expected pressure reading from both feet sensors will be about half of the maximum possible value $P=P_b/2$. If (case 3, Fig. 3c, d) the subject is in the stage of transiting the weight from, e.g. leg 1 to leg 2 while standing on both legs, then the reading from sensor F_1 will gradually reduce from its half value $P_b/2$ to zero while the reading from sensor F_2 will gradually increase from its half value $P_b/2$ to its maximum possible value P_b. The pressure reading P at the shoe-ground sensor F is due to both object's and exoskeleton's weights.
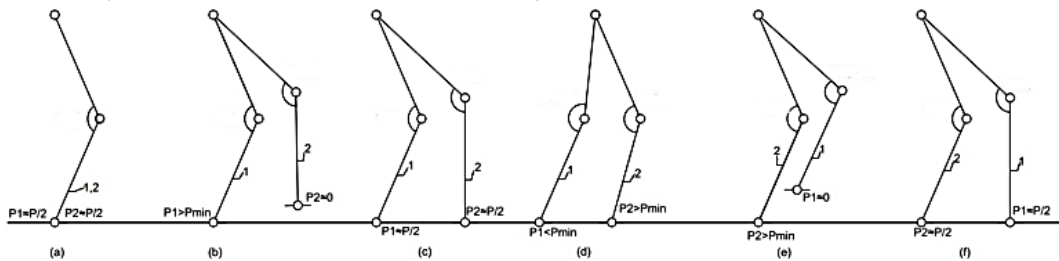

Fig. 3 Gaits of the exoskeleton

Several rules have been established to control the operation of the actuators during the subject walk. The first rule establishes a condition when the knee joint motion has to be inhibited, i.e. should be blocked by cylinder. Simultaneously, the hip and knee motors M_1 and M_2 have to be deactivated. At this condition the object puts its one foot on the ground and prepares to move the body in forward direction (leg 2 in Fig.3c). It is exactly the case when the exoskeleton is ready to carry the

weight with no assistance from the leg muscles and the deactivated motors. The signal to initiate this action comes from the respective foot sensor, i.e. when the reading from the sensor is $P>0$ and it is growing. The cylinder is actuated and the motors deactivates when the contact with the ground is confirmed. This condition implies a stilt type of walk when the object's weight rests on the "rigid" leg while the object takes a step forward with another leg.

The second rule establishes a condition when the knee motion is unblocked, i.e. cylinder is deactivated and respective hip and knee motors M_1 and M_2 have to be reactivated instead. Obviously, it is the case when the reading of pressure sensors $P=0$, i.e. the foot is not in touch with the ground. Alternatively, if the foot is in touch with the ground it depends on gradually decreasing pressure signal from the foot sensors and the minimum allowed pressure value P_{min} that should initiate this action. At this condition the exoskeleton leg mechanism is ready to follow the intended motion of the object leg and to take a new step without hindering the leg motion (leg 1 in Fig.3d). Motors M_1, M_2 and flexible sensors S_1 and S_2 are used to execute this action (Fig. 2).

Based on the rules discussed above, the following control strategy for the walk is proposed:

• Motors M_1 and M_2 of each leg are actuated only and only if the pressure reading from the corresponding pressure sensors at the foot either zero or keeps decreasing until $P \leq P_{min}$ (second rule) in order to pick up the leg from the ground and take a step

• Cylinder's solenoid valves C_1 and C_2 are actuated only and only if the pressure reading from the corresponding pressure sensors at the foot become be $P>0$ and keeps increasing (i.e. confirm the ground touch, first rule).

The control strategy for the motors M_1 and M_2 is aimed to make sure that the exoskeleton structure will follow the subject's leg physical motion without hindering it. The set of sensors S_1 and S_2 (flexible strips with bonded strain gages) are attached to the links of the exoskeleton (Fig. 2). When the subject limbs commence the motion the limbs will touch and bend the strips. The sensors will detect in real time any intended tiny motions of the subject's limbs and send the signals to the PID controller. The controller will react immediately by activating hip and knee motors M_1 and M_2 in order to move the links of the exoskeleton away from the object limbs and thus to restore the original shape of the strips. The set point of the PID controller is zero signals from the sensors. The PID controller can provide fast system response and accurate positioning of the exoskeleton links with respect to subject's limps. As a result, object limp can move free with no obstruction from the exoskeleton.

The system operational or logic flow chart is shown in Fig. 4. If the common switch is on then the system start receiving data from pressure F sensors (Fig. 2). If $P>0$ that means that the foot is in contact with the ground. If the value of P is growing that means the subject is stepping of that foot and the motors have to be deactivated and the cylinder has to be activated. This is weight supporting condition for the exoskeleton. If instead P is decreasing that means the subject is transmitting the weight from this leg to another one and if $P \geq P_{min}$ then motors should be kept

deactivated and the cylinder is activated to support the weight. If $P \leq P_{min}$ that means the limit is reached and the subject is ready to move this leg one step forward.
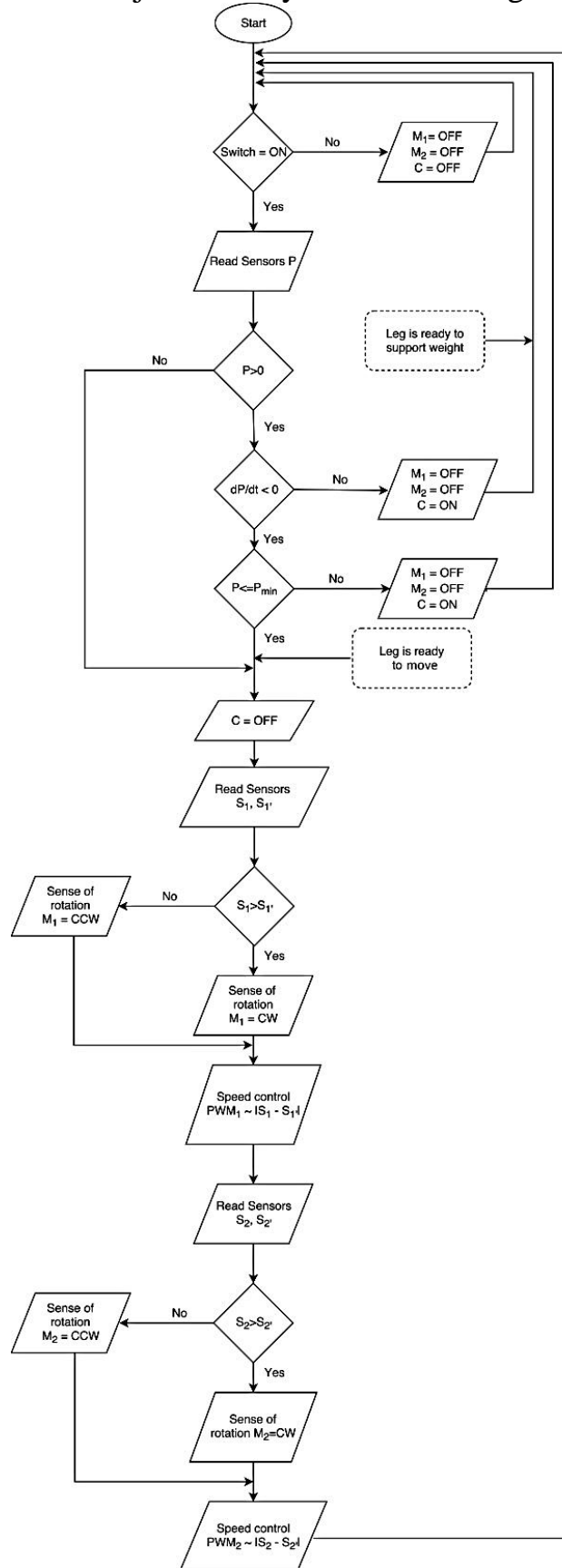

Fig. 4 Flow chart of controller operation

Therefore, the cylinder valve is deactivated to allow the motion of the exoskeleton components. In this condition the reading of strain gages S_1, $S_1´$, and S_2, $S_2´$ and operation of both motors M_1 and M_2 are initiated. By comparing the reading from the pair of sensors S_1, $S_1´$, and S_2, $S_2´$ the sense of motors rotation can be established. For example, if the reading $S_1 > S_1´$ the rotation of M_1 can be set in clockwise direction. Conversely, if $S_1 < S_1´$ then the rotation of M1 can be set in counterclockwise direction. Same is true for the data received from sensors S_2, $S_2´$ that control the sense of rotation of motor M_2. The speed of motor rotation is controlled by the motor driver and PWM signal received from the microcontroller. PWM is selected to be proportional to the absolute difference between the readings of the pair of sensors, i.e. $| S_1 – S_1´ ||S_2 – S_2´|$. It is very effective way of monitoring the speed of the motor response to the object intention to move a limb. The higher is the pressure applied by the user to the strip the higher is the acceleration of the motor to restore the shape of the strip with attached strain gages. It is in a way implementation of proportional control strategy for the motor speed control. The microcontroller operates in loop continuously checking status of all sensors, making decision and actuating either cylinder valves or the motors as long as the common switch is on (Fig. 4).

Computer Simulation of Human-Machine Interface with MATLAB Simulink. The main control system for the exoskeleton is divided into four subsystems where each subsystem is responsible for the sensing and actuation of each joint. For simulation purpose, the subject movement is taken from the recorded data of typical human lower limb movement during walking. Figure 5 shows the top layer of the program that controls the overall logic of the exoskeleton motion.
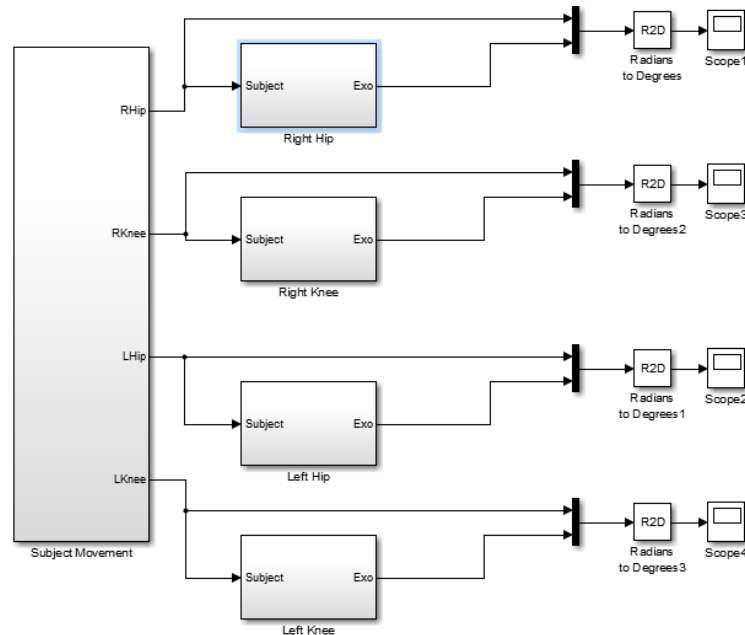

Fig. 5 Top layer of exoskeleton simulation program

The "Subject Movement" block provides the data to simulate the subject movement input to the individual joint controller which runs a closed-loop control algorithm to control the movement of its actuator

Fig. 6 and Fig. 7 show the second layer of the simulation program for hip and knee joint respectively where the closed-loop controller is implemented. The controller setup is identical for both hip and knee joint except for the addition of inhibition logic for knee joint. The controller consists of a "PID" block, "DC Motor" block, "Load Torque" block and "Sensor" block. The "PID" block calculates the desired output to be applied to the actuator, "DC Motor" block simulates the response of the DC motor towards the voltage applied, "Load Torque" block calculates the static and dynamic loads acting on the joint actuator and "Sensor" block simulate the electrical signal given by the sensing system in response to the subject movement. The DC motor model is constructed based on classical DC motor equivalent circuit as well as on the closed loop simulation technique based on the motor torque-current and speed-voltage relations. The load for the joints are constructed and calculated based on the dynamic model derived based on classical Lagrangian mechanics [19]. To simplify the code management, each torque component is grouped into a separate function block.

Fig. 8 shows the detail of the "Sensor" block. The "Cantilever Beam" block is constructed from the mathematical model of strain gages responses to the deflection of cantilever beam that is to which it is bonded. The thigh or shank movement of the human object will result in the displacement of the deformable material (beams) which will further result in the deformation of the strain gauges. Foil type strain gauge can be attached to the deformable materials such as Low Density Polyethylene (LDPE) sheet to achieve the measurement with maximum sensitivity. The block receives the input from the movement of the thigh or shank which will create the deflection of the cantilever beam. Depending on the beams length and thickness, materials properties of the material and the position of strain gauge on the cantilever beam, the amount of strain of each gauge can be calculated as a result of this deflection. Once the strain is calculated it can be converted to output voltage by means of Wheatstone bridge circuit. In order to follow closely the subjects legs motion the output voltage from Wheatstone bridge is then compared to the zero voltage reference to generate the error for the PID controller. The PID controller then instantly applies the output to the joint DC motor to actuate and drive the exoskeleton link in order to follow the subject movement with accuracy and fast response.
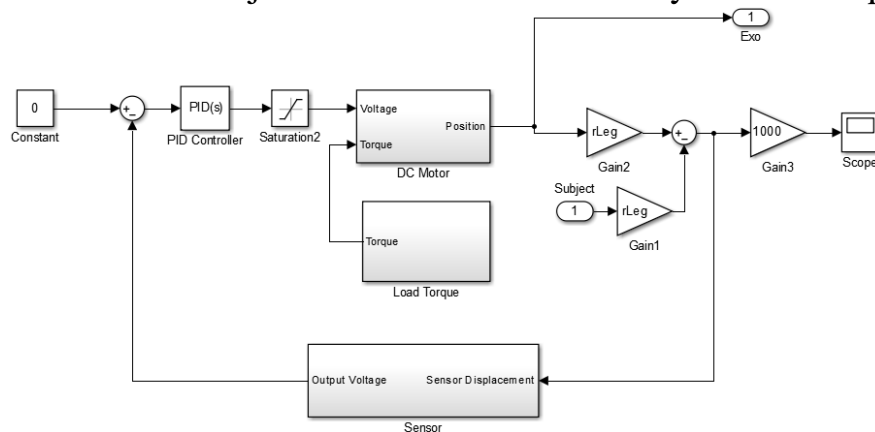

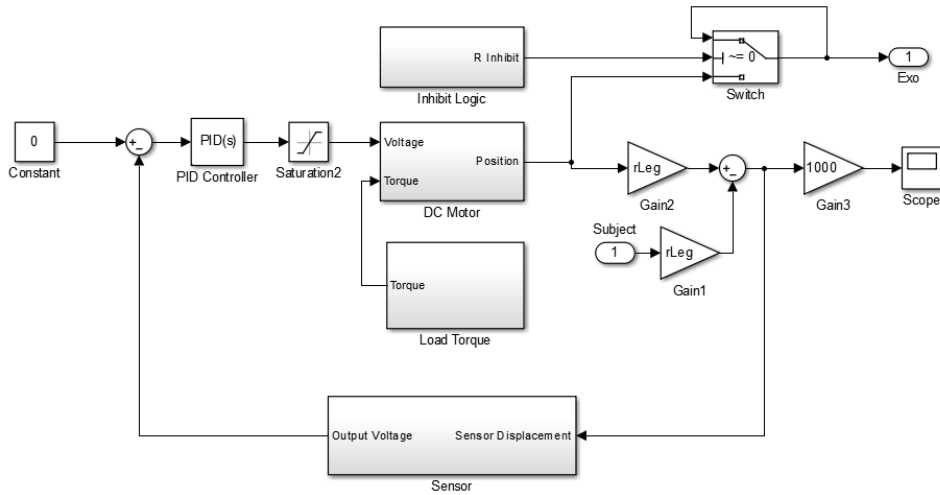*Fig.6 Closed-loop controller for hip joint*
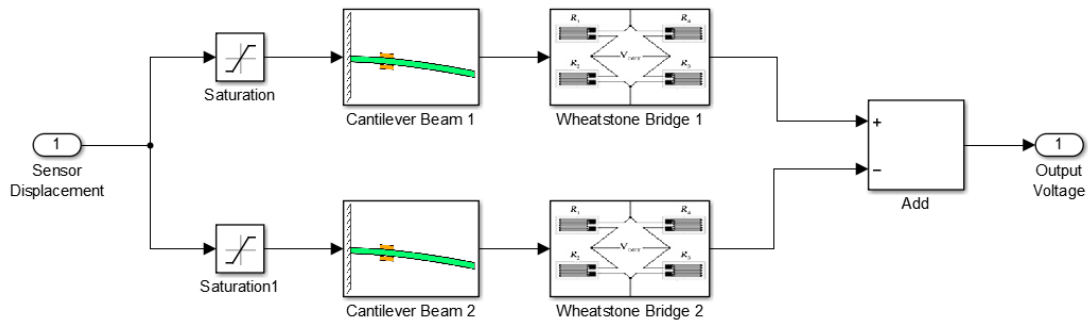
Fig 7 Closed-loop controller for knee joint

Fig. 8 Simulink model of the sensing subsystem

The parameters used in the simulation work are shown in Table 1.

| TABLE I SIMULATION PARAMETERS		
Symbol	Quantity	Value
Mechanical Parameters		
r_{leg}	Length of leg (thigh and shank)	0.4 m
m_{thigh}	Mass of thigh	4 kg
m_{shank}	Mass of shank	3 kg
m_{knee}	Mass of knee	1 kg
m_{ankle}	Mass of ankle	0.5 kg
Motor Parameters (Maxon DCX32L 24V)		
K_t	Torque constant	27.3 mNm/A
R	Terminal resistance	0.331 Ω
L	Terminal inductance	0.103 mH
J	Rotor inertia	72.8 gcm^2
b	Viscous friction	5.17x10^{-3} mNm/rad/s
Sensor Parameters		
h	Thickness of cantilever beam	5 mm
x	Strain gauge distance	35 mm
l	Length of cantilever beam	70 mm
G	Gauge factor	31
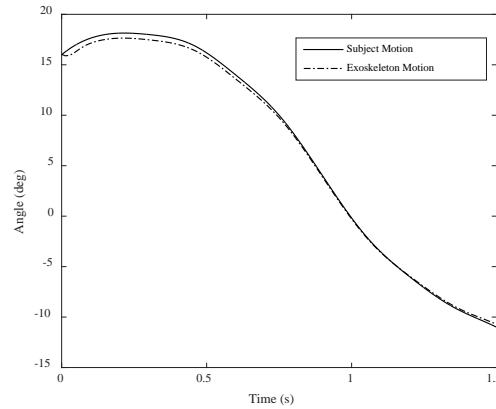
Fig.9 Hip joint angle during leg swinging motion

Fig. 9 and Fig. 10 show the hip and knee joint angles variation of one leg during part of walking cycle (free swing of the leg). In these figures the angle of the subject's leg is shown in solid line and the angle of the exoskeleton is shown in dashed line. As it can be seen from the figures the dynamic motion of the exoskeleton leg very closely traces the motion of subject leg during its free swing in space. It proves the efficiency of the developed control system and its subcomponents.

Conclusion. The paper describes the methodology of mechanical design and effective control of a new exoskeleton system to enhance walk capabilities of people. It also can be used for rehabilitation of people with leg injuries. The core idea is to use exoskeleton to decouple weight carrying capabilities of the legs from its body advancing capabilities. This has been done by special logic and intelligent management of electrical motors and motion inhibiting passive pneumatic cylinders operation. The operation is managed and controlled by the microcontroller which receives the necessary data from the strain gauge sensors located at the subject's thighs and shanks and the pressure sensors located at the feet. The paper also demonstrates the MATLAB Simulink modelling of the exoskeleton leg dynamic behavior that proves fast and precise response to the human motion intentions. This approach in exoskeleton design enables the user to focus on just forward motion that takes much less muscle tension and leave to the exoskeleton to carry the heavy body weight. This makes the exoskeleton more power efficient because electrical motors are smaller in size and did not participate in supporting the weight like in all other existing exoskeleton designs. The motors just provide a synchronous fast motion of the exoskeleton leg in response to human intention to take a step.
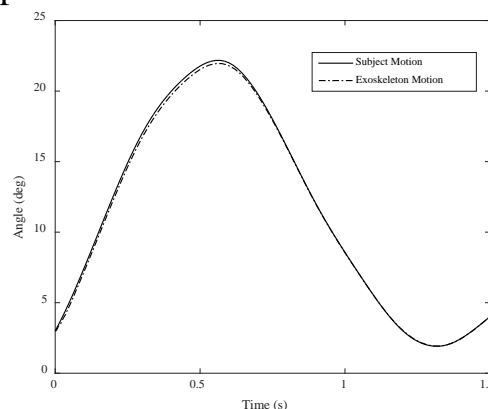

Fig.10 Knee joint angle during leg swinging motion

REFERENCES:

[1] Zoss, A.B., Kazerooni, H. & Chu, A., *"Biomechanical design of the Berkeley lower extremity exoskeleton (BLEEX),"* IEEE/ASME Transactions on Mechatronics, 11(2), pp. 128–138, (2006).

[2] Suzuki K., Mito G., Kawamoto H., Hasegawa Y., Sankai Y., *Intention-based walking support for paraplegia patients with robot suit HAL*, Journal of Advanced Robotics, 21, pp. 1441-1469, (2007).

[3] Mao Y., Agrawal S.K., *Design of a Cable Driven Arm Exoskeleton (CAREX) for Neural Rehabilitation*, IEEE Transactions on Robotics, vol. 28, no. 4, pp. 922-931, (2012).

[4] Jamwal P.K., Sheng Q.X., Shahid H., John G.P., *An adaptive wearable parallel robot for the treatment of ankle injuries*, IEEE/ASME Transactions on Mechatronics, 19(1), pp. 64-75, (2014).

[5] Iqbal J., Baizid K., *Stroke rehabilitation using exoskeleton-based robotic exercisers*, Mini Review, Biomedical Research, 26 (1), pp. 197-201, (2015).

[6] Pons J. L., Wearable Robots: Bio-mechatronic Exoskeletons, Wiley & Sons, Ltd.: Hoboken, NJ, USA. (2008).

[7] De Santis, Siciliano B., De Luca A., Bicchi A., *An atlas of physical human-robot interaction," Mechanisms and Machines Theory*, vol. 43, pp. 253-270, (2008).

[8] Veneman J. F., Kruidhof R., Hekman E.E., Ekkelenkamp R., Van Asseldonk E. H., H. van der Kooij, *Design and evaluation of the LOPES exoskeleton robot for interactive gait rehabilitation*, IEEE Trans. on Neural Systems and Rehabilitation Engineering, vol. 15, pp. 379-86, (2007).

[9] Banala S., Agrawal S., Scholz J., *Robot assisted gait training with active leg exoskeleton (ALEX)*, IEEE Trans. Neural Syst. Rehabilitation Engineering., vol. 17, pp. 2-8, (2009).

[10] Kawamoto H., Y. Sankai, "Power assists method based on phase sequence and muscle force condition for HAL," Journal of Advanced Robotics, 19(7), pp. 717–734, (2005).

[11] Kawabata T., Satoh H., Sankai Y., *Working posture control of robot suit HAL for reducing structural stress*, in Proc. of IEEE International Conference on Robotics and Biomimetics (ROBIO), , Guilin, pp. 2013–2018, (2009).

[12] Kao P., Ferris D. P., *Motor adaptation during dorsiflexion-assisted walking with a powered orthosis*, Journal of Gait Posture., vol. 29, pp. 230-236, (2009).

[13] Kazerooni H., Steger R., Huang L., H*ybrid control of the Berkeley lower extremity exoskeleton (bleex)*, The International Journal of Robotics Research, 25(5-6), pp. 561–573, (2006).

[14] Ghan J., Kazerooni H., *System identification for the Berkeley lower extremity exoskeleton (BLEEX)*, In Proc. of IEEE International Conference on Robotics and Automation (ICRA), Florida, pp. 3477–3484, (2006).

[15] Heng C., Jun Z., Chunming X., Hong Z., Xiao C., Yu W., *Design and Control of a Hydraulic-Actuated Leg Exoskeleton for Load-Carrying Augmentation*, in Proc. Of IEEE International Conference on Intelligent Robotics and Automation (ICIRA), Part I, vol. 6424, Shanghai, 2010, pp. 590–599.

[16] Walsh C. J., Paluska D., *Development of a lightweight, underactuated exoskeleton for load-carrying augmentation*, in Proc. of IEEE International Conference on Robotics and Automation (ICRA), Florida, pp. 3485–3491, (2006).

[17] Ikeuchi Y., Ashihara J., Hiki Y., Kudoh H., Noda T., *Walking assist device with bodyweight support system*, in Proc. of IEEE/RSJ International Conference on Intelligent Robots and Systems, St. Louis, pp. 4073–4079, (2009).

[18] Leslie M., *The next generation of exoskeletons*, A Magazine of the IEEE Engineering in Medicine and Biology Society, vol. 3, no. 4, pp. 56-61, (2012).

[19] Tawakal H. B., Adnan M., Javaid I., Umer I., Umer S. K., *Kinematic and dynamic Analysis of Lower Limb Exoskeleton*, WASET International Journal of Mechanical, Aerospace, Industrial, Mechatronic and Manufacturing Engineering, , vol.6, no.9, pp. 1945-1949, (2012).

DEVELOPMENT OF SOFTWARE FOR THE SELECTION OF PARAMETERS FOR STANDARD GRINDING CYCLES OF THE SIEMENS SINUMERIK 802D SL SYSTEM

Leonid SHIPULIN[1], Evgeniya OBUKHOVA[2], Arnold FROLOV[3]

[1,3]South Ural State University, Chelyabinsk, Russia, [2]«PTC» LLC, Chelyabinsk, Russia

E-mail: shipulinlv@susu.ru[1], oev@rts-eng.ru[2], arni-frolov@mail.ru[3]

Abstract: An overview of the standard cycles used in the preparation of control programs for cylindrical grinding machines with the Siemens SINUMERIK 802D sl CNC system, as well as the problems associated with the assignment of their parameters, is carried out. The developed software for assigning the parameters of standard cycles used in the preparation of control programs for cylindrical grinding machines with the Siemens SINUMERIK 802D sl CNC system is being carried out.

Keywords: cylindrical grinding, automatic cycles, parameters of grinding cycles.
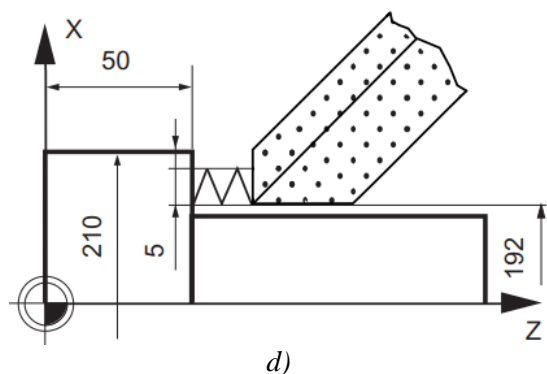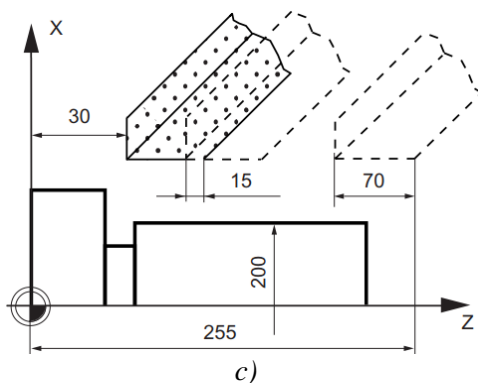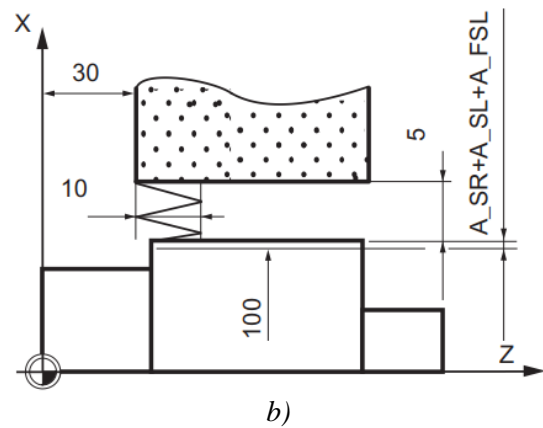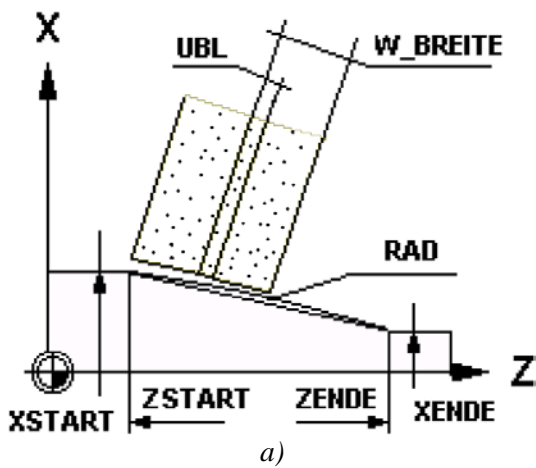
Introduction. Features of the current stage of development of mechanical engineering is characterized by the proliferation of CNC grinding machines. The use of this type of equipment can significantly increase machining productivity and improve the quality of manufactured parts. The main feature of this equipment is that the movement of the tool relative to the workpiece is pre-programmed and recorded in the form of a control program written in G codes according to the ISO standard.

The control program is a sequence of frames. It is recommended to compose the control program in such a way that only the geometric, technological and auxiliary information that changes with respect to the previous frame is recorded in the frame. To increase the performance of CNC cylindrical grinding operations, cycles are used to adapt the machining cycle to specific technological conditions [1–8]. Cycles represent the specified trajectories of movement of the working bodies of the machine. Modern CNC systems have pre-programmed machining cycles. The use of typical cycles (libraries of subprograms) for machining workpiece elements in programming greatly simplifies the compilation of a control program, reduces labor intensity and reduces the possibility of programming errors.

There are several types of single machining cycles: typical, fixed and flexible. Typical cycles reflect available cycle design guidelines for a wide range of possible machining options. Permanent (automatic) cycles are small, hard programs that cannot be changed. Flexible cycles are made as subprograms that can be changed during programming. Permanent cycles and subprograms can be repeated anywhere in the program and thus greatly simplify the programming of machining parts with several identical elements.

According to the Siemens SINUMERIK 802D sl [9] programming and operating manual for cylindrical grinding machines with CNC systems, there is the following list of cycles, for which you must enter the parameters indicated in brackets:

Leonid SHIPULIN, Evgeniya OBUKHOVA, Arnold FROLOV.
Development of software for the selection of parameters for standard
grinding cycles of the siemens sinumerik 802D sl system

– cone grinding CYCLE 405 (N_SITZ, Z_START, Z_ENDE, X_START, X_ENDE, W_BREITE, UBL, RAD, B_ART, ZU_ART, BVU1, BVU2, X_A_LU, X_A_SR, X_A_SL, X_A_FS, SRZ, SLZ, FSZ, N_SR, N_SL, N_FS, D_SR, D_SL, D_FS, ESL, EFS, FX_SR, FX_SL, FX_FS, FZ_SR, FZ_SL, FZ_FS, MZ, KS, F_KS, UWERK) (see fig. 1, a);

– plunge-cut CYCLE 410 (N_SITZ, X_SOLL, Z_ST, B_ART, A_LU, A_SR, A_SL, A_FSA, F_SR, F_SL, F_FSL, TIME, MZ, KS, F_KS, OSW, F_OSCILL, UWERK) (see fig. 1, b);

– repeated plunge-cut CYCLE 411 (N_SITZ, X_SOLL, Z_ST, Z_END, UBL, B_ART, A_LU, A_SR, A_SL, A_FSL, SLZ, FSZ, ZU_ART, BVU1, BVU2, F_PE, F_SR, F_SL, F_FSL, N_FR, MZ, KS, F_KS, UWERK) (see fig. 1, c);

–plunge-cut edge grinding CYCLE412 (N_SITZ, Z_SCH, X_ST, B_ART, A_LU, A_SR, A_SL, F_SR, F_SL, TIME, KS, F_KS, OSW, F_OSCILL, UWERK) (see fig. 1, d);

– plunge-cut grinding with angle feed CYCLE413 (N_SITZ, X_SOLL, Z_SCH, WIN, B_ART, A_LU, A_SR, A_SL, A_FSL, F_SR, F_SL, F_FSL, TIME, MZ, KS, F_KS, UWERK) (see fig. 1, e);

– swing CYCLE415(N_SITZ, X_SOLL, Z_ST, Z_END, B_ART, A_LU, A_SR, A_SL, A_FSL, SRZ, SLZ, FSLZ, ZU_ART, BVU1, BVU2, F_PE, FP_SL, FP_FS F_SR, F_SL, F_FSL, N_FR, MZ, KS, F_KS, UWERK) (see fig. 1, f);

– fillet grinding CYCLE414 (N_SITZ, Z_SCH, X_ST, RAD, LAGE, A_LU, A_SR, F_SR, KS, F_KS, UWERK) (see fig. 1, g).
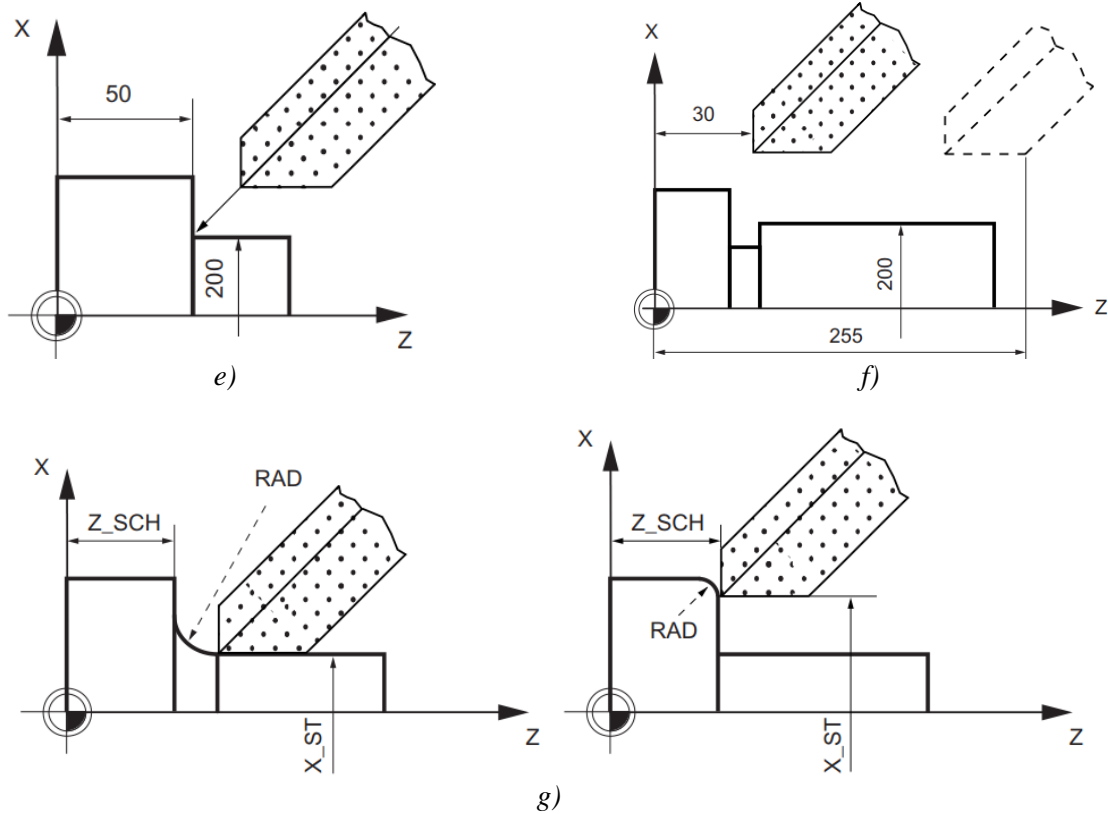

a)

b)

c)

d)

Leonid SHIPULIN, Evgeniya OBUKHOVA, Arnold FROLOV.
Development of software for the selection of parameters for standard
grinding cycles of the siemens sinumerik 802D sl system

Figure. 1. SINUMERIK 802D sl CNC cylindrical grinding machine cycles [7]:
a) CYCLE 405; b) CYCLE 410; c) CYCLE 411;
d) CYCLE412; e) CYCLE413; f) CYCLE415; g) CYCLE414.

When developing a control program using the above cycles, problems arise related to the assignment of cycle parameters (for example, for the swing cycle CYCLE415, shown in Table 1), namely:
– a large number of strictly regulated parameters;
– lack of recommendations on the assignment of parameters;

Table 1. Description of swing cycle parameters CYCLE415 [7]

Parameter	Data type	Meaning
N_SITZ	INT	Support number
X_SOLL	REAL	Specified diameter (abc.)
Z_ST	REAL	Start position in Z (abc.)
Z_END	REAL	End position in Z (abc.)
B_ART	INT	Machining mode: 1= roughing 2= finishing + tweaking 3=roughing + finishing + tweaking
A_LU	REAL	Air gap (increment)
A_SR	REAL	Cut amount - Roughing (incr.)
A_SF	REAL	Cut amount - Finishing (incr.)
A_FSL	REAL	Cut amount - Tweaking (incr.)
SRZ	REAL	Feed rate value in roughing (incr.)
SLZ	REAL	Feed rate value in finishing (incr.)
FSLZ	REAL	Feed rate value in tweaking (incr.)

72

Leonid SHIPULIN, Evgeniya OBUKHOVA, Arnold FROLOV.
Development of software for the selection of parameters for standard
grinding cycles of the siemens sinumerik 802D sl system

ZU_ART	INT	Feed rate -1 = only from left 0 = from both sides 1 = only from right
BVU1	INT	Dwell time at point of return 1
BVU2	INT	Dwell time at point of return 2
F_PE	REAL	Pendulum roughing feed
FP_SL	REAL	Pendulum finishing feed
FP_FS	REAL	Pendulum tweaking feed
F_SR	REAL	Feed in roughing
F_SL	REAL	Feed in tweaking
F_FSL	REAL	The number of moves to exit
N_FR	INT	Active control J=1 / N=0
MZ	INT	Structure-borne noise J=1 / N=0
KS	INT	Feed for grinding wheel idle passes [mm/min]
F_KS	REAL	Peripheral speed of workpiece [m/min]

To solve these problems, it is proposed to develop software that makes it easier for the technologist-programmer to choose the parameters of the cycles, which ultimately will greatly simplify the compilation of the control program. The Microsoft Excel program was considered as a software implementation tool. The functions of the program allow you to carry out almost any manipulation of numbers. The spreadsheet is the main tool that is used to process and analyze digital information using computer technology.

The peculiarity of Microsoft Excel lies in the fact that in the process of calculating, you can simultaneously operate with data that is located in different zones of the spreadsheet and at the same time are connected with a certain dependency. Such calculations are carried out due to the possibility of introducing various formulas into the cells of the table. After performing the calculation, the result will be displayed in the cell with the formula. An important feature of using a spreadsheet is the automatic recalculation of results if cell values change.

In the Microsoft Excel software environment, eight sheets were created, seven of which correspond to each of the considered cycles and one sheet contains reference information. In fig. 2 shows an example of an Excel sheet with recommendations for assigning parameters for a
canned cycle for radius grinding CYCLE414.

The worksheet (see fig. 2) is divided into 2 zones:

– zone "Initial data", here the user specifies all the necessary data for assigning parameters, such as length, required diameter, etc., depending on the type of cycle;

– parameter assignment zone. Most of the cells are filled in automatically using the original data. However, to fill in some cells it is necessary to perform a number of actions: follow the hyperlink to the sheet with reference information from the reference book of the Chelyabinsk Research Institute of Abrasives and Grinding [9], select the required variable and write in the indicated place. Finally, all data is automatically copied into one record, resulting in a cycle record that can be used on the machine.

Leonid SHIPULIN, Evgeniya OBUKHOVA, Arnold FROLOV.
Development of software for the selection of parameters for standard
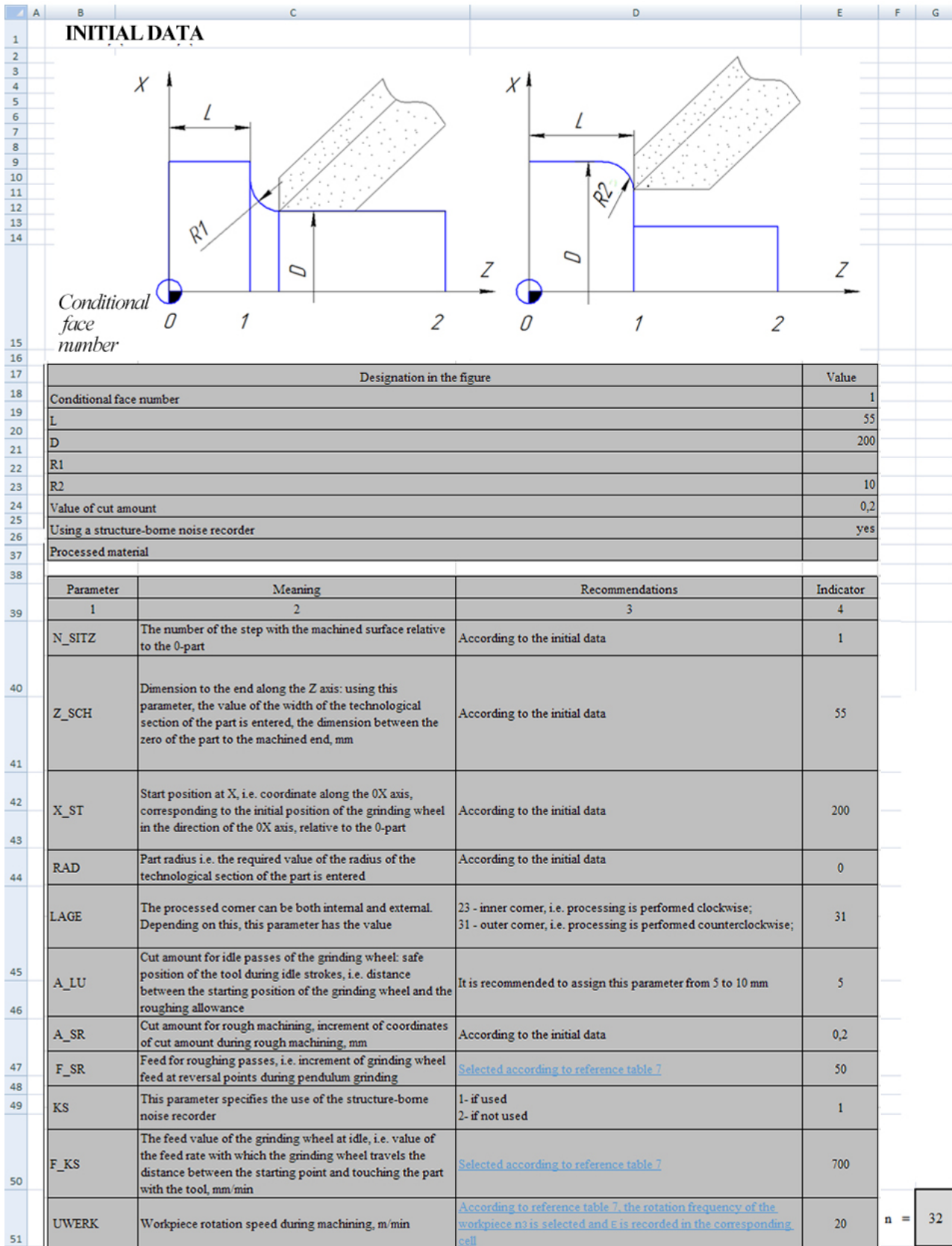**grinding cycles of the siemens sinumerik 802D sl system**

Fig. 2. Parameter assignment for radius grinding CYCLE414.

Leonid SHIPULIN, Evgeniya OBUKHOVA, Arnold FROLOV.
Development of software for the selection of parameters for standard
grinding cycles of the siemens sinumerik 802D sl system

Results. A software tool has been developed in the form of a Microsoft Excel book containing tables from the reference book of the Chelyabinsk Research Institute of Abrasives and Grinding. The software tool allows you to determine the parameters of the standard grinding cycles of the Siemens SINUMERIK 802D sl system using reference data.

REFERENCES:

[1]. Pereverzev P, Pimenov D., *Optimization of control programs for numerically controlled machine tools by dynamic programming.* Russian Engineering Research 35(2):135–142, (2015)

[2]. Guzeev V., Nurkenov A., *Designing the plunge-grinding cycle on the basis of the rigidity of the technological system.* Russian Engineering Research 35(2):150–153, (2015).

[3]. Pereverzev P., Akintseva A., *Optimal internal grinding cycles in multidimensional control-parameter space.* Russian Engineering Research 36(11):974–978, (2016).

[4]. Malkin S., Koren Y., Ber A., *Off-Line Grinding Optimization with a Micro-Computer.* CIRP Annals 29(1):213–216. https://doi.org/10.1016/S0007-8506(07)61324-9, (1980).

[5]. Malkin S., *Grinding Cycle Optimization.* CIRP Annals 30(1):223–226. https://doi.org/10.1016/S0007-8506(07)60930-5 , (1981).

[6]. Xiao G., Malkin S., *On-Line Optimization for Internal Plunge Grinding.* CIRP Annals – Manufacturing Technology 45(1):287–292, (1996).

[7]. Ivester R., Danai K., Malkin S. *Optimization of cylindrical plunge grinding by recursive constraint bounding.* American Society of Mechanical Engineers, Dynamic Systems and Control Division 57-1:529–537, (1995).

[8]. Aravind M., Periyasamy Dr. *Optimization of Surface Grinding Process Parameters By Taguchi Method And Response Surface Methodology.* IJERT 3(5):1721–1727, (2000).

[9]. SIEMENS SINUMERIK 802D sl. *Cylindrical Grinding: A Guide to Programming and Operation. Software version 1.4. for access:* https://cache.industry.siemens.com/dl/files/125/28436125/att_76624/v1/802Dsl_BPRS_0709_ru_ru-RU.pdf. – 04.06.2021.

[10]. Ardashev D.V., *Cutting modes for work performed on grinding and lapping machines with manual control and semiautomatic devices: reference book / [and others].* Chelyabinsk: Publishing house of ATOKSO, 384 p (2007).

SUBMISSION GUIDELINES

General requirements.
Article should not be earlier published in any edition, stated in the short form and edited. The scientific article maintenance should correspond to one of the following scientific directions: Designing of machines; Materials technology; Mechanics; Manufacturing engineering; Economy and management; Automatics and ICT; Technical information.

The documents applied to article.
The conclusion of the corresponding organization (chair, etc.); The expert opinion on expediency of the publication of the article; The covering letter; The Information on the authors (name, patronymic, surname, the exact address, place of work and position, scientific degree, area of scientific activity, contact phones, e-mail address ,etc.).

Preparation rules.
Format - A4; *Margins from each party* - 20 mm; *Program* - Microsoft Office Word; *Font* - Times New Roman, a font size - 14, an interval - 1,5.
The scientific article can be written only in English language, and it is represented in duplicate.
 Article volume - 5 … 8 pages.

Sequence of compilation:
1. Article name - on the center;
2. Names and surnames of the authors - on the center;
3. Full addresses of a place of work of authors - on the center;
4. Co-ordinates of authors: e-mail address, phone numbers.
5. The abstract: not less than two-three offers, and no more than 100 words. In the summary: article summary, problem statement, and the information on the received results should be reflected.
6. Keywords: often used $3 \div 5$ terms under the article.
7. The basic text.
8. The references.

The main text of article should be divided as follows:
For example: "*Introduction*", "*Problem statement*", "*Decision or test methods*", "*Results of the decision or tests and their estimation*".
In introduction: the description of the problem statement, the work purpose and etc.;
In the main part: formation of problem statements; research and methods of the decision, their advantage and difference from existing methods; examples confirming efficiency of the offered method of the decision and the results received.
In the conclusion: evaluation of the results.
Drawings. *Formats* - DOC, JPEG, TIFF and PDF (600 dpi). *The size* – min. 5×5, max. 10×15. *Arrangement* - ("In the text", in the center). Images of drawings should be accurately visible, and all symbols well are read.
Drawings, paintings, schedules and algorithms should correspond to standard requirements.
Tables are located in the text and are numbered, and the name of each table should be specified in the right top corner.
Formulas should be written down in format *Equation* in the separate line. It is not recommended to use special symbols in the text written on the same line in format *Equation*. Formulas should be written down in certain sequence and are numbered on the right.
The references should correspond to the text and sequence of article. It is recommended to refer to sources published in last 10 years.
The additional information. Edition has the right to spend necessary updating and reductions. Authors bear a scientific article maintenance responsibility. To the publication those articles which have received a positive response are represented only. If article is not published, the edition decision is possible to data of authors, the manuscript and disks do not come back.

MACHINE SCIENCE № 1, 2021